THE UNIVERSITY OF MANITOBA

TURBULENCE IN A CONICAL DIFFUSER WITH FULLY DEVELOPED FLOW AT ENTRY

by

Paul Akazua Christopher Okwuobi

A THESIS

SUBMITTED TO THE FACULTY OF GRADUATE STUDIES

IN PARTIAL FULFILMENT OF THE REQUIREMENTS FOR THE DEGREE

OF DOCTOR OF PHILOSOPHY

DEPARTMENT OF MECHANICAL ENGINEERING

WINNIPEG, MANITOBA

October 1972

ABSTRACT

An experimental study of the structure of turbulence in a conical diffuser having a total divergence angle of 8° and an area ratio of 4:1 with fully developed flow at entry is described. Quantitative data are presented for pipe entry Reynolds numbers of 152,000 and 293,000 of profiles of the mean pressure, mean velocity, turbulence intensities, correlation coefficients and the one-dimensional energy spectra.

The results show that the rate of turbulent energy production approximately reaches a maximum value at the edge of the wall layer defined by the point of maximum u_1-fluctuation. It is found that within the layer, $\overline{u_1^2}$ varies linearly with the distance from the wall and the linear range grows with distance in the downstream direction; the surfaces of maximum $\overline{u_1^2}$ and $\overline{u_1 u_2}$ closely coincide; and at the edge of the layer, the energy production is about two orders of magnitude greater than the direct viscous dissipation.

The spectral profiles and characteristics are very similar to those reported for pipe flows; the normalised spectra of $\overline{u_1^2}$ exhibit the $\kappa_1^{-5/3}$ dependence for about one decade of the one-dimensional wave-number κ_1.

From the turbulent kinetic energy balance, it is found that the magnitude of the energy convective diffusion due to kinetic and pressure effects is comparable to that of the energy production.

ACKNOWLEDGEMENTS

The author would like to take this opportunity to express his appreciation to Dr. R. S. Azad for his encouragement and guidance as research adviser. Sincere thanks are due to Dr. J. Tinkler for his comments and careful review of the thesis.

Thanks are also due to Professor R. E. Chant, Head of the Department of Mechanical Engineering, and to Professor O. Hawaleshka for their warm and cheerful suggestions which made it possible to conduct the research at the University of Manitoba.

Special thanks are due to my wife Lucy, and children Azu, Nkihu, Ike and Uche for their patience and interest.

Finally, the support provided by the National Research Council of Canada through the grant held by Professor O. Hawaleshka is gratefully acknowledged.

TABLE OF CONTENTS

LIST OF TABLES

LIST OF FIGURES

NOMENCLATURE

A	constant
AR	diffuser area ratio, A_{x_1}/A_{in}
A_{x_1}	local cross-sectional area
A_{in}	inlet plane cross-sectional area
B	constant
c_f	skin friction coefficient, $\tau_W/\frac{1}{2}\rho U_{1,m}^2$
$\overline{C}_p$	pressure recovery coefficient, $(\langle P\rangle_{x_1} - \langle P\rangle_{in})/\frac{1}{2}\rho\langle U_1\rangle_{in}^2$
$\overline{C}_{p,i}$	ideal pressure recovery coefficient, $1 - 1/(AR)^2$
$C_{P,R}$	pressure recovery coefficients;
$C_{P,S}$	$C_{P,S} = (P_S - P_{W,ref})/\frac{1}{2}\rho\langle U_1\rangle_{ref}^2$
$C_{P,T}$	etc.
$C_{P,W}$	etc.
D	local diameter of pipe or diffuser
D_{ij}	deformation tensor
F_{ij}	unnormalised spectra at $\overline{u_i u_j}$
H	shape factor, δ^*/θ
K_1, K_2	structure parameters
L	length of pipe separating the diffuser from the contraction cone
M'	instantaneous value of an unspecified parameter
M	mean value of an unspecified parameter
m	fluctuating value of an unspecified parameter
P'	instantaneous static pressure (mean plus fluctuating)

P	mean static pressure
p	instantaneous static pressure fluctuation
$(P_r)_c$	cumulative turbulence energy production rate
$(P_r)_*$	dimensionless turbulent energy production rate
q	resultant velocity fluctuation
r	radial direction
R	local radius of pipe or diffuser
Re	Reynolds number, $(<U_1>D/\nu)_{ref}$
Re,m	Reynolds number, $RU_{1,m}/\nu$
R_θ	Reynolds number based on momentum thickness, $U_{1,m}\theta/\nu$
t	time
T	averaging time
U_1', U_2', U_3'	instantaneous velocity in the x_1, x_2, x_3 directions, respectively
U_1, U_2, U_3	local mean velocity in the x_1, x_2, x_3 directions, respectively
u_1, u_2, u_3	instantaneous velocity fluctuation in the x_1, x_2, x_3 directions, respectively
$\tilde{u}_1, \tilde{u}_2, \tilde{u}_3$	root-mean-square of velocity fluctuation in the x_1, x_2, x_3 directions, respectively
U_x, U_r, U_θ	local mean velocity in the x, r, θ directions, respectively
u_x, u_r, u_θ	instantaneous velocity fluctuation in the x, r, θ directions, respectively

$U_{l,m}$	pipe or diffuser center-line velocity
U_*	friction velocity, $(\tau_W/\rho)^{1/2}$
U^+	U_l/U_*
W	work done per unit of mass and time
$(W_\mu)_*$	dimensionless direct viscous dissipation rate
x_1, x_2, x_3	axial, radial and circumferential directions, respectively
x, r, θ	axial, radial and circumferential directions, respectively
y	radial distance from pipe or diffuser wall
y^+	yU_*/ν
α	total divergence angle of diffuser
β	angle between the principal axis of the turbulent stress tensor and the x_1-axis
δ^*	displacement thickness
δ_{ij}	Kroeneker delta
∇^2	Laplacian operator
ε_{ijk}	alternating tensor
ε	turbulent energy dissipation rate, $\overline{\nu(\frac{\partial u_i}{\partial x_j} + \frac{\partial u_j}{\partial x_i})\frac{\partial u_i}{\partial x_j}}$
ε^*	turbulence energy dissipation rate, $\overline{\nu(\frac{\partial u_i}{\partial x_j})^2}$ for homogeneous flow
κ_1	one-dimensional wave number in x_1-direction
λ_{u_i}	Taylor microscale
θ	momentum thickness
Ω_k	vorticity
Φ	dilation of the fluid

ϕ_{ij}	normalised spectral density
ρ	air density
σ_{ij}	stress tensor
τ	total shearing stress
μ	dynamic viscosity
ν	kinematic viscosity
ξ_1, ξ_2	dimensionless distance, x_1/R, x_2/R
$\overline{(\quad)}$	denotes time-average quantity
$\langle \quad \rangle$	denotes cross-section average quantity
$\underline{(\quad)}$	denotes vector quantity

Subscripts

CORR	corrected
i,j	indices
in	diffuser inlet plane
iso	isotropic
MEAS	measured
out	diffuser outlet plane
ref	reference station
R	reverse-facing pitot tube measurement
S	static tube pressure measurement
T	forward-facing pitot tube measurement
W	wall

1. INTRODUCTION

The importance of the diffuser as a simple, useful, fluid-mechanical element in closed-circuit wind tunnels and in turbomachinery has been known ever since Venturi (1797) and his contemporaries tried to determine the geometry for the most efficient diffuser. In a broad sense, a diffuser is a device for converting the velocity head of a moving fluid to static pressure head. The details of the actual process (at Reynolds numbers of engineering interest) involve the production, diffusion and dissipation of turbulent energy; these characteristics are difficult to describe or to predict. As a result, many investigators (e.g. Cocanower, Kline and Johnston 1965) have studied the diffuser problem with the following objectives:

(i) to measure the pressure recovery;

(ii) to determine the effect of various geometric parameters on the pressure recovery process;

(iii) to determine the over-all flow patterns.

1.1 Brief review of diffuser research

An early comprehensive study of diffuser flow was reported by Gibson (1910); on the basis of systematic experiments with water, he correlated pressure recovery

coefficient with divergence angle for a fixed area ratio. Patterson (1938) surveyed all the available data and deduced general rules for diffuser design. Since then a vast number of experimental and theoretical studies (e.g., Nikuradse 1929; Fraser 1956; Sprenger 1959; Kline, Abbott and Fox 1959; Cocanower, Kline and Johnston 1965; Sovran and Klomp 1967; Ackeret 1967; Cockrell and King 1967) has been devoted to the subject. The results of these investigations have led to the following insight on the performance of diffusers: the pressure recovery coefficient $(\langle P\rangle_{out}-\langle P\rangle_{in})/\frac{1}{2}\rho\langle U_1\rangle^2_{in}$ tends to

(i) increase as the thickness of the turbulent boundary layer at inlet decreases;

(ii) decrease as the region of boundary layer separation increases within the diffuser;

(iii) decrease for curved diffusers as the angle of deflection of the axis increases;

(iv) become independent of Reynolds number as the Reynolds number increases to the range of most engineering applications;

(v) vary as the diffuser divergence angle is increased and the area ratio kept constant with a maximum occurring at about 8°.

1.2 Diffuser turbulence research

The one aspect of diffuser study which until

recently has received little attention is the investigation of the turbulence characteristics of the flow field. Despite many years of research on diffuser operation, it is not always possible to predict the performance accurately even when the initial flow conditions are well defined; when the inlet boundary layer is fully developed, the prediction methods serve as no more than a general guide to diffuser performance (Cockrell and King 1967). Sprenger (1959), Bradley and Cockrell (1970) among others have expressed the need for turbulence information as a means of improving the understanding of diffuser operation.

The structure of turbulent shear flow in a diffuser was probably first studied by Ruetenik and Corrsin (1955). They investigated the turbulence properties of fully developed, plane diffuser flow at a total divergence angle $\alpha = 2°$; comparison of their results with those of Laufer (1951) for parallel wall channel flow showed that there were large increases in turbulent energy and average shear levels. Previously published turbulence measurements in a conical diffuser include those of Robertson and Calehuff (1957) for $\alpha = 7\frac{1}{2}°$ and Trupp et al (1971) for $\alpha = 8°$. Robertson and Calehuff observed that the turbulence levels, the rates of turbulence production and dissipation were greatly in excess of similar quantities for zero pressure gradient boundary layers and that the longitudinal micro-scales of turbulence remained remarkably constant across

and along the developing diffuser flow. Trupp et al investigated diffuser flow with a partly developed pipe flow at entry; they found that the effect of Reynolds number (within the range tested) on the distribution of the turbulence intensities was negligible, and that the relationship between the turbulent shear stress and the turbulent kinetic energy was approximately linear as noted by Harsha and Lee (1970).

Flow through diffusers does not usually possess the simplified features of fully developed flow and it may be expected that any mathematical model of turbulence formulated with reference to the existing experimental data for symmetric equilibrium flows will be inadequate when used to predict diffuser flows in moderate to strong adverse pressure gradients. It thus appeared desirable to provide more quantitative data than has hitherto been available on the turbulence properties of conical diffuser flow. This information should also be useful as a test case for future calculation methods for predicting the distribution of mean and turbulent quantities in a diffuser.

1.3 Objectives

The primary objective of the present investigation was to make extensive measurements of mean and turbulent flow quantities in a conical diffuser; emphasis was to be placed on fully developed flow conditions at entry.

Measurements were to include, for two Reynolds numbers, profiles of the mean pressure, mean velocity, turbulence intensities, correlation coefficients and the one-dimensional energy spectra. Other objectives were

(i) to examine the data for any similarity or dissimilarity between the flow properties at the inlet (fully developed pipe flow) and in the diffuser.

(ii) to examine the flow characteristics in the wall layer defined as extending to the point of maximum u_1-fluctuation.

(iii) to investigate at a station about halfway along the diffuser (station 7) how the rates of production, diffusion and dissipation of turbulent energy are distributed.

Measurements of the turbulence quantities were to be made using the hot wire technique; the choice of the diffuser geometry was guided by the work of Sprenger (1959) and Sovran and Klomp (1967) whose results show that the 8° conical diffuser of area ratio 4:1 possesses optimum pressure recovery characteristics.

2. PRELIMINARY CONSIDERATIONS

2.1 Fundamental concepts

The basic equations of incompressible turbulent flow are derived from the Navier-Stokes and continuity relationships. These equations hold for both laminar and turbulent flow fields as long as the scale of motion of the turbulence exceeds the molecular mean free path. Townsend (1956) has shown that the molecular mean free path of air, under standard conditions, is approximately three orders of magnitude less than the dimensions of the smallest turbulent eddy; the Navier-Stokes and continuity equations should be adequate to describe turbulent air flow under such conditions.

The equations of motion are based upon the instantaneous values of velocity, pressure, body forces and fluid properties. The analysis of turbulent flow fields can be greatly simplified by considering the instantaneous property (M') to be made up of a mean component (M) and a fluctuating component (m) expressed as (Reynolds 1895)

$$M' = M + m \tag{2.1}$$

For stationary flows such as those usually studied in laboratory experiments, the mean component (M) is defined

by

$$M(x_i) = \frac{1}{T_2-T_1} \int_{T_1}^{T_2} M'(x_i,t)\, dt \quad , \tag{2.2}$$

and the time average value of the fluctuating component (m) by

$$\overline{m} = \frac{1}{T_2-T_1} \int_{T_1}^{T_2} m(x_i,t)\, dt = 0. \tag{2.3}$$

The averaging time (T_2-T_1) should be taken long enough to ensure a representative sample of the averaged quantity; for laboratory experiments it usually ranges from 1 to 100 seconds.

2.2 Governing equations

The flow of an incompressible turbulent fluid may be described by the following system of equations (Cartesian coordinates):

(i) Continuity equation:

$$\frac{\partial U_i'}{\partial x_i} = 0. \tag{2.4}$$

(ii) Momentum equation (Navier-Stokes):

$$\frac{\partial U_i'}{\partial t} + U_j' \frac{\partial U_i'}{\partial x_j} = - \frac{1}{\rho} \frac{\partial P'}{\partial x_i} + \nu \frac{\partial}{\partial x_j} \left(\frac{\partial U_i'}{\partial x_j}\right) . \tag{2.5}$$

Taking the time average of each term in equation (2.5) yields the equation of mean motion

$$\frac{\partial U_i}{\partial t} + U_j \frac{\partial U_i}{\partial x_j} = - \frac{1}{\rho} \frac{\partial P}{\partial x_i} + \frac{\partial}{\partial x_j}(\nu \frac{\partial U_i}{\partial x_j} - \overline{u_i u_j}) \quad . \tag{2.6}$$

One objective of the experimental investigation was directed at measuring the Reynolds (or turbulent) stresses $\overline{u_i u_j}$ which appear in equation (2.6). It may be noted that this stress term arises from momentum exchange effect.

Mechanical energy consideration:

The mean energy in a turbulent field is affected by the existence of turbulent velocity fluctuation through the mechanism of energy production, diffusion and dissipation. In what follows, some physical aspects of turbulent fields will be presented and the contribution of turbulence to the mean flow energy identified.

Multiplying the momentum equation (2.6) by U_i and rearranging the terms yields the mechanical mean energy equation

$$\begin{aligned} \frac{\partial}{\partial t} (\frac{1}{2} U_i U_i) = & - \frac{\partial}{\partial x_j} U_j (\frac{P}{\rho} + \frac{1}{2} U_i U_i) \\ & + \nu U_i \frac{\partial}{\partial x_j} (\frac{\partial U_i}{\partial x_j}) \\ & - U_i \frac{\partial}{\partial x_j} \overline{u_i u_j} \quad . \end{aligned} \tag{2.7}$$

The energy balance of the mean plus turbulent kinetic energy can readily be obtained by multiplying the momentum equation (2.5) by U_i' and carrying out appropriate transformations. However, to bring out the meaning of some of the terms of the energy equation, it is worth while to consider the work done by the total stress σ_{ij} acting on a fluid particle per unit mass during the deformation of the flowing fluid. This work W per unit mass may be written as

$$W = \frac{1}{\rho} \frac{\partial}{\partial x_i} \sigma_{ij} U_j'$$

$$= \frac{1}{\rho}\left[\frac{\partial}{\partial x_1} \sigma_{11}U_1' + \frac{\partial}{\partial x_2} \sigma_{21}U_1' + \frac{\partial}{\partial x_3} \sigma_{31}U_1' + \frac{\partial}{\partial x_1} \sigma_{12}U_2' + \ldots\right], \tag{2.8}$$

but

$$\frac{\partial}{\partial x_i} \sigma_{ij}U_j' = \sigma_{ij} \frac{\partial U_j'}{\partial x_i} + U_j' \frac{\partial \sigma_{ij}}{\partial x_i}, \tag{2.9}$$

and from Newton's second law,

$$\frac{\partial}{\partial x_i} \sigma_{ij} = \rho \frac{dU_j'}{dt}, \tag{2.10}$$

therefore

$$U_j' \frac{\partial}{\partial x_i} \sigma_{ij} = \rho U_j' \frac{dU_j}{dt} = \frac{\rho}{2} \frac{d}{dt} U_j'U_j', \tag{2.11}$$

and represents the total change of the kinetic energy of the fluid. The first term on the right-hand side of equation (2.9) may be evaluated by considering the details of the

stress tensor

$$\sigma_{ij} = - P'\delta_{ij} + \mu(D_{ij} - \frac{2}{3}\Phi\delta_{ij}).$$

For an incompressible fluid, $\Phi = 0$ and σ_{ij} reduces to

$$\sigma_{ij} = - P'\delta_{ij} + \mu D_{ij} \tag{2.12}$$

The total spatial change $\partial U_i'/\partial x_j$, of a deforming fluid may be divided into a symmetrical and antisymmetrical part as

$$\frac{\partial U_i'}{\partial x_j} = \frac{1}{2}(\frac{\partial U_i'}{\partial x_j} + \frac{\partial U_j'}{\partial x_i}) + \frac{1}{2}(\frac{\partial U_i'}{\partial x_j} - \frac{\partial U_j'}{\partial x_i})$$

$$= \frac{1}{2} D_{ij} + \frac{1}{2} \Omega_k \varepsilon_{ijk}.$$

The symmetrical part D_{ij} determines the deformation of the fluid while the antisymmetrical part $\Omega_k \varepsilon_{ijk}$ determines the pure rotation of the fluid. Substituting for D_{ij} in equation (2.12) yields

$$\sigma_{ij} = - P'\delta_{ij} + \mu(\frac{\partial U_i'}{\partial x_j} + \frac{\partial U_j'}{\partial x_i}). \tag{2.13}$$

Thus the work done by the stresses σ_{ij} may be written as

$$W = \frac{1}{\rho} [\sigma_{ij} \frac{\partial U_j'}{\partial x_i} + U_j' \frac{\partial \sigma_{ij}}{\partial x_i}]$$

$$= \frac{1}{\rho} [- P'\delta_{ij} \frac{\partial U_j'}{\partial x_i} + \mu(\frac{\partial U_i'}{\partial x_j} + \frac{\partial U_j'}{\partial x_i}) \frac{\partial U_j'}{\partial x_i} + \frac{\rho}{2} \frac{d}{dt} U_j' U_j']$$

$$= \frac{1}{2} \frac{d}{dt} U_j' U_j' + \nu \left(\frac{\partial U_j'}{\partial x_i} + \frac{\partial U_i'}{\partial x_j}\right) \frac{\partial U_j'}{\partial x_i}. \qquad (2.14)$$

Since

$$\delta_{ij} \frac{\partial U_j'}{\partial x_i} = \frac{\partial U_i'}{\partial x_i} = 0.$$

Also, introducing the expression for the stress tensor, equation (2.13), into equation (2.8) yields

$$W = \frac{1}{\rho} \frac{\partial}{\partial x_i} \sigma_{ij} U_j'$$

$$= \frac{1}{\rho} \frac{\partial}{\partial x_i} \{U_j' [- P' \delta_{ij} + \mu \left(\frac{\partial U_i'}{\partial x_j} + \frac{\partial U_j'}{\partial x_i}\right)]\}$$

$$= \frac{\partial}{\partial x_i} [- \frac{P'}{\rho} U_i' + \nu U_j \left(\frac{\partial U_i'}{\partial x_j} + \frac{\partial U_j'}{\partial x_i}\right)]$$

$$= - \frac{\partial}{\partial x_i} \frac{P'}{\rho} U_i' + \nu \frac{\partial}{\partial x_i} U_j' \left(\frac{\partial U_i'}{\partial x_j} + \frac{\partial U_j'}{\partial x_i}\right). \qquad (2.15)$$

Equating equations (2.14) and (2.15) give the balance of the mean plus turbulent kinetic energy as

$$\frac{1}{2} \frac{\partial}{\partial t} (U_j' U_j') = - \frac{\partial}{\partial x_i} U_i' \left(\frac{P'}{\rho} + \frac{U_j' U_j'}{2}\right)$$

(1) *(2)*

$$+ \nu \frac{\partial}{\partial x_i} U_j' \left(\frac{\partial U_i'}{\partial x_j} + \frac{\partial U_j'}{\partial x_i}\right)$$

(3)

$$- \nu \left(\frac{\partial U_i'}{\partial x_j} + \frac{\partial U_j'}{\partial x_i}\right) \frac{\partial U_j'}{\partial x_i}, \qquad (2.16)$$

(4)

where

$$\frac{1}{2}\frac{d}{dt}U_j'U_j' = \frac{1}{2}\frac{\partial}{\partial t}U_j'U_j' + \frac{1}{2}U_k'\frac{\partial}{\partial x_k}U_j'U_j'$$

$$= \frac{1}{2}\frac{\partial}{\partial t}U_j'U_j' + \frac{1}{2}\frac{\partial}{\partial x_k}U_k'U_j'U_j' \quad .$$

Term *(1)* in equation (2.16) represents the local change of the kinetic energy of the fluid per unit mass.

Term *(2)* may be interpreted as the rate of convection per unit mass of the total dynamic pressure by the velocity U_i'.

Term *(3)* represents the rate of convection by the velocity U_j' of the total viscous stresses per unit mass.

Term *(4)* is the energy dissipation per unit mass.

To identify the contribution of the turbulence motion, the velocity and pressure quantities may be written in terms of their mean and fluctuating parts as

$$U_i' = U_i + u_i,$$

$$P' = P + p \quad ,$$

and

$$U_i'U_i' = U_iU_i + 2U_iu_i + u_iu_i.$$

Substituting these expressions into equation (2.16) and averaging with respect to time yield

$$\frac{1}{2}\frac{\partial}{\partial t}U_jU_j + \frac{1}{2}\frac{\partial}{\partial t}\overline{u_ju_j} = -\frac{\partial}{\partial x_i}U_i\left(\frac{P}{\rho} + \frac{U_jU_j}{2}\right)$$

$$+ \nu\frac{\partial}{\partial x_i}U_j\left(\frac{\partial U_i}{\partial x_j} + \frac{\partial U_j}{\partial x_i}\right)$$

$$- \nu\left(\frac{\partial U_i}{\partial x_j} + \frac{\partial U_j}{\partial x_i}\right)\frac{\partial U_j}{\partial x_i}$$

$$- \frac{\partial}{\partial x_i}\overline{u_i\left(\frac{P}{\rho} + \frac{u_ju_j}{2}\right)}$$

$$- \frac{\partial}{\partial x_i}\overline{U_ju_iu_j} - \frac{1}{2}\frac{\partial}{\partial x_i}\overline{U_iu_ju_j}$$

$$+ \nu\frac{\partial}{\partial x_i}\overline{u_j\left(\frac{\partial u_i}{\partial x_j} + \frac{\partial u_j}{\partial x_i}\right)}$$

$$- \nu\overline{\left(\frac{\partial u_i}{\partial x_j} + \frac{\partial u_j}{\partial x_i}\right)\frac{\partial u_j}{\partial x_i}}\ . \qquad (2.17)$$

The turbulent energy equation is then obtained by subtracting equation (2.7) from equation (2.17) to give

$$\frac{1}{2}\frac{\partial}{\partial t}\overline{u_ju_j} + \frac{1}{2}\frac{\partial}{\partial x_i}\overline{U_iu_ju_j} = -\frac{\partial}{\partial x_i}\overline{u_i\left(\frac{P}{\rho} + \frac{u_ju_j}{2}\right)}$$

$$- \frac{\partial}{\partial x_i}\overline{U_ju_iu_i} + U_j\frac{\partial}{\partial x_i}\overline{u_iu_j}$$

$$+ \nu\frac{\partial}{\partial x_i}\overline{u_j\left(\frac{\partial u_i}{\partial x_j} + \frac{\partial u_j}{\partial x_i}\right)}$$

$$- \nu\overline{\left(\frac{\partial u_i}{\partial x_j} + \frac{\partial u_j}{\partial x_i}\right)\frac{\partial u_j}{\partial x_i}}\ ,$$

or rearranged in the form

$$\frac{\partial}{\partial t}\left(\frac{\overline{u_j^2}}{2}\right) + U_i \frac{\partial}{\partial x_i}\left(\frac{\overline{u_j^2}}{2}\right) + \frac{\partial}{\partial x_i}\left[\overline{u_i\left(\frac{P}{\rho} + \frac{u_j^2}{2}\right)}\right]$$

$$+ u_i u_j \frac{\partial U_j}{\partial x_i} - \nu \frac{\partial}{\partial x_i}\left[\overline{u_j\left(\frac{\partial u_i}{\partial x_j} + \frac{\partial u_j}{\partial x_i}\right)}\right]$$

$$+ \nu\overline{\left(\frac{\partial u_i}{\partial x_j} + \frac{\partial u_j}{\partial x_i}\right)\frac{\partial u_j}{\partial x_i}} = 0 \ . \qquad (2.18)$$

The terms arising from this equation have usually been considered as the key to the understanding of the turbulence problem, namely the production, diffusion and dissipation of turbulence; these terms will be considered in relation to the diffuser flow.

For axisymmetric mean flow, equation (2.18) for the turbulent kinetic energy balance of the mean flow may be non-dimensionalised and written in the form (Appendix A)

$$(I) + (II) + (III) + (IV) + (V) = 0, \qquad (2.19)$$

where the terms have the following meanings.

Mean flow equation:

$$(I) = \frac{1}{2}\left[\left(\frac{U_1}{U_{1,m}}\right)\frac{\partial}{\partial \xi_1}\left(\frac{\overline{q^2}}{U_{1,m}^2}\right) + \left(\frac{U_2}{U_{1,m}}\right)\frac{\partial}{\partial \xi_2}\left(\frac{\overline{q^2}}{U_{1,m}^2}\right)\right.$$

Convective diffusion by kinetic and pressure effects:

$$(II) = \frac{1}{2\xi_2} \left\{ \frac{\partial}{\partial \xi_1} \left[\xi_2 \overline{\left(\frac{u_1}{U_{1,m}}\right) \left(\frac{q^2}{U_{1,m}^2} + \frac{2p}{\rho U_{1,m}^2}\right)} \right] + \frac{\partial}{\partial \xi_2} \left[\xi_2 \overline{\left(\frac{u_2}{U_{1,m}}\right) \left(\frac{q^2}{U_{1,m}^2} + \frac{2p}{\rho U_{1,m}^2}\right)} \right] \right\} ,$$

Production:

$$(III) = \left[\left(\frac{\overline{u_1 u_2}}{U_{1,m}^2}\right) \frac{\partial}{\partial \xi_2} \left(\frac{U_1}{U_{1,m}}\right) + \left(\frac{\overline{u_1^2}}{U_{1,m}^2} - \frac{\overline{u_2^2}}{U_{1,m}^2}\right) \frac{\partial}{\partial \xi_1} \left(\frac{U_1}{U_{1,m}}\right) + \frac{\overline{u_1 u_2}}{U_{1,m}^2} \frac{\partial}{\partial \xi_1} \left(\frac{U_2}{U_{1,m}}\right) + \frac{1}{\xi_2} \left(\frac{U_2}{U_{1,m}}\right) \left(\frac{\overline{u_3^2}}{U_{1,m}^2} - \frac{\overline{u_2^2}}{U_{1,m}^2}\right) \right] .$$

Viscous work:

$$(IV) = - \left(\frac{1}{2Re,m} \left\{ \frac{1}{\xi_2} \frac{\partial}{\partial \xi_2} \left[\xi_2 \frac{\partial}{\partial \xi_2} \left(\frac{\overline{q^2}}{U_{1,m}^2}\right) \right] + \frac{\partial^2}{\partial \xi_1^2} \left(\frac{\overline{q^2}}{U_{1,m}^2}\right) \right\} + \frac{\nu R}{U_{1,m}^3} \overline{\frac{\partial u_i}{\partial x_j} \frac{\partial u_j}{\partial x_i}} \right) .$$

Dissipation:

$$(V) = \frac{R\varepsilon}{U_{1,m}^3} .$$

Where

$$q^2 = u_i u_i ,$$

$$\xi_1 = x_1/R , \quad \xi_2 = r/R , \quad Re,m = RU_{1,m}/\nu ,$$

$$\varepsilon = \nu\overline{\left(\frac{\partial u_i}{\partial x_j} + \frac{\partial u_j}{\partial x_i}\right)\frac{\partial u_i}{\partial x_j}}$$

and the normalising quantities R and $U_{1,m}$ at station 7 are taken as constants.

Each of the terms of equation (2.19) represents a rate of change of turbulent energy per unit mass, where a positive sign indicates energy entering the fluid element.

Term I represents the convection of energy by the mean velocity; it reduces to zero for fully developed pipe flow, but is non-zero for flows which are developing in the axial direction (ξ_1) as in a diffuser.

Term II represents the convective diffusion of energy due to kinetic and pressure effects.

Term III is the energy transferred from the mean motion through the turbulence shear stresses and is known as the production term.

Term IV denotes the work done by the viscous shear stresses of the turbulent motion.

Term V represents the dissipation of turbulence by turbulent motion.

2.3 Wall friction velocities

The characteristic velocity parameter U_* is important in the correlation of both mean and fluctuating velocity components near a smooth wall. The methods for accurately calculating U_* in pipe flow and constant

pressure boundary layers are well established unlike the case in adverse pressure gradients. In consequence, values of U_* obtained by various methods have been considered.

(i) The 'law of the wall': A method considered for evaluating the friction velocity assumes the validity of 'the law of the wall'; the law is an hypothesis which states that there exists a region near a smooth wall where the mean velocity data in turbulent flow fall on one universal curve independent of the governing boundary conditions; that is, it is valid for pipes, channels and boundary layers with or without pressure gradients. In general, results from many experimental data (Cole and Hirst 1969) indicate that the law provides a plausible method for estimating the wall friction velocity.

The procedure requires looking for a parameter U_* which fits the formula

$$\frac{U_1}{U_*} = A \log_{10} \frac{yU_*}{\nu} + B \ , \qquad (2.20)$$

in the range

$$100 \leq \frac{yU_*}{\nu} \leq 300 \ .$$

Typical values for the constants A and B are as follows:

A = 5.60 , B = 4.90 (Clauser 1954);

A = 5.50 , B = 5.45 (Patel 1965);

A = 5.75 , B = 5.50 (Nikuradse, referenced in Schlichting 1968).

The fitting procedure to be carried out will be that, at each station, a U_* will be found (for each of the A and B values listed above) such that the residual of

$$f(U_*) = \frac{U_1}{U_*} - A \log_{10} \frac{yU_*}{\nu} - B$$

is less than 0.01 and the arithmetic mean of U_* determined in the range of $100 \leq yU_*/\nu \leq 300$.

(ii) Ludweig and Tillman equation: A second method for evaluating the friction velocity will make use of the formula

$$U_* = U_{1,m} \, (c_f/2)^{1/2} \, , \tag{2.21}$$

where c_f will be determined from the Ludweig and Tillman (1950) equation

$$c_f = 0.246 \times 10^{-0.678H} \times R_\theta^{-0.268} \, ,$$

with

$$H = \delta^*/\theta \, ,$$

$$\theta = \int_o^R \left(1 - \frac{U_1}{U_{1,m}}\right) \left(\frac{U_1}{U_{1,m}}\right) (1 - \tfrac{y}{R}) \, dy,$$

$$\delta^* = \int_o^R \left(1 - \frac{U_1}{U_{1,m}}\right) (1 - \tfrac{y}{R}) \, dy \, ,$$

and

$$R_\theta = U_{1,m}\theta/\nu \, .$$

(iii) Total shear stress extrapolation to the wall: The friction velocity will also be evaluated by finding the intercept of the shear stress

$$\frac{\tau}{\rho} = \nu\frac{\partial U_1}{\partial y} - \overline{u_1 u_2} \quad , \tag{2.22}$$

at the wall.

3. EXPERIMENTAL EQUIPMENT AND PROCEDURES

3.1 Wind tunnel and diffuser

The low speed open circuit wind tunnel used in the experiment has been described by Azad and Hummel (1971). The fan was driven by a 25 h.p. DC motor; the settling chamber, 92 cm in diameter and 366 cm long, was provided with two sets of fine mesh screens; the contraction cone with an area ratio of 89:1 was fabricated from mahogany plywood; seventy-eight diameters of straight pipe separated the contraction cone from the start of the diffuser.

The diffuser (Figure 1) was machined from cast aluminum. The inner surface was finished with a smooth curve from the inlet to a distance of 3 cm along the wall. Static pressure holes, 0.6 mm in diameter and spaced 90° apart were inserted at each station; these were connected to a static pressure ring. A machined reinforcement ring which could be rotated to any angular position was adapted to the outlet end to support the traversing mechanism (Figure 2(a)) with a micrometer head graduated in 0.001 inches. The probes were mounted on a tube entering the diffuser from the downstream end. (The size of the tube, 2.5 cm in diameter, was determined by the hot wire probe lead connectors; a long taper (Figure 2(b)) was fitted

between the end of the tube and the probe support to minimise any flow blockage effect upstream of the probe.) The hot wire holder could be rotated about its axis to align the X-probe sensors with the x_1x_2 or x_1x_3 planes; the line of traverse was normal to the diffuser axis.

3.2 Measuring equipment

Mean static and total pressures across the diffuser at each station were measured by means of round tubes with external and internal diameters of 1 mm and 0.76 mm, respectively. The flow near the wall was examined for evidence of separation using flattened-tip forward- and reverse-facing pitot-tubes with external and internal tip heights of 0.45 mm and 0.15 mm, respectively. The width of the tubes at the tip was 2.5 mm. The probe readings were recorded on a Betz* projection manometer (discrimination 0.1 mm of water) for large pressure differences and a Hero† precision micromanometer (discrimination, 0.01 mm of alcohol) for small pressure differences.

Velocity fluctuations were measured with standard Disa hot wire equipment (constant temperature anemometers 55D01; linearizers 55D10; DC voltmeter 55D30; random signal indicators and correlators 55A06; and X-probe 55A38). A block diagram of the turbulence measuring equipment is shown in Figure 3. The X-probe sensors were platinum-plated

---

*Betz Manometer AVA

†Hero Präzisions-Mikromanometer

tungsten probe wires, 0.005 mm in diameter, 1.2 mm long, spaced 1 mm apart and operated at an overheat ratio of 0.8. Calibrations of the hot wires were performed at the centre of the reference station (by fitting the probe stem to the pipe traversing mechanism) before and after each run. The linearizer exponent setting of 2.3 was found to yield a linear calibration curve in the velocity range of $15 \leq (U_{1,m})_{ref} \leq 60$ m/sec. The X-probe sensors showed nearly equal sensitivity; the small differences were reduced by adjusting the linearizer gains.

The frequency spectra were measured with a Hewlett-Packard model 3590A wave analyzer. The signals from the X-probes were recorded on a seven channel Lyric TR 61-2 F.M. magnetic tape recording system which could operate at tape speeds of 0.6, 6.0 and 60.0 in/sec with corresponding upper frequency limits of 200, 2,000, and 20,000 Hz, respectively. The recording and playback speed of 60.0 in/sec was used. The signal-to-noise ratio for the combined hot wire, anemometer, tape recorder and wave analyzer system was maintained in excess of 40 db. Other instrumentation included a dual beam oscilloscope for monitoring the signals from the hot wires and a pressure manometer Disa type 55D41 for monitoring the pressure drop across the contraction cone.

3.3 Measurements

The mean flow parameters at the reference station

are given in Table 1. Wall static pressure was recorded at positions upstream of the reference station and along the diffuser wall. Pressure measurements were also taken at 1 mm from the wall at stations 1 to 12 with (i) the flattened-tip forward-facing pitot-tube (ii) the flattened-tip reverse-facing pitot-tube and (iii) the static pressure tube. Measurements recorded in the radial traversers at stations 1 to 10 were the total and static pressures, the r.m.s. turbulence intensities and the correlation coefficients. To obtain the correlation coefficient, two random signal correlators were used as outlined in the Disa manual* The frequency spectra were measured at station 7.

3.4 Corrections

Considerable care was taken to minimize possible measurement errors in data acquisition; measurements were repeated whenever it appeared necessary. The hot wire and pitot-tube were traversed to 1 mm distance from the wall where the accuracy for the probe positioning was estimated at about ± 0.05 mm. Correction for wall effect was thus assumed to be negligible and was not applied. The X-probe effective cooling velocity and the corrections for non-linearities caused by high intensity turbulence were assumed and applied in the form proposed by Champagne et al

---

*Instruction Manual 55A06, Disa Elektronik A/S, Herlev, Denmark.

(1967) for the linearized constant temperature operation (Appendix B). The corrected mean velocity data obtained from pitot and static tube measurements using the method suggested by Kaye (1968), and outlined in Appendix B, showed good agreement with those of hot wire measurements; close to the wall, the deviation was about 5%.

The magnetic tape recorder input-output values of the r.m.s. velocity fluctuations were compared at five radial positions in station 7; the ratio varied from 1.0 to 0.97.

4. RESULTS AND DISCUSSION

4.1 Flow specification

Mean velocity traverses taken along two perpendicular diameters at the reference station showed that the mean velocity profile was symmetric to within ± 0.4%; at station 10, the symmetry was within ± 1%.

At the reference station, the ratio of the cross section average to maximum velocity $(\langle U_1 \rangle / U_{1,m})_{ref}$, which is an indication of the degree of development of the flow, was 0.82 and 0.83 for the two flows of Re 152,000 and 293,000. Nikuradse (referenced in Schlichting 1968) obtained values of $\langle U_1 \rangle / U_{1,m}$ in the range 0.81 - 0.83 for $23{,}000 \leq Re \leq 1100{,}000$ and $L/D_{ref} = 120$; Lawn (1971) reported values of $\langle U_1 \rangle / U_{1,m}$ in the range 0.806 - 0.833 for $35{,}000 < Re < 250{,}000$ and $L/D_{ref} = 59$. The present values of $(\langle U_1 \rangle / U_{1,m})_{ref}$ therefore suggest that the flow is fully developed. A more rigorous criterion for establishing fully developed pipe flow is that the rate of change of all mean quantities (excluding pressure) with respect to the axial flow direction is zero. Experimental evidence (e.g. Laufer 1954) has shown that a value for L/D_{ref} of 50 is adequate. Here a value for L/D_{ref} of 78 is used; therefore the flow can be claimed to be fully

developed turbulent pipe flow.

The universal velocity profile (Figure 4), the distribution of the turbulence intensities and correlation coefficient (Figure 5) at the reference station are shown in relation to Laufer's (1954) and Lawn's (1971) data to indicate the condition of the flow entering the diffuser. Here, the wall shear stress was evaluated from the wall pressure gradient upstream of the reference station.

4.2 Mean pressure

The mean pressure distributions along the diffuser wall as well as at 1 mm from the wall is presented in Figure 6. Sandborn and Liu (1968) investigated turbulent boundary layer separation employing a dual pressure probe with one tip pointing upstream and the other downstream; they traversed the pressure probe along the curved surface of their diverging duct until the point of the minimum differential pressure was located. A similar approach by way of comparing the readings of the forward- and reverse-facing pitot tube was employed in the experiment. The readings of the wall pressure, the static pressure and the reverse-facing pitot tube pressure were practically the same; the forward-facing pitot tube indicated correspondingly higher readings all along the diffuser wall up to the exit, thus showing that there was forward flow very close to the wall and that separation had not been reached.

Previous studies have shown that in the diffuser, the pressure recovery coefficient decreases with the increase of the boundary layer thickness at entry; this coefficient thus approaches a lower limiting value when the flow at the inlet is fully developed as in the present case. Figure 7 shows the pressure recovery line on the triangular plot discussed by Sovran and Klomp (1967); the ratio $\overline{C}_p/\overline{C}_{p,i}$ was found to be 0.78.

The radial distribution of the measured mean static pressure is plotted in Figures 8(a) to (d) as a pressure coefficient $(P_S - P_W)/\frac{1}{2}\rho\langle U_1\rangle^2_{ref}$. The variation of the pressure coefficient in the region $0.02 < y/R \leq 1.0$ is less than 0.01 at stations 1 to 5 but approaches a value of 0.02 at stations 6 to 10.

For turbulent flow fields in which it is possible to distinguish one main flow direction, both theoretical and experimental investigations can be greatly simplified if a relationship describing the flow field in the transverse direction can be found. For fully developed pipe flow, the relationship takes the form of

$$P_S + \rho\overline{u_2^2} + \rho\int_o^y \frac{\overline{u_3^2} - \overline{u_2^2}}{R - y'}\,dy' = P_W \,. \qquad (4.1)$$

From boundary layer type order-of-magnitude analysis of the Reynolds equation in the radial direction, equation (4.1) turns out to be a 'second-order' approximation for moderately

diverging flow. (The order of magnitude analysis has been developed in detail in Hinze 1959.) By rearranging equation (4.1) to give

$$\frac{P_S - P_W}{\frac{1}{2}\rho\langle U_1\rangle^2_{ref}} = -\frac{\rho\overline{u_2^2} + \rho\int_o^y \frac{\overline{u_3^2} - \overline{u_2^2}}{R - y'}\,dy'}{\frac{1}{2}\rho\langle U_1\rangle^2_{ref}}, \qquad (4.2)$$

it is seen that the term on the L.H.S. of equation (4.2) is the static pressure expressed in the same form as the measured pressures. When $\rho\overline{u_2^2}$ and $\rho\overline{u_3^2}$ increase, $(P_S - P_W)$ tends to decrease; thus the profile of $(P_S - P_W)$ may be expected to show a maximum variation toward the diffuser exit with a trend similar to those of $\rho\overline{u_2^2}$ and $\rho\overline{u_3^2}$. A noteworthy feature of the radial pressure distribution in the nondimensionalised form is that the profiles show a good agreement for the two Reynolds numbers of 293,000 and 152,000.

A comparison of the profiles of both sides of equation (4.2) is shown in Figures 8(a) and (b). Except for the trend in the profiles, there is hardly any agreement. This lack of agreement may be due to the effect of the curvature of the mean streamlines in the diverging flow; another possibility may be that equation (4.1) does not adequately apply as it represents an approximation for diffuser flow; the lack of agreement may also be due to the fact that the comparison is between relatively small quantities which are not totally free of experimental

errors. It appears from the foregoing discussion that the use of equation (4.1) for the diffuser flow investigated, as well as correction required in measured values of static pressure will require further justification.

4.3 Mean velocity

The corrected mean axial velocities obtained from hot wire measurements are plotted in Figure 9. The decrease in slope and magnitude of the profiles especially near the wall is due to the retardation of the fluid layers relative to each other caused by the rising pressure in the downstream direction. Physically, the change in the diffuser cross-section in the axial direction produces a reduction in U_1 as demanded by flow continuity and a simultaneous rise in pressure; because the radial variation of the static pressure is comparatively small, the amount by which the axial velocity is reduced would tend to be of the same order of magnitude across the diffuser but is modified by the shear forces. The velocity profiles therefore show the biggest change of shape in regions of low velocity (near the wall). It is from stations 6 to 10 that the velocity profiles start exhibiting points of inflexion usually observed in boundary layers in adverse pressure gradients. The data are plotted in universal co-ordinates in Figure 10(a). The wall shear stress was determined by extrapolating to the wall as shown in Figure 10(b) the total mean shear stress calculated from the sum of the viscous

shear and the directly measured Reynolds stress using equation (2.22). Table 2 compares the values of the friction velocity U_* obtained from different methods.

The noteworthy feature of Figure 10(a) is the absence of the logarithmic region of the 'law of the wall'; a semi-logarithmic variation occurs near the axis in a region which, for fully developed pipe flow, would be associated with the velocity defect law. The velocity profiles in the U^+ and Y^+ scales using the other friction velocities listed in Table 2 do not indicate any noticeable logarithmic portion of the law of the wall.

The mean radial velocity distribution shown in Figure 11 was evaluated from the continuity relation

$$\frac{U_2}{\langle U_1 \rangle_{ref}} = -\frac{1}{r}\int_o^r \frac{\partial}{\partial x_1}\left(\frac{x_2 U_1}{\langle U_1 \rangle_{ref}}\right) dx_2 \ . \qquad (4.3)$$

By comparing the values of $U_2/\langle U_1 \rangle_{ref}$ with the corresponding values of $U_1/\langle U_1 \rangle_{ref}$ in Figure 9, it is seen that for $y/R_{ref} > 0.02$ the ratio U_2/U_1 is generally less than 6%.

4.4 Turbulence intensities

The distributions of the three components of the r.m.s. relative turbulence intensities are shown in Figure 12. The $\tilde{u}_1$ profiles are those obtained from the average values of the X-probe readings in the $x_1\ x_2$ and $x_1\ x_3$ planes. At each station, the $\tilde{u}_1$ component has the highest

value with $\tilde{u}_1/U_1 > \tilde{u}_3/U_1 > \tilde{u}_2/U_1$ and the degree of anisotropy decreasing from the wall to the diffuser axis. The $\tilde{u}_2$ component shows a peak away from the wall; this is a result of the more restrictive influence of the wall on the $\tilde{u}_2$ component than on either the $\tilde{u}_1$ or $\tilde{u}_3$ components. For a given relative position y/R, the relative turbulence intensities increases in the downstream direction. The tendency may be explained by noting that U_1 decreases as the fluid moves through the diffuser. Thus, in a flow with rising pressure as in the diffuser, the tendency is towards an increase in turbulence. The trend in the distribution of the intensity levels in the radial direction are qualitatively similar to those of measurements by Klebanoff (1954) for boundary layer flow, Laufer (1954) for fully developed pipe flow, Ruetenik and Corrsin (1955) for slightly divergent channel flow, Robertson and Calehuff (1957) and Trupp et al (1971) for diffuser flow.

The components of the turbulence intensity non-dimensionalised with the friction velocity (obtained by total shear stress extrapolation) are plotted in Figure 13. The peak which is developed very close to the wall near the diffuser inlet moves progressively away from the wall in the downstream direction; the trend is in qualitative agreement with the observations of Sandborn and Slogan (1955) in two dimensional adverse pressure gradients.

4.5 Correlation coefficients

The correlation coefficient $\overline{u_1 u_2}/\tilde{u}_1\tilde{u}_2$ (Figure 14) varies appreciably in the radial direction. The noteworthy features of the data are the progressive contraction of the region of constant coefficient which at the reference station (Figure 5) is in the region $0.05 \leq y/R \leq 0.5$ and the development of peaks with a trend similar to those noted for the turbulence intensities $\tilde{u}_1/U_*$, $\tilde{u}_2/U_*$ and $\tilde{u}_3/U_*$. Close to the wall, the correlation coefficient exhibits an approximate linear variation with the distance from the wall and the linear range grows with downstream distance.

The distribution of the correlation coefficient $\overline{u_1 u_3}/\tilde{u}_1\tilde{u}_3$ is shown in Figure 15. The vertical lines indicate the range of the distribution of the coefficient for a given relative position y/R from stations 1 to 10; the values of the coefficient vary from 0.0 to 0.05 and are small in relation to those of $\overline{u_1 u_2}/\tilde{u}_1\tilde{u}_2$.

4.6 Wall turbulent layer

In fully developed pipe flow, the edge of the viscous sublayer approximately corresponds to the point of the maximum u_1-fluctuation. This region $Y^+ \tilde{<} 12$ is usually of interest because the bulk of the direct viscous dissipation takes place within it; at the edge, the energy production reaches a maximum value with production equal to dissipation; within the layer, $\tilde{u}_1/U_*$ is linear with the

distance from the wall as shown by the work of Laufer (1954), Bakewell and Lumley (1967).

It is perhaps of interest to examine for the diffuser the flow characteristics in the layer between the wall and the point of maximum u_1-fluctuation. As in pipe flow, the energy production (Figure 16) attains a maximum value approximately at the edge of the layer and the bulk of the direct viscous dissipation takes place within it. When the mean square of the streamwise velocity fluctuation $\overline{u_1^2}$ is plotted in universal coordinates (Figure 17) there is a linear variation in this layer; the surfaces of maximum $\overline{u_1^2}$ and $\overline{u_1 u_2}$ closely coincide as shown in Figure 18; at the edge of the layer, the energy production rate is not in local equilibrium with the direct viscous dissipation rate as in the boundary layer and pipe flow, rather, production is about two orders of magnitude greater than direct viscous dissipation (Figure 16); and about 60% of the total energy production (Figure 19) takes places within the layer as compared to about 40% for boundary layers and pipes.

4.7 Turbulent flow features with partly developed flow at entry

Complementary to the investigation reported here, turbulent flow properties were examined, using the same wind tunnel and diffuser, for four flow conditions at entry (Okwuobi and Azad 1972b) defined in terms of the entry pipe

conditions by

L/D = 2.5 , Re = 300,000 ;

L/D = 2.5 , Re = 150,000 ;

L/D = 19 , Re = 300,000 ;

L/D = 19 , Re = 150,000 .

Measurements included profiles of mean velocity, turbulence intensities and correlation coefficients. In general, the data showed trends similar to the observation in the diffuser for fully developed pipe flow entry conditions. The turbulent flow characteristics exhibited in the wall turbulent layer were also similar irrespective of the inlet flow conditions: namely, $\overline{u_1^2}$ varied linearly with the distance from the wall (Figures 20(a) and Ib)); the energy production rate approximately reached a maximum value at the edge of the layer; and the surfaces of maximum $\overline{u_1^2}$ and $\overline{u_1 u_2}$ closely coincided. For a fixed L/D_{ref} ratio, the relative turbulence intensity profiles showed a slight dependence on Reynolds number.

4.8 Structure parameters

A feature of interest with regard to the turbulent stress tensor is the direction along which the maximum stress acts. The orientation of one of the principal axes of the turbulent stress tensor is shown in Figure 22 where β_1 is evaluated from the expression

$$\beta_1 = \tan^{-1}\left[\frac{2\overline{u_1 u_2}}{\overline{u_1^2} - \overline{u_2^2}} \right], \qquad (4.4)$$

and is positive away from diffuser axis.

The variation of β_1 in the radial direction is between 13° and 20° over the large region $0.15 < y/R < 0.9$ for the two Reynolds numbers: elsewhere, the variation is considerable. In particular, β_1 decreases as the diffuser wall is approached and its direction is aligned closely parallel to the wall.

The structure parameters,

$$K_1 = \frac{\overline{u_3^2} - \overline{u_2^2}}{\overline{u_3^2} + \overline{u_2^2}} ,$$

and

$$K_2 = \frac{3\overline{u_1^2}}{\overline{q^2}} - 1 , \qquad (4.5)$$

which give an indication of the relative values of the components of the turbulence intensities, were investigated to see whether they would reveal any interesting features in the diffuser flow field. These parameters have been employed e.g. by Townsend (1956), Tucker and Reynolds (1968) to predict the equilibrium structure of the turbulence subjected to a homogeneous uniform plain straining in suitably shaped distorting ducts. The

assumption embodied in these experiments were first that the mean flow was irrotational and second that $\tilde{u}_1/U_1 << 1$, so that the major contribution to the distortion came from changes in the mean flow. Viscous effects were neglected as the distortion was assumed to take place in a short time. For the diffuser flow investigated, none of the above simplifying conditions is satisfied. The strain field is inhomogeneous and the turbulent fluid is subjected to plain straining, rotation and the effect of adverse pressure gradient. Figures 23 and 24 illustrate how K_1 and K_2 are distributed in the diffuser. At the various stations, the distributions of K_1 (Figure 23) are similar and have a low value except near the wall. As the wall is approached, the value of K_1 increases due to the high degree of anisotropy of the flow in this region. The variation of K_1 in the radial direction appears to limit the usefulness of the parameter in deciding when the diffuser turbulence has been fully compressed.

The structure parameter K_2 (Figure 24), which for isotropic homogeneous turbulence is zero, varies from about 0.9 near the wall to about 0.35 at the diffuser axis. The distributions emphasize that the energy component of the u_1-fluctuation considerably exceeds the combined energy components of the u_1 and u_2 fluctuations over the large portion $0.01 < y/R < 0.8$.

A study of the structure parameters $(\overline{u_1^2} - \overline{u_2^2})/$

$(\overline{u_1^2} + \overline{u_2^2})$, $\overline{u_1^2}/\overline{q^2}$, $\overline{u_2^2}/\overline{q^2}$ and $\overline{u_2^2}/\overline{u_1^2}$, using the same experimental equipment, is reported in Okwuobi, Azad and Hawaleshka (1972a); the study indicates that along the diffuser axis the parameters remain practically constant and independent of both pipe entry Reynolds numbers (within the range tested) and changes in the turbulent kinetic energy along the axis.

4.9 One-dimensional spectra

Spectral analysis provides an important description of the structure of turbulence; it gives an idea of the way in which eddies of different sizes exchange energy with one another. The low wave-number part of the energy spectrum consists of energy containing eddies whose structure is determined by the mean flow. The structure of eddies at the high wave-number range of the spectrum is determined by viscosity; it is in this region that the turbulent energy is dissipated into heat. The eddies which lie between the two ends of the spectrum are not directly affected by viscosity; this range is called the inertial subrange. In this investigation, the spectral analysis has been employed as a method for estimating the energy dissipation.

The normalised spectral density ϕ_{ij} is defined by

$$\phi_{ij}(\kappa_1 R) = \frac{F_{ij}(\kappa_1)}{R\overline{u_i u_j}}, \qquad (4.6)$$

where F_{ij} is the unnormalised spectrum of $\overline{u_i u_j}$, such that

$$\int_0^\infty \frac{F_{ij}(\kappa_1)}{R}\, d(\kappa_1 R) = \overline{u_i u_j}$$

The profiles of ϕ_{11} and ϕ_{22} measured at station 7 are plotted in Figures 25 and 26, respectively. The spectra ϕ_{11} (Figure 25) at varying distance from the wall for $y/R > 0.02$ exhibit the $\kappa_1^{-5/3}$ dependence in the portion $9 < \kappa_1 R < 95$; the contribution to the turbulent energy in the low wave-number range increases with distance from the wall and reaches a maximum value at about mid-radius. The difference between the profiles of the ϕ_{11} and ϕ_{22} spectra, Figures 25 and 26, respectively is that, in the low wave-number range, the energy contents of the ϕ_{11} spectra are relatively greater than those of the ϕ_{22} spectra as can be explained by the trend that $\overline{u_1^2} > \overline{u_2^2}$; also, the range of the -5/3 power law for the ϕ_{22} spectra is less than that of the ϕ_{11} spectra.

4.10 Energy balance

The distribution, at station 7, of the terms in the energy equation (2.10) are shown in Figure 27. The mean flow convection (Term I), the production (Term III) and the viscous work

$$\frac{1}{2Re,m}\left\{\frac{1}{\xi_2}\frac{\partial}{\partial \xi_2}\left[\xi_2 \frac{\partial}{\partial \xi_2}\left(\frac{\overline{q^2}}{U_{1,m}^2}\right)\right] + \frac{\partial^2}{\partial \xi_1^2}\left(\frac{\overline{q^2}}{U_{1,m}^2}\right)\right\}$$

were evaluated directly from the data.

The dissipation (Term V) was evaluated using the dissipation rate ε^* calculated from the $\overline{u_1^2}$ energy spectra by the method proposed by Bradshaw (1967) as

$$\varepsilon^* = \left[F_{11}(\kappa_1)\kappa_1^{5/3}/0.53 \right]^{3/2} . \tag{4.7}$$

For comparison a second estimate of the dissipation rate was obtained from the isotropic relationship

$$\varepsilon^*_{iso} = 15\ \nu\tilde{u}_1^2/\lambda^2_{u_1} , \tag{4.8}$$

where λ_{u_1} is the Taylor microscale evaluated from

$$\lambda_{u_1} = \left[\int_o^\infty \kappa_1^2\ \phi_{11}(\kappa_1 R)\ d(\kappa_1 R) \right]^{-1/2} .$$

The dissipation rates from equations (4.7) and (4.8) are given in Table 3. At about mid-radius, the magnitudes are approximately the same; from mid-radius to the diffuser axis, $\varepsilon^* > \varepsilon^*_{iso}$; and from the diffuser wall to mid-radius, $\varepsilon^* < \varepsilon^*_{iso}$. These values thus provide an estimate of the maximum value of the dissipation rate at station 7.

Equation (2.19) has been employed to determine the diffusion (Term II) as the closing entry in the

energy balance. The viscous work is about two orders of magnitude less than the production. The profile of the energy production shows a local minimum value near the wall ($y/R \doteq 0.03$); this trend is a result of the decrease of $\partial U_1/\partial y$ close to the wall due to the effect of adverse pressure gradient as can be observed from Figure 9 (station 7).

From the energy balance shown in Figure 27, the following conclusions may be drawn.

(i) In the region $0.8 < y/R < 1.0$, the dissipation is mostly balanced by the mean flow convection; here, the picture is different from that for fully developed pipe flow (e.g. Laufer 1954) in that, in the latter case, the dissipation is mostly balanced by the kinetic energy diffusion, while the mean flow convection is zero.

(ii) For $0.2 < y/R < 0.8$, the energy production and the convective diffusion due to kinetic and pressure effects are approximately equal in magnitude while the mean flow convection which is comparatively less than the production is approximately equal in magnitude to the dissipation. The increased significance of the convective diffusion of turbulence due to kinetic and pressure effects in the diffuser flow is attributable to the fact that the portion,

$$\frac{1}{2\xi_2}\left\{\frac{\partial}{\partial\xi_1}\left[\xi_2\left(\frac{u_1}{U_{1,m}}\right)\left(\frac{q^2}{U_{1,m}^2}+\frac{2p}{\rho U_{1,m}^2}\right)\right]\right\}$$

of Term II, equation (2.19), is zero in fully developed pipe flow but non-zero for the diffuser flow; the convective diffusion of turbulence may therefore be viewed here as taking place both in the streamwise and transverse directions.

(iii) For $0.01 < y/R < 0.2$, the rate of energy production and convection by mean motion is mostly balanced by the rate of energy convective diffusion due to kinetic and pressure effects.

The picture which emerges from the energy balance is that the magnitude of the convective diffusion of turbulence due to kinetic and pressure effects is increased in relation to that of the dissipation and is comparable to that of the production; the picture is different from those in constant pressure boundary layer and fully developed pipe flow, where the rate of turbulence production is comparable to the rate of turbulence dissipation.

4.11 Turbulence mechanism in diffuser flow

To convey a vivid appreciation of the basic features of diffuser turbulent flow in the present study, the results such as the turbulent intensities, the

correlation coefficients and the turbulent kinetic energy balance have been presented in the form of their spatial distributions. The discussion of these results has examined in turn the various properties of the mean and turbulent flow. This section considers the turbulence mechanism of the flow as conveyed by the data. The words 'turbulence mechanism' have been used in a restricted sense to describe observations and conjectures based on the present study. It is clear that for an indepth understanding of the detailed mechanism of diffuser turbulent flow, knowledge is required of the double and triple velocity correlations, pressure correlations and the turbulent vorticity distributions in the flow field.

Initially, the fully developed pipe flow entering the diffuser is in a state of dynamic balance between pressure force and shear-stress force. When the flow enters the diffuser, the mean velocity U_1 decreases to preserve continuity. Simultaneously, the pressure increases resulting in a change in momentum with maximum effect on the velocity profile near the wall. This changing momentum flux in the wall proximity produces a thickening wall layer and a displacing effect of the position of maximum velocity fluctuations and turbulent shear stress toward the diffuser axis. The retardation of the mean velocity U_1 increases the relative turbulence intensity. The equilibrium between the production and

dissipation of turbulent energy which existed in the flow entering the diffuser is upset by convective acceleration which is now present and further distorts the turbulence intensity profiles.

One interesting observation in the present study is that the convective diffusion of turbulent energy is comparable in magnitude with the energy production. This observation can be viewed from another approach. If the turbulence were spatially homogeneous, one would expect that the terms describing the diffusion of turbulent energy would be zero since there would be no spatial transfer of energy. When the turbulence is inhomogeneous in one direction as in the radial direction in fully developed pipe flow, experimental evidence indicates that there is a net transfer of turbulent energy by diffusion toward the pipe axis; the magnitude of the diffusion is everywhere small except near the pipe axis where it is comparable to that of the dissipation; there is of course no diffusion in the axial direction. In the diffuser, the turbulence is inhomogeneous both in the axial and radial directions as shown in Figures 12 and 13. Thus, not all the energy produced at a cross-section is dissipated there as would be the case in fully developed pipe flow. It turns out that an appreciable proportion of the energy produced is convected and diffused both in the radial and downstream directions. The deduction that may be made on the basis of

the foregoing consideration is that when the diffuser divergence angle α is zero (continuation of the straight pipe), the convective diffusion is negligible; as α increases and the dissipation decreases but production increases.

Turbulence production leads to a loss in mean flow energy. It thus appears plausible to conjecture that as the diffuser divergence angle α increases to the optimum pressure recovery limit for a given area ratio, the total energy production throughout the diffuser flow field approaches the lower limiting value. For, when α is very small, the diffuser is very long and the total energy production is very large. As α increases beyond the optimum angle, separation occurs; eddies are formed leading to a very large total energy production. Thus, within the range of these values of α, there is an α at which the total energy production is a minimum. It is surmised, here, that the optimum pressure recovery occurs at the same α.

It was remarked in section (4.3) that the velocity profiles plotted in the universal coordinates did not indicate any appreciable logarithmic portion of the law of the wall. For a logarithmic portion to exist, the mean velocity gradient has to be inversely proportional to the distance from the wall in a region of constant shear stress. In fully developed pipe flow, the region of constant shear

stress (equilibrium layer) approximately corresponds to the region where a balance exists between the production and the dissipation of turbulent energy. From the turbulent energy balance Figure 27, it is seen that the absence of the equilibrium layer is due to the fact that production is greater than dissipation and the excess energy is carried out of the element by convective diffusion due to kinetic and pressure effects. In fact Figure 10(b) indicates that the shear stress increases linearly from the wall to a maximum value before decreasing to zero at the diffuser axis with no region of constant shear stress. Thus a plausible explanation for the absence of the usual wall logarithmic portion in the semi-logarithmic plot of the velocity profiles is that the flow does not exhibit an equilibrium layer.

The foregoing considerations tend to suggest that there is a need for turbulence measurements of higher order correlations in diffuser flow in order to further the understanding of the turbulence mechanism associated with the flow.

5. CONCLUDING REMARKS

An experimental study of mean and turbulent flow properties in a conical diffuser with fully developed flow at entry has been described. Quantitative data presented have included, for entry Reynolds numbers of 152,000 and 293,000, measurements of the mean pressure, mean velocity, turbulence intensities, correlation coefficients and the one-dimensional energy spectra.

The general feature of the radial distribution of the turbulent fluctuations and the correlation coefficients is the occurrence of a peak very close to the wall near the diffuser inlet; the peak progressively shifts away from the wall with the distance in the streamwise direction. The distribution of the turbulence intensity levels is qualitatively similar, but quantitatively much in excess of those in pipe flow.

The results show that the rate of turbulent energy production approximately reaches a maximum value at the edge of the wall layer defined by the point of maximum u_1-fluctuation. It is found that within the layer, $\overline{u_1^2}$ varies linearly with the distance from the wall and the linear range grows with distance in the downstream direction. The surfaces of maximum $\overline{u_1^2}$ and $\overline{u_1 u_2}$ closely

coincide. At the edge of the layer, the energy production is about two orders of magnitude greater than the direct viscous dissipation and about 60% of the total energy production takes place in the layer.

The spectral profiles and characteristics are very similar to those reported for pipe flows; the normalised spectra of $\overline{u_1^2}$ exhibit the $\kappa_1^{-5/3}$ dependence for about one decade of the one-dimensional wave-number κ_1.

From the turbulent kinetic energy balance it is found that the magnitude of the energy convective diffusion due to kinetic and pressure effects is comparable to that of the energy production.

6. RECOMMENDATIONS

As pointed out in the 'Introduction' (section 1), the primary objective of the present investigation was to obtain quantitative information on the distribution of some mean a turbulence quantities in a conical diffuser with optimum pressure recovery characteristics. To gain further insight into the structure of turbulence in diffuser flow, future investigations along the following lines are recommended.

(i) Measurement of the double and triple velocity correlations. The double velocity correlation will be useful in providing information regarding the size of the turbulent eddies and the way in which energy is transferred from one size of an eddy to another. The triple velocity correlation will make it possible to assess the separate contribution made to the convective diffusion of turbulence by kinetic effects only.

(ii) Measurement of the pressure diffusion term of the turbulent kinetic energy balance.

(iii) Measurement of the turbulence vorticity field. As is well-known, turbulence is rotational, three-dimensional and characterized by high levels of fluctuating vorticity. Evidence suggests (Tennekes and Lumley 1972)

that the eddies most effective in maintaining a correlation between the fluctuating velocities (e.g., u_1 and u_2) and in extracting energy from the mean flow are vorticies whose principal axes are approximately aligned with those of the mean strain rate; the energy transfer mechanism for such eddies is believed to be linked with vortex stretching. Thus a study of the vorticity field can shed more light on the turbulence mechanism in diffuser flow.

APPENDIX A

TURBULENT ENERGY EQUATION IN CYLINDRICAL COORDINATES FOR AXISYMMETRIC MEAN FLOW

The turbulent energy equation (2.18) may be written for mean flow in the form

$$U_i \frac{\partial}{\partial x_i}\left(\frac{\overline{u_j^2}}{2}\right) + \frac{\partial}{\partial x_i}\left[\overline{u_i\left(\frac{p}{\rho} + \frac{u_i^2}{2}\right)}\right]$$

$$+ \overline{u_i u_j}\frac{\partial U_j}{\partial x_i} - \nu\frac{\partial^2}{\partial x_i^2}\left(\frac{\overline{u_j^2}}{2}\right) + \nu\overline{\left(\frac{\partial u_j}{\partial x_i}\right)^2}$$

$$= 0 \ , \qquad \text{(A.1)}$$

by noting that

$$\frac{\partial}{\partial x_i}\ \overline{u_j\left(\frac{\partial u_i}{\partial x_j} + \frac{\partial u_j}{\partial x_i}\right)} \ - \overline{\left(\frac{\partial u_i}{\partial x_j} + \frac{\partial u_j}{\partial x_i}\right)\frac{\partial u_j}{\partial x_i}}$$

$$= \frac{\partial}{\partial x_i}\overline{\left(u_j\frac{\partial u_i}{\partial x_j}\right)} + \frac{\partial^2}{\partial x_i^2}\left(\frac{\overline{u_j^2}}{2}\right) - \overline{\frac{\partial u_i}{\partial x_j}\frac{\partial u_j}{\partial x_i}} - \overline{\left(\frac{\partial u_j}{\partial x_i}\right)^2}$$

$$= \frac{\partial^2}{\partial x_i^2}\left(\frac{u_j^2}{2}\right) - \overline{\left(\frac{\partial u_j}{\partial x_i}\right)^2} \ ,$$

since

$$\frac{\partial}{\partial x_i}\left(\overline{u_j \frac{\partial u_i}{\partial x_j}}\right) = \overline{\frac{\partial u_j}{\partial x_i}\frac{\partial u_i}{\partial x_j}} + \overline{u_j \frac{\partial^2 u_i}{\partial x_i \partial x_j}} \quad ,$$

and

$$\overline{u_j \frac{\partial^2 u_i}{\partial x_i \partial x_j}} = \overline{u_j \frac{\partial}{\partial x_j}\frac{\partial u_i}{\partial x_i}} = 0 \quad .$$

For cylindrical coordinates, let

U_i be represented by U_x , U_r , U_θ

u_i by u_x , u_r , u_θ

and x_i by x , r , θ.

Application of the identities

$$\frac{\partial U_i}{\partial x_i} = \nabla \cdot \underline{U} = \frac{\partial (rU_r)}{r\partial r} + \frac{\partial U_\theta}{r\partial \theta} + \frac{\partial U_x}{\partial x} \quad ,$$

$$\frac{\partial^2}{\partial x_i^2} = \nabla^2 = \frac{\partial}{r\partial r}\left(\frac{r\partial}{\partial r}\right) + \frac{\partial^2}{r^2 \partial \theta^2} + \frac{\partial^2}{\partial x^2} \quad ,$$

$$\frac{\partial U_j}{\partial x_i} = \nabla \underline{U} = \begin{bmatrix} \frac{\partial U_r}{\partial r} & \frac{\partial U_\theta}{\partial r} & \frac{\partial U_x}{\partial r} \\ \frac{\partial U_r}{r\partial \theta} - \frac{U_\theta}{r} & \frac{\partial U_\theta}{r\partial \theta} + \frac{U_r}{r} & \frac{\partial U_x}{r\partial \theta} \\ \frac{\partial U_r}{\partial x} & \frac{\partial U_\theta}{\partial x} & \frac{\partial U_x}{\partial x} \end{bmatrix} \quad ,$$

and the conditions that

$$U_\theta = 0 \quad , \quad \frac{\partial}{\partial\theta}\overline{(\quad)} = 0 \quad ,$$

$$\nabla\cdot\underline{U} = 0 \quad ,$$

to equation (A.1) yields on expansion,

$$(U_x \frac{\partial}{\partial x} + U_r \frac{\partial}{\partial r}) \left(\frac{\overline{u_x^2} + \overline{u_r^2} + \overline{u_\theta^2}}{2}\right)$$

$$+ \frac{\partial}{\partial x}\left[\overline{u_x\left(\frac{p}{\rho} + \frac{u_x^2 + u_r^2 + u_\theta^2}{2}\right)}\right] + \frac{1}{r\partial r}\, r\left[\overline{u_r\left(\frac{p}{\rho} + \frac{u_x^2 + u_r^2 + u_\theta^2}{2}\right)}\right]$$

$$+ \left[\overline{u_x u_r}\frac{\partial U_x}{\partial r} + (\overline{u_x^2} - \overline{u_r^2})\frac{\partial U_x}{\partial x}\right.$$

$$\left. + \overline{u_x u_r}\frac{\partial U_r}{\partial x} + \frac{U_r(\overline{u_\theta^2} - \overline{u_r^2})}{r}\right]$$

$$- \nu\left(\frac{\partial}{r\partial r}\left(r\frac{\partial}{\partial r}\right) + \frac{\partial^2}{\partial x^2}\right)\left(\frac{\overline{u_x^2} + \overline{u_r^2} + \overline{u_\theta^2}}{2}\right) - \nu\overline{\left(\frac{\partial u_i}{\partial x_j}\right)\left(\frac{\partial u_j}{\partial x_i}\right)}$$

$$+ \nu\overline{\left(\frac{\partial u_i}{\partial x_j} + \frac{\partial u_j}{\partial x_i}\right)\frac{\partial u_i}{\partial x_j}} = 0 \qquad \text{(A.2)}$$

The non-dimensional form of the turbulent energy balance equation (2.19) is finally obtained by re-arranging and multiplying equation (A.2) by $R/U_{l,m}^3$, replacing u_j^2 by q^2 and returning to the index notation.

APPENDIX B

CORRECTIONS TO THE MEASUREMENTS

(i) Correction to the X-probe measurements

Errors arise from many sources when making turbulence measurements. These errors have been discussed extensively by Hinze (1959) and Corrsin (1963). Here, the hot-wire response to yaw and non-linearities caused by high intensity turbulence is assumed to be significant; the correction factors applied to the measured turbulence quantities were in the form suggested by Champagne et al (1967), as follows:

$$\left(\frac{\overline{u_1^2}}{U_1^2}\right)_{CORR^*} = \left(\frac{\overline{u_1^2}}{U_1^2}\right)_{MEAS^+} , \qquad (B.1)$$

$$\left(\frac{\overline{u_2^2}}{U_1^2}\right)_{CORR} = 1.17 \left(\frac{\overline{u_2^2}}{U_1^2}\right)_{MEAS} , \qquad (B.2)$$

and

$$\left(\frac{\overline{u_1 u_2}}{U_1^2}\right)_{CORR} = 1.08 \left(\frac{\overline{u_1 u_2}}{U_1^2}\right)_{MEAS} , \qquad (B.3)$$

---

*CORR denotes corrected.

+MEAS denotes measured; in connection with hot-wire, it denotes normal component cooling only (assuming cosine law cooling).

(ii) Correction to mean velocity obtained from pitot and static tube measurements

Considerable theoretical and experimental investigations have been directed in the past to the study of pitot and static tube measurements in turbulent flow; these investigations are discussed in considerable detail for example in Hinze (1959) and Kaye (1968). In the present experiment, the mean static and total pressures were referenced to the local wall pressure.

The mean velocities obtained from pitot and static tube measurements were corrected with Kaye's results as follows:

$$P_T - P_S = \frac{1}{2}\rho \left\{ A_o(U_1^2 + \overline{u_1^2}) + (A_o + A_2)\ (\overline{u_2^2} + \overline{u_3^2}) + (A_2 + A_4) \left[\frac{3(\overline{u_2^2})^2 + 2\overline{u_2^2}\ \overline{u_3^2} + 3(\overline{u_3^2})^2}{U_1^2} \right] \right\}_{CORR} , \quad (B.4)$$

where

$$A_o = \left[f(\alpha) \right]_{\alpha=o} ,$$

$$A_2 = \left[\frac{1}{2} \frac{d^2 f(\alpha)}{d\alpha^2} \right]_{\alpha=o} ,$$

$$A_4 = \left[\frac{1}{4!} \frac{d^4 f(\alpha)}{d\alpha^4} \right]_{\alpha=o} .$$

[$f(\alpha)$ is given in Kaye, Figure 11, page 104 for hemispherical nose probe (0.072 ins external diameter and 0.0135 internal diameter; this probe is closest in dimension to the one used in the present experiment)].

By combining equation (B.4) with the measured quantity

$$P_T - P_S = \frac{1}{2} \rho (U_1^2)_{MEAS} , \qquad (B.5)$$

the corrected mean velocity was obtained.

REFERENCES

ACKERET, J. 1967 Aspects of internal flow. Gen. Motors Symposium on Internal Flow, Amsterdam: Elsevier.

AZAD, R. S. AND HUMMEL, R. 1971 Measurement of the intermittency factor in diffuser-flow. Can. J. Physics, 49, 2917.

BAKEWELL, P. H. AND LUMLEY, J. L. 1967 Viscous sublayer and adjacent wall region in turbulent pipe flow. Phys. Fluids, 10, 1880.

BRADLEY, C. I. AND COCKRELL, D. J. 1970 Boundary layer methods applied to internal fluid problems. Proc. Heat Transfer and Fluid Mech. Inst. Stanford Univ.

BRADSHAW, P. 1967 Conditions for the existence of the inertial subrange in turbulent flows. NPL Aero. Rep. 1220, A. R. C. 28 664.

CHAMPAGNE, F. H., SLEICHER, C. A. AND WEHRMANN, O. H. 1967 Turbulence measurements with inclined hot wires. J. Fluid Mech. 28, 153.

CHAMPAGNE, F. H. AND SLEICHER, C. A. 1967 Turbulence measurements with inclined hot wires. J. Fluid Mech. 28, 177.

CLAUSER, F. H. 1954 Turbulent boundary layers in adverse pressure gradients. J. Aero. Sci. 21, 91.

COCANOWER, A. B., KLINE, S. J. AND JOHNSTON, J. P. 1965 A unified method for predicting the performance of subsonic diffusers of several geometries. Stanford University, Dept. of Mech. Eng. Rep. PD-10.

COCKRELL, D. J. AND KING, A. L. 1967 A review of the literature on subsonic fluid flow through diffusers. The British Hydromechanics Research Association Rep. TN 902.

COLES, D. AND HIRST, E. A. (eds.) 1969 Computation of turbulent boundary layers. Proceedings 1968 AFOSR-IFP-Stanford Conference, vol. 2. Stanford University.

CORRSIN, S. 1963 Turbulence: experimental methods. Encyclopedia of Physics, 8, 524, Berlin: Springer-Verlag.

FRASER, H. R. 1956 Study of an incompressible turbulent boundary layer in a conical diffuser. Ph.D. Thesis, Dept. of Theoretical and Appl. Mech., University of Illinois.

GIBSON, A. H. 1910 On the flow of water through pipes and passages having converging or diverging boundaries. Proc. Roy. Soc. A 83, 366.

HARSHA, P. T. AND LEE, S. C. 1970 Correlation between turbulent shear stress and turbulent kinetic energy. AIAA Journal 8, 1508.

HINZE, J. O. 1959 Turbulence. New York: McGraw-Hill.

KAYE, K. S. 1968 Rapid acceleration of high intensity turbulent shear flow. Ph.D. Dissertation, The Johns Hopkins University, Baltimore, Maryland.

KLEBANOFF, P. S. 1954 Characteristics of turbulence in a boundary layer with zero pressure gradient. NACA TN 3178.

KLINE, S. J., ABBOTT, D. E. AND FOX, R. W. 1959 Optimum design of straight-walled diffusers. ASME Trans. J. Basic Eng. 81, 321.

LAUFER, J. 1951 Investigation of turbulent flow in a two-dimensional channel. NACA Rep. 1053.

LAUFER, J. 1954 The structure of turbulence in fully developed pipe flow. NACA Rep. 1174.

LAWN, C. J. 1971 The determination of the rate of dissipation in turbulent pipe flow. J. Fluid Mech. 48, 477.

LUDWEIG, H. AND TILLMAN, W. 1950 Investigation of the wall-shearing stress in turbulent boundary layers. NACA TM 1285.

NIKURADSE, J. 1929 Untersuchungen über die Strömungen des Wassers in konvergenten und divergenten kanälen. Forsch. Geb. Ing. Wes., Heft 289.

OKWUOBI, P. A. C., AZAD, R. S. AND HAWALESHKA, O. 1972a Turbulence structure parameters in an inhomogeneous strain field. To appear in AIAA Journal.

OKWUOBI, P. A. C. AND AZAD, R. S. 1972b Turbulence investigation in a conical diffuser with partly developed flow at entry. The University of Manitoba, Dept. of Mech. Eng. Rep. ER 25.17.

PATEL, V. C. 1965 Calibration of the Preston tube and limitations on its use in pressure gradients. J. Fluid Mech. 23, 185.

PATTERSON, G. N. 1938 Modern diffuser design. Aircraft Engineering, 10, 267.

REYNOLDS, O. 1958 On the dynamical throry of incompressible viscous fluids and the determination of the criterion. Trans. Roy. Soc. 186A, 123.

ROBERTSON, J. M. AND CALEHUFF, G. L. 1957 Turbulence in civil engineering: turbulence in a diffuser boundary layer. Proc. ASCE 83, HY5, paper 1393.

RUETENIK, J. R. AND CORRSIN, S. 1955 Equilibrium turbulent flow in a slightly divergent channel. 50 Jahre Grenzschichtforschung, pp. 446-459, Brauschweig: Vieweg & Sohn.

SANBORN, V. A. AND SLOGAR, J. 1955 Study of the momentum distribution of turbulent boundary layers in adverse pressure gradients. NACA TN 3264.

SANBORN, V. A. AND LIU, C. Y. 1968 On turbulent boundary-layer separation. J. Fluid Mech. 32, 293.

SCHLICHTING, J. 1968 Boundary-layer Theory., 6th ed. Toronto: McGraw-Hill.

SOVRAN, G. AND KLOMP, E. D. 1967 Experimentally determined optimum geometries for rectilinear diffusers with rectangular, conical or annular cross-section. Gen. Motors Symposium on Internal Flow, Amsterdam: Elsevier.

SPRENGER, H. 1959 Experimental investigations of straight and curved diffusers. Mitt. Inst. Aero. Zurich, 27; The British Ministry of Aviation Rep. TIL/T. 5134, 1962.

TENNEKES, H. AND LUMLEY, T. L. 1972 A First Course in Turbulence. Cambridge, Massachusetts: The MIT Press.

TOWNSEND, A. A. 1956 The Structure of Turbulent Shear Flow. Cambridge University Press.

TRUPP, A.C., AZAD, R.S., WILSON, N. W. AND OKWUOBI, P. A. C. 1971 Turbulence characteristics in a straight conical diffuser. University of Salford Symposium on Internal Flows, paper 9.

TUCKER, H. J. AND REYNOLDS, A. J. 1968 The distortion of turbulence by irrotational plain strain. J. Fluid Mech. 32, 657.

VENTURI, G. B. 1797 Recherches experimentales sur le principle de communication lateral dans les fluides. Nicholson's Journal of Natural Philosophy, vol. 3, London, 1802.

Reynolds number $\langle U_1 \rangle D/\nu$	293,000	152,000
Cross-section average velocity $\langle U_1 \rangle$, m/sec	45.7	22.9
Centre line velocity $U_{1,m}$, m/sec	54.9	27.8
Friction velocity U_* , m/sec	1.94	0.99
Kinematic viscosity ν, m^2/sec	1.59×10^{-7}	1.53×10^{-7}
Density ρ , kg.f. sec^2/m^4	0.118	0.120

TABLE 1. Mean flow parameters at the reference station.

Station (1)	$100 \leq Y^+ \leq 300$ Clauser (2)	Patel (3)	Nikuradse (4)	Ludwieg & Tillman (5)	Total shear extra-polation (6)
Re = 293,000					
1	1.496	1.475	1.432	1.522	1.612
2	1.155	1.134	1.113	1.231	1.367
3	0.904	0.883	0.861	0.987	1.170
4	0.708	0.687	0.665	0.790	1.011
5	0.612	0.591	0.569	0.641	0.881
6	0.548	0.534	0.527	0.536	0.773
7	0.495	0.484	0.473	0.454	0.685
8	0.431	0.420	0.431	0.374	0.613
9	0.399	0.388	0.378	0.325	0.553
10	0.372	0.367	0.351	0.286	0.503
11	0.346	0.346	0.346	0.258	0.461
12	0.324	0.324	0.308	0.231	0.427
Re = 152,000					
1	0.793	0.782	0.787	0.791	0.884
2	0.618	0.607	0.586	0.625	0.782
3	0.488	0.484	0.484	0.480	0.695
4	0.410	0.410	0.399	0.372	0.620
5	0.330	0.324	0.308	0.288	0.555
6	0.308	0.303	0.298	0.244	0.499
7	0.282	0.282	0.276	0.208	0.450
8	0.250	0.250	0.239	0.175	0.407
9	0.232	0.228	0.225	0.148	0.370
10	0.212	0.207	0.207	0.130	0.338
11	0.202	0.191	0.191	0.117	0.309
12	0.188	0.188	0.183	0.106	0.284

TABLE 2. The friction velocities in m/sec.

$\frac{y}{R}$	ε^*_{iso} $\frac{m^2}{sec^3}$	ε^* $\frac{m^2}{sec^3}$	$\frac{R\varepsilon^*}{U^3_{1,m}}$
0.017	160.0	8.30	0.013×10^{-3}
0.080	240.0	38.5	0.058×10^{-3}
0.205	407.0	186.0	0.281×10^{-3}
0.268	435.0	305.0	0.463×10^{-3}
0.331	497.0	546.0	0.828×10^{-3}
0.393	635.0	609.0	0.924×10^{-3}
0.582	526.0	709.0	1.076×10^{-3}
0.770	360.0	608.0	0.923×10^{-3}
0.957	239.0	545.0	0.826×10^{-3}

TABLE 3. Dissipation rate in the diffuser at station 7 for the Re = 293,000.

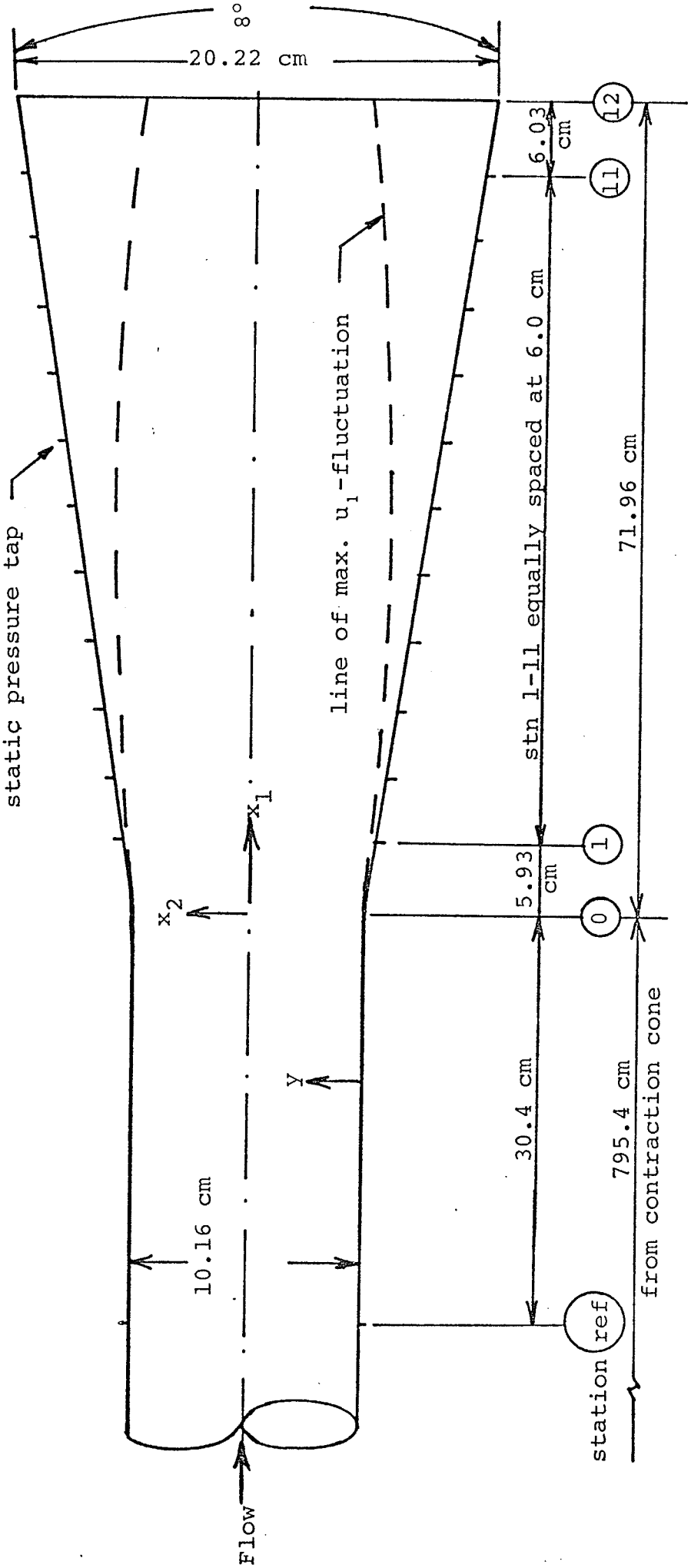

FIGURE 1. Diffuser geometry

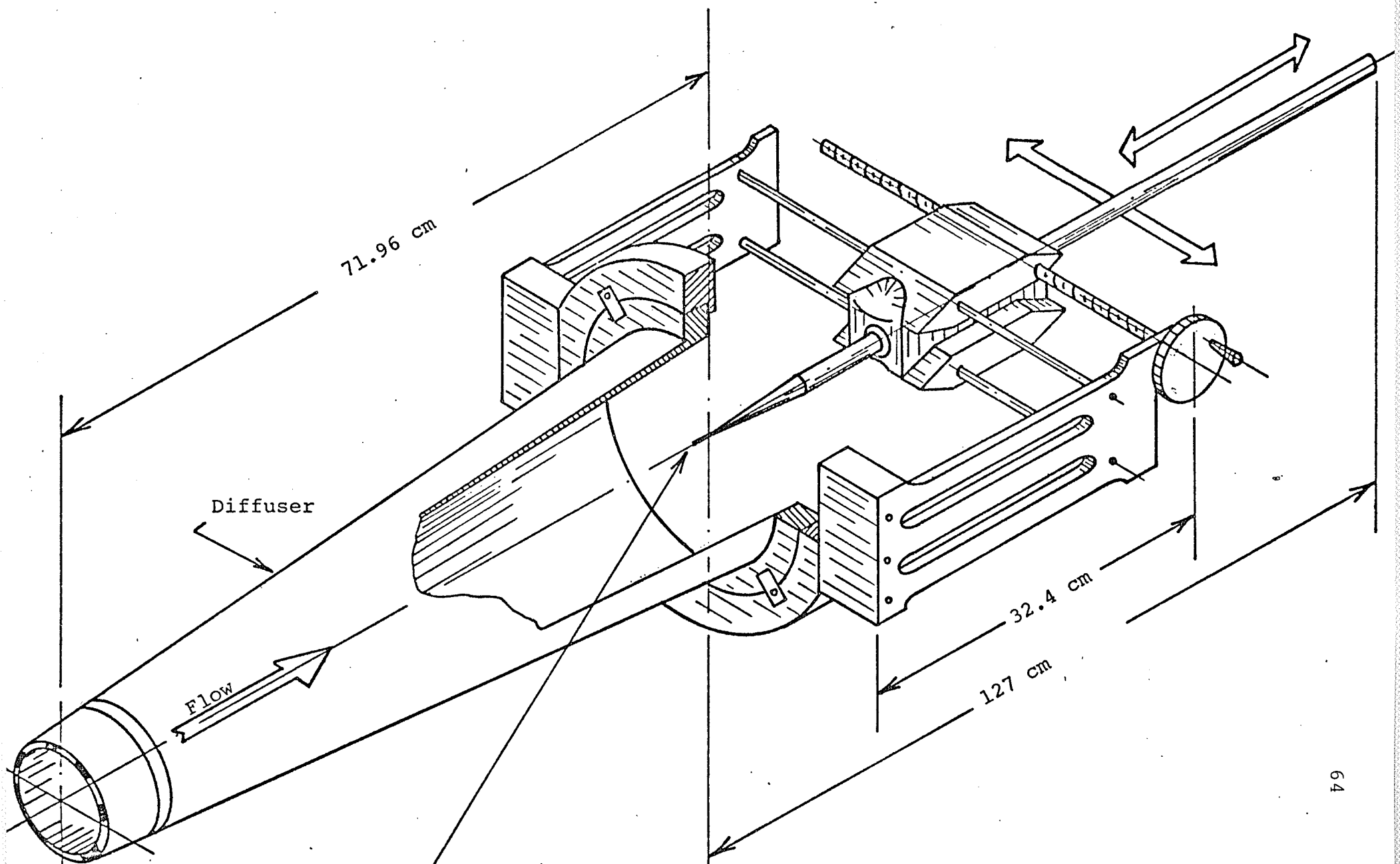

FIGURE 2 (a). Diffuser traversing mechanism.

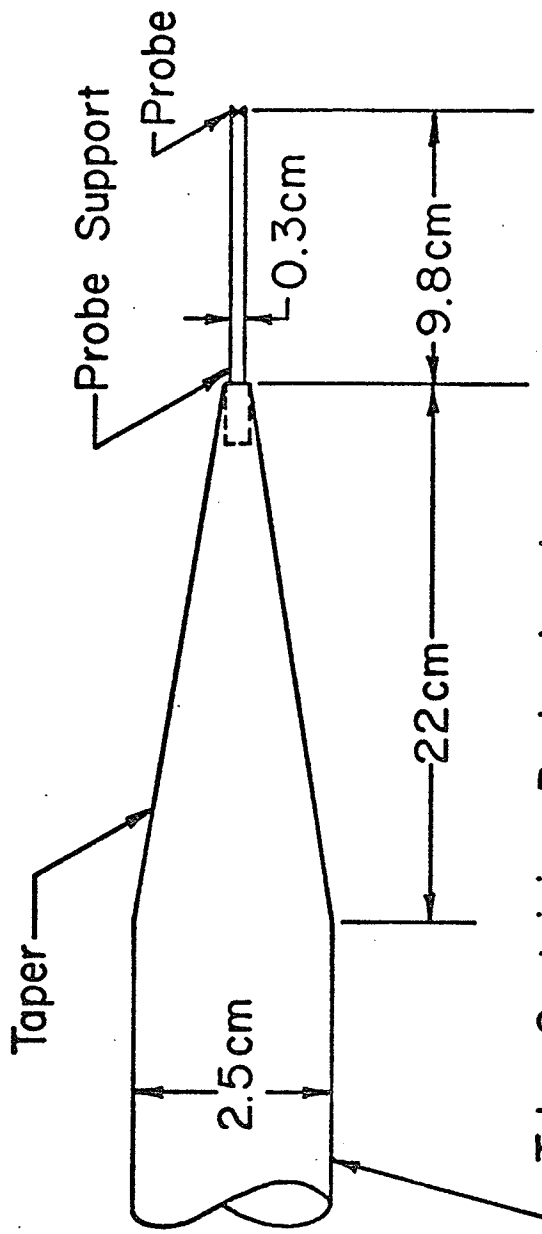

FIGURE 2(b). Detail of traversing probe head.

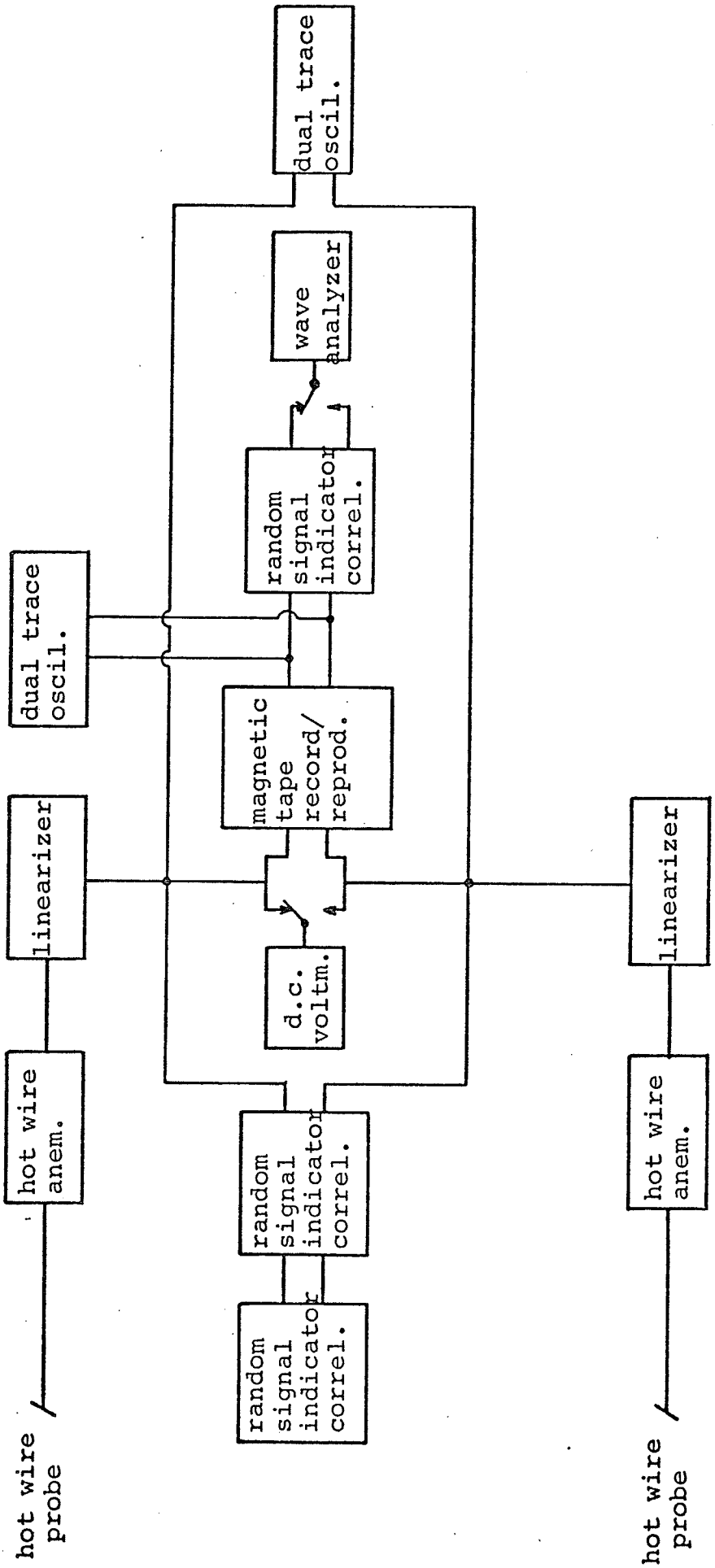

FIGURE 3. Block diagram of the turbulence measuring equipment.

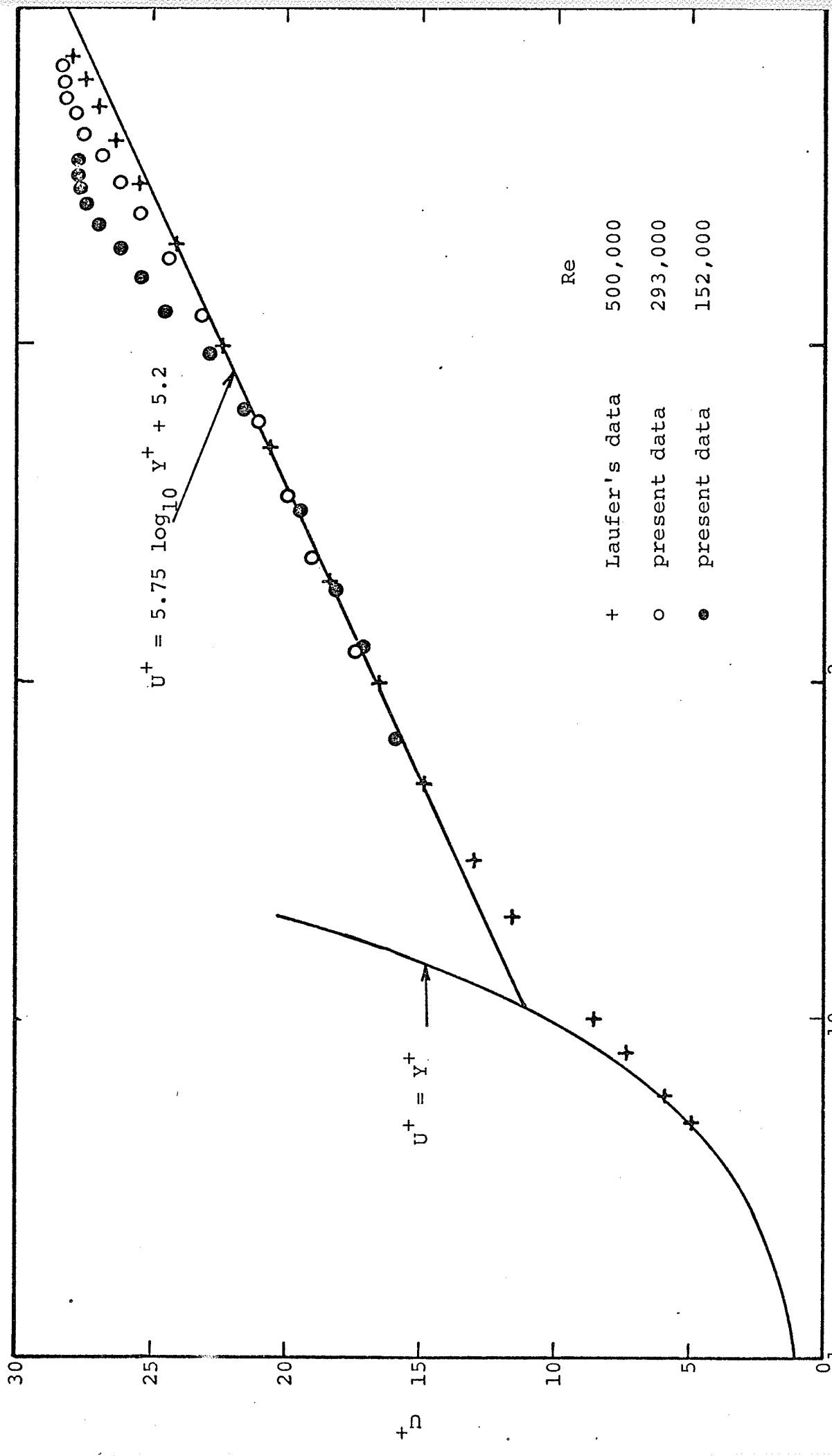

FIGURE 4. Universal velocity profile at the reference station.

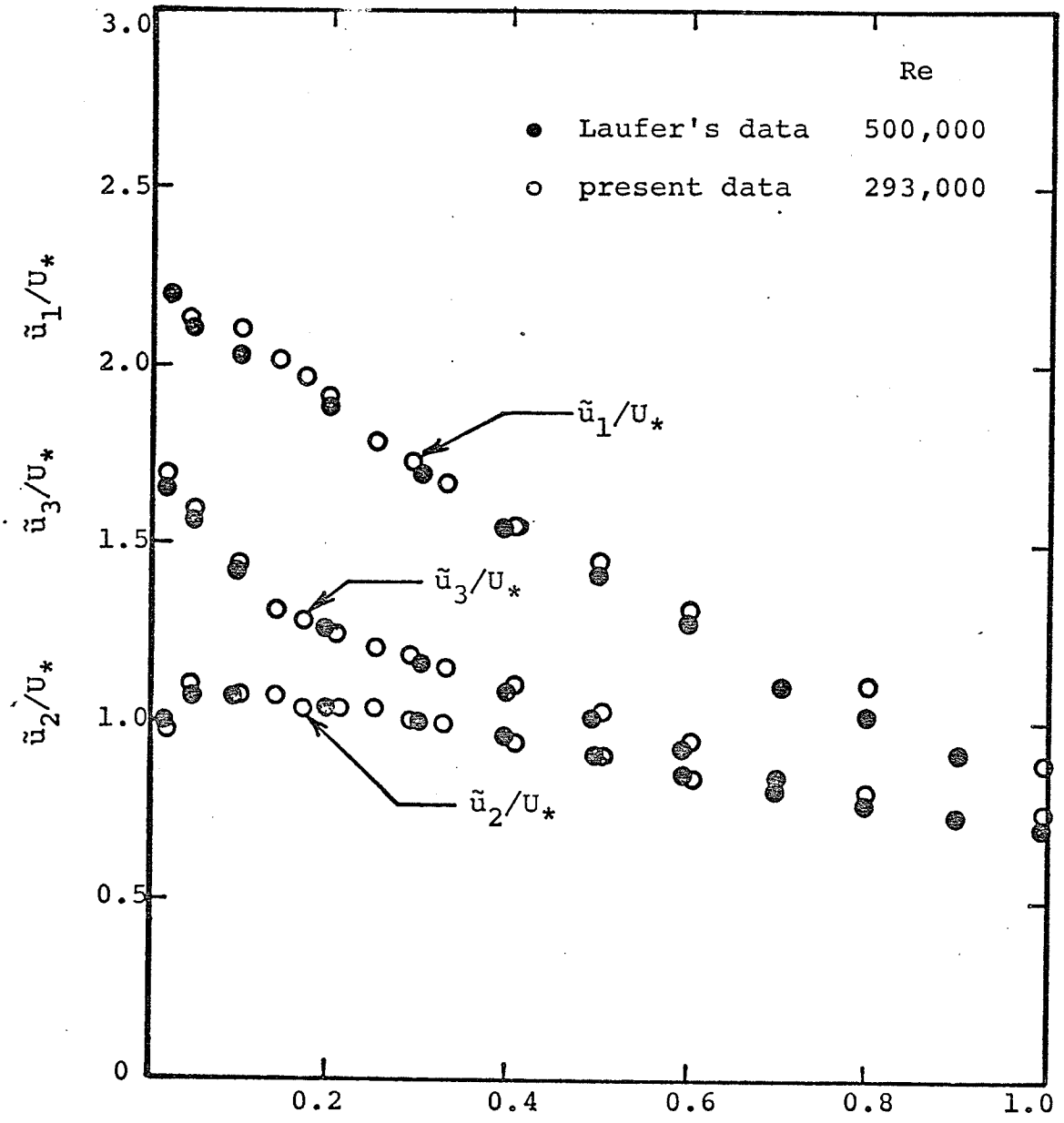

FIGURE 5(a). Turbulence intensities at the reference station.

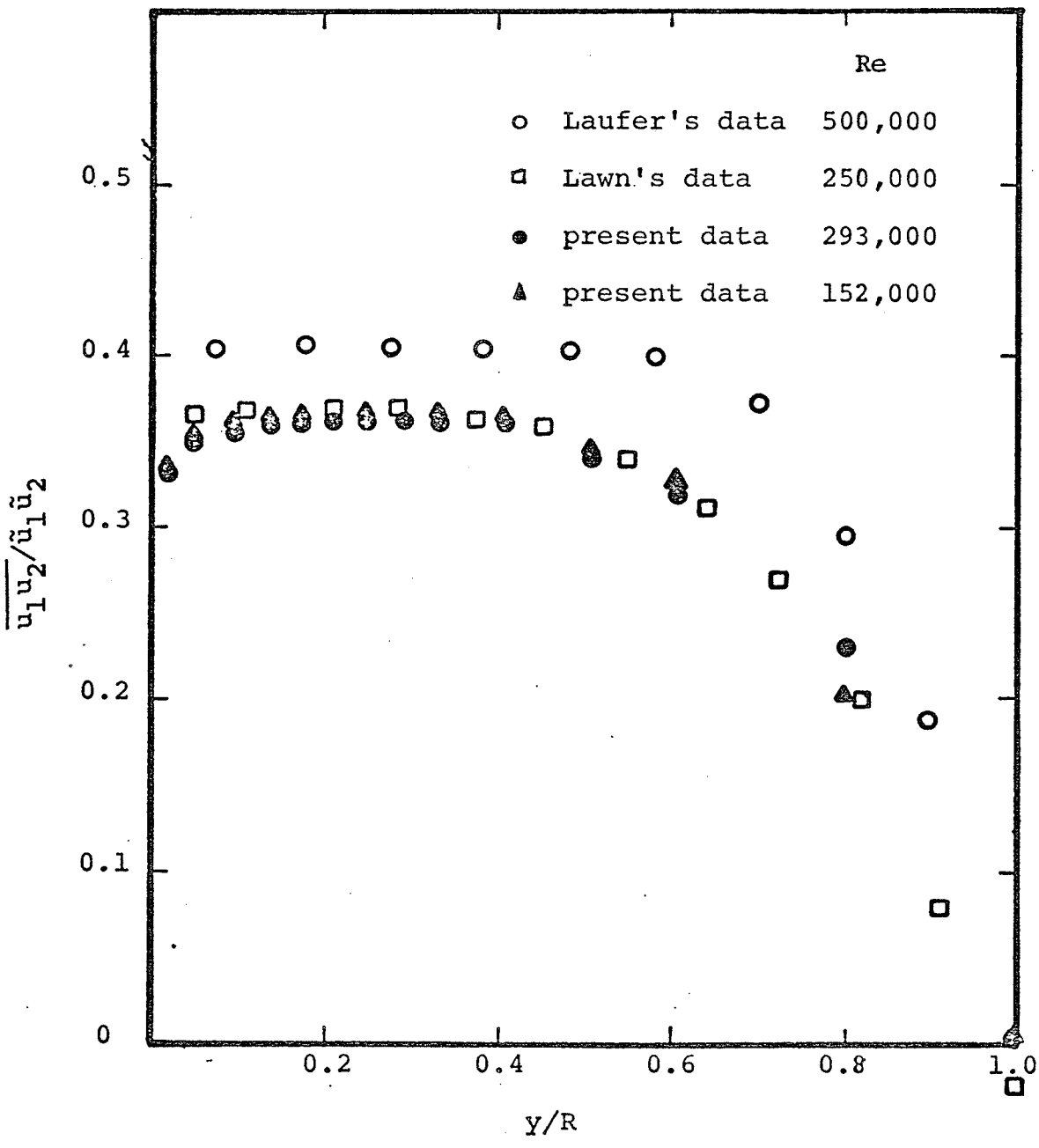

FIGURE 5(b). Correlation coefficient at the reference station.

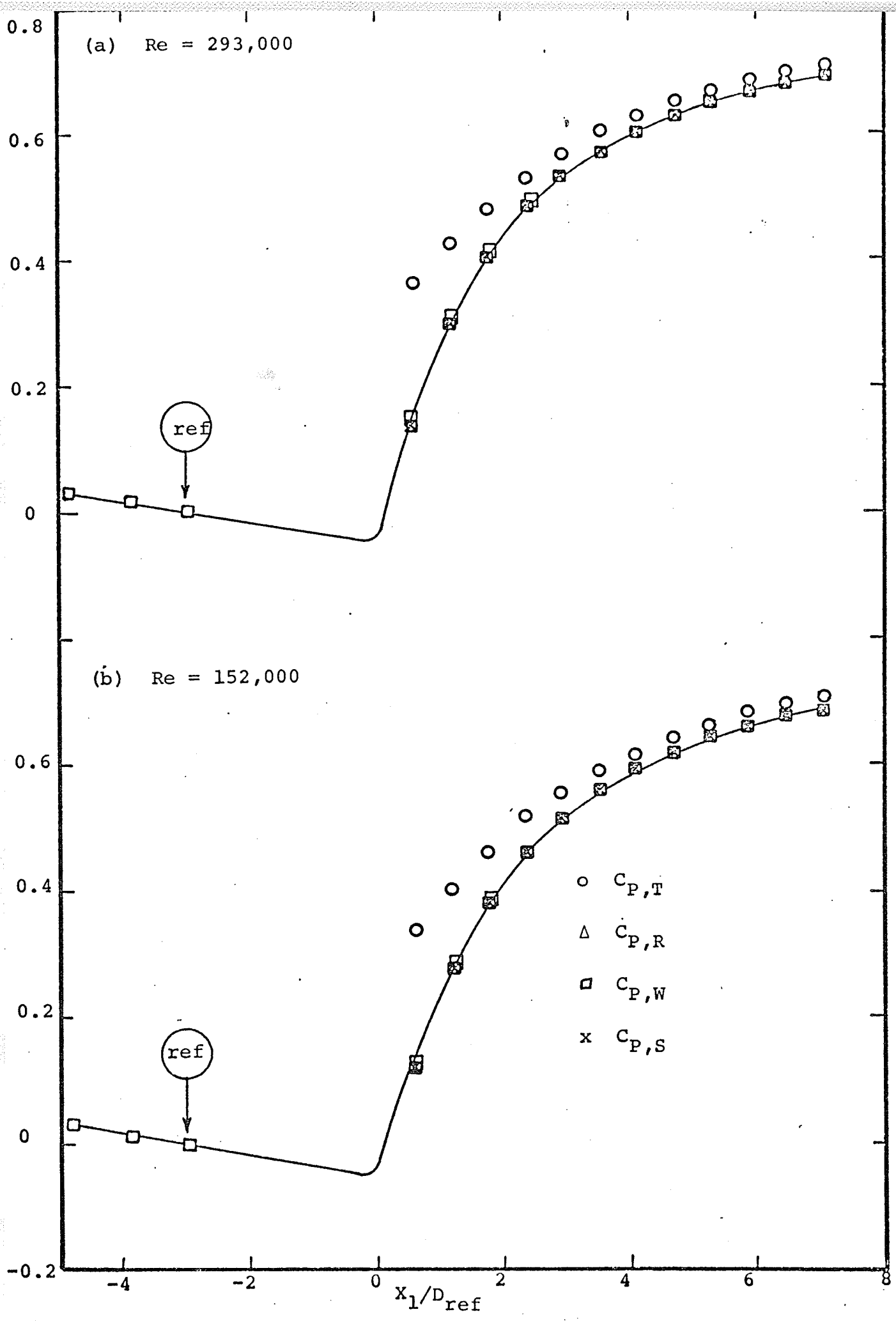

FIGURE 6. Mean pressure distribution.

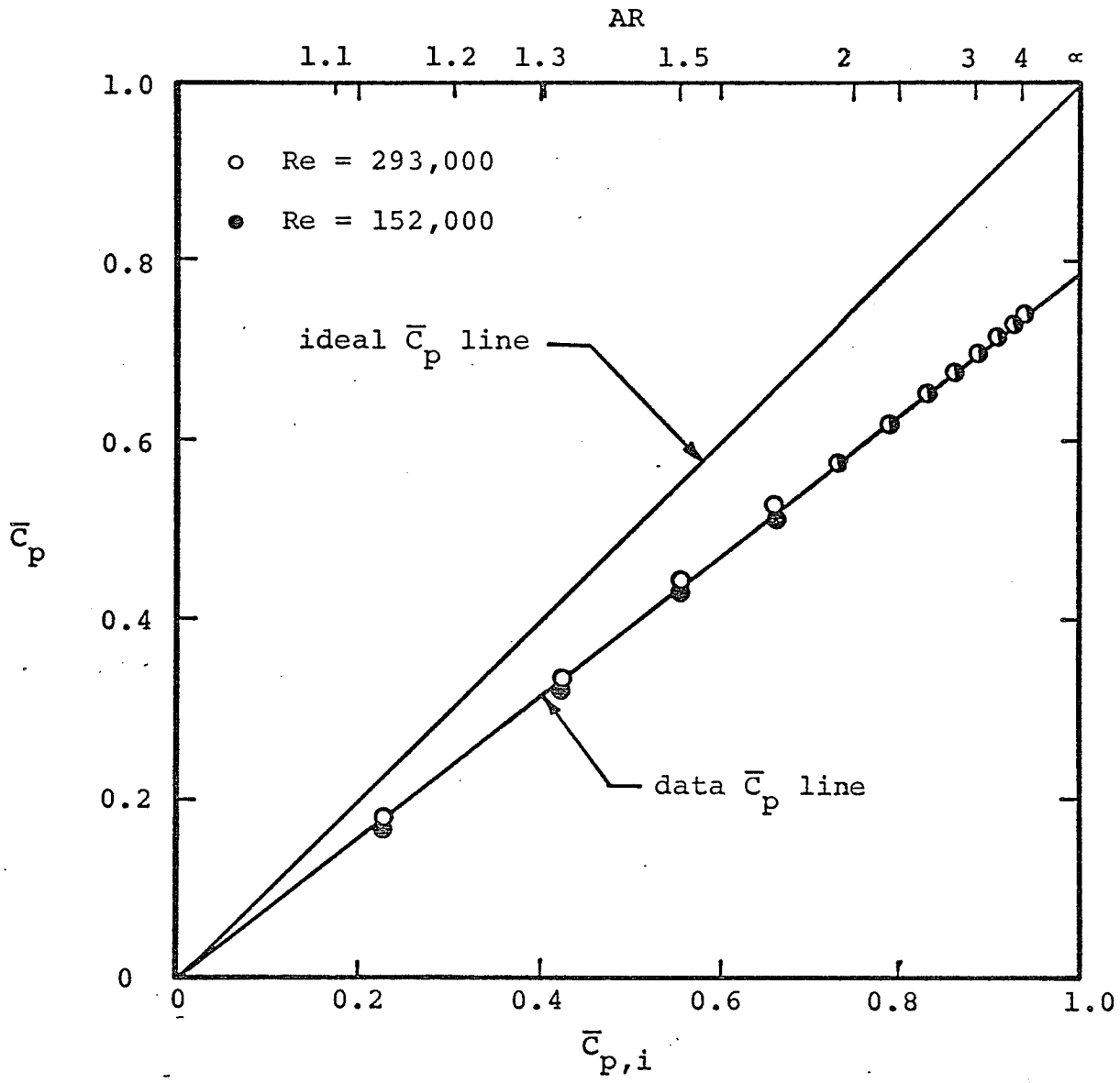

FIGURE 7. Triangular effectiveness plot for the pressure recovery coefficient.

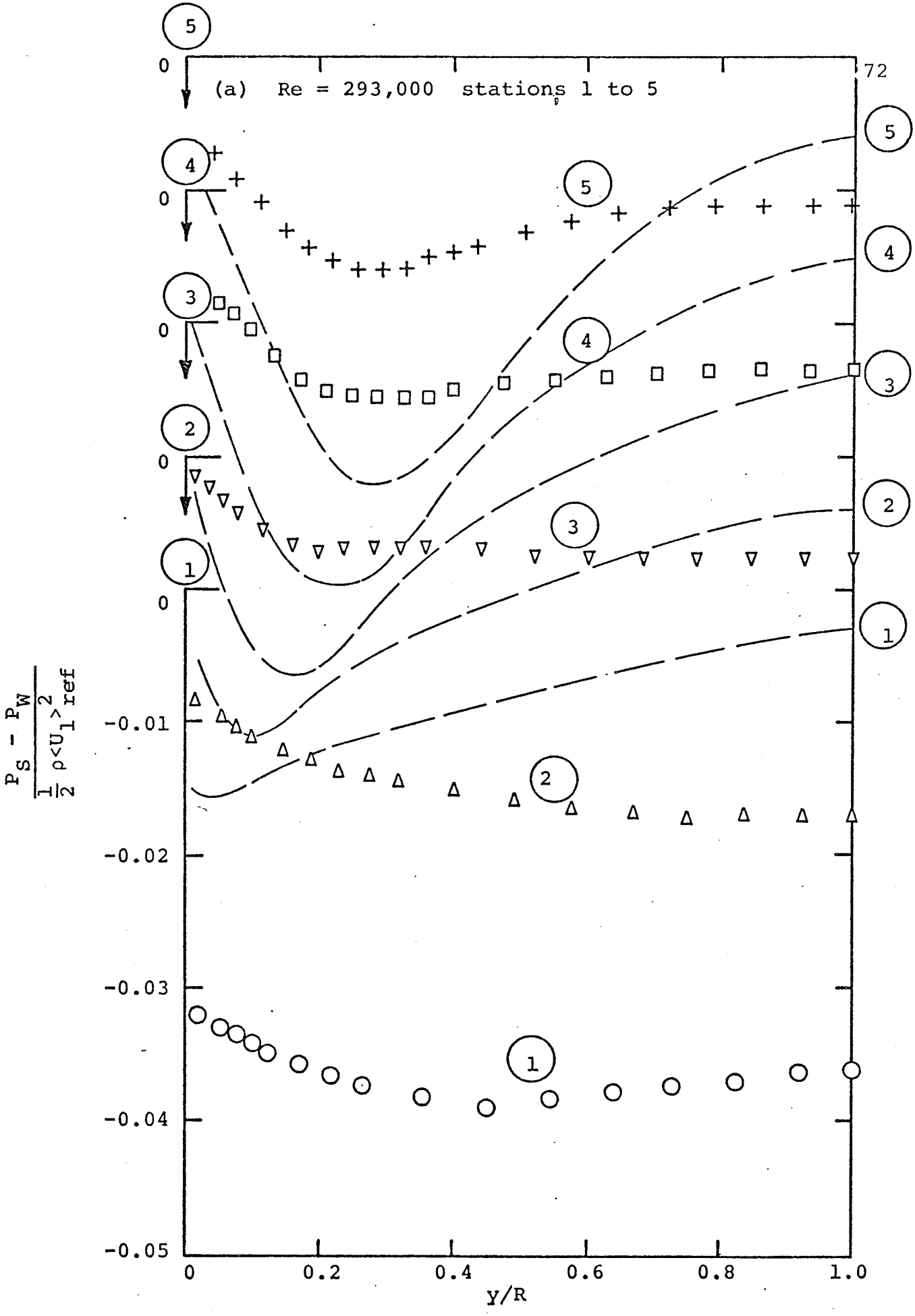

FIGURE 8. Variation of mean static pressure. (Legend as in Figure 8(b)).

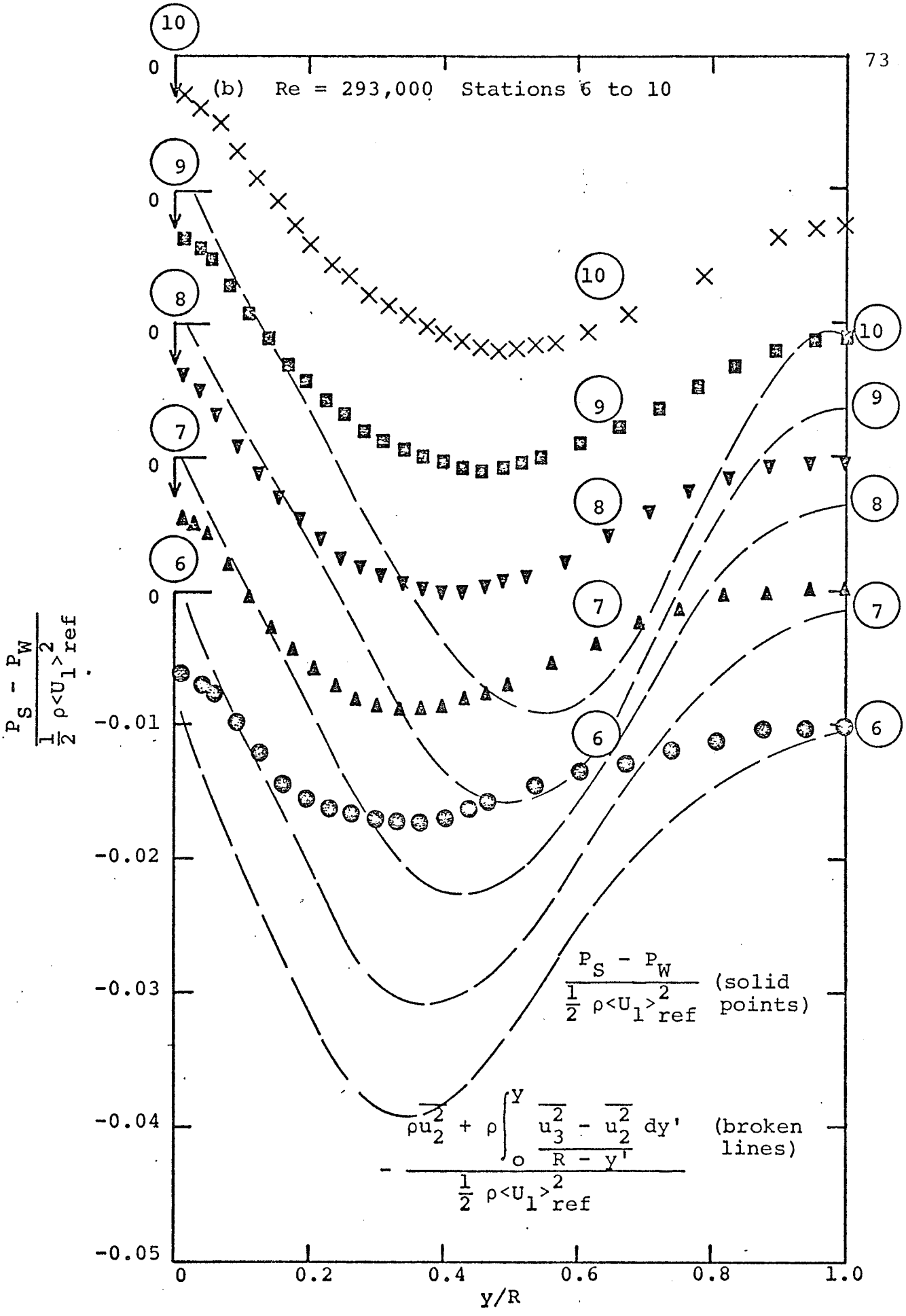

FIGURE 8. Variation of mean static pressure.

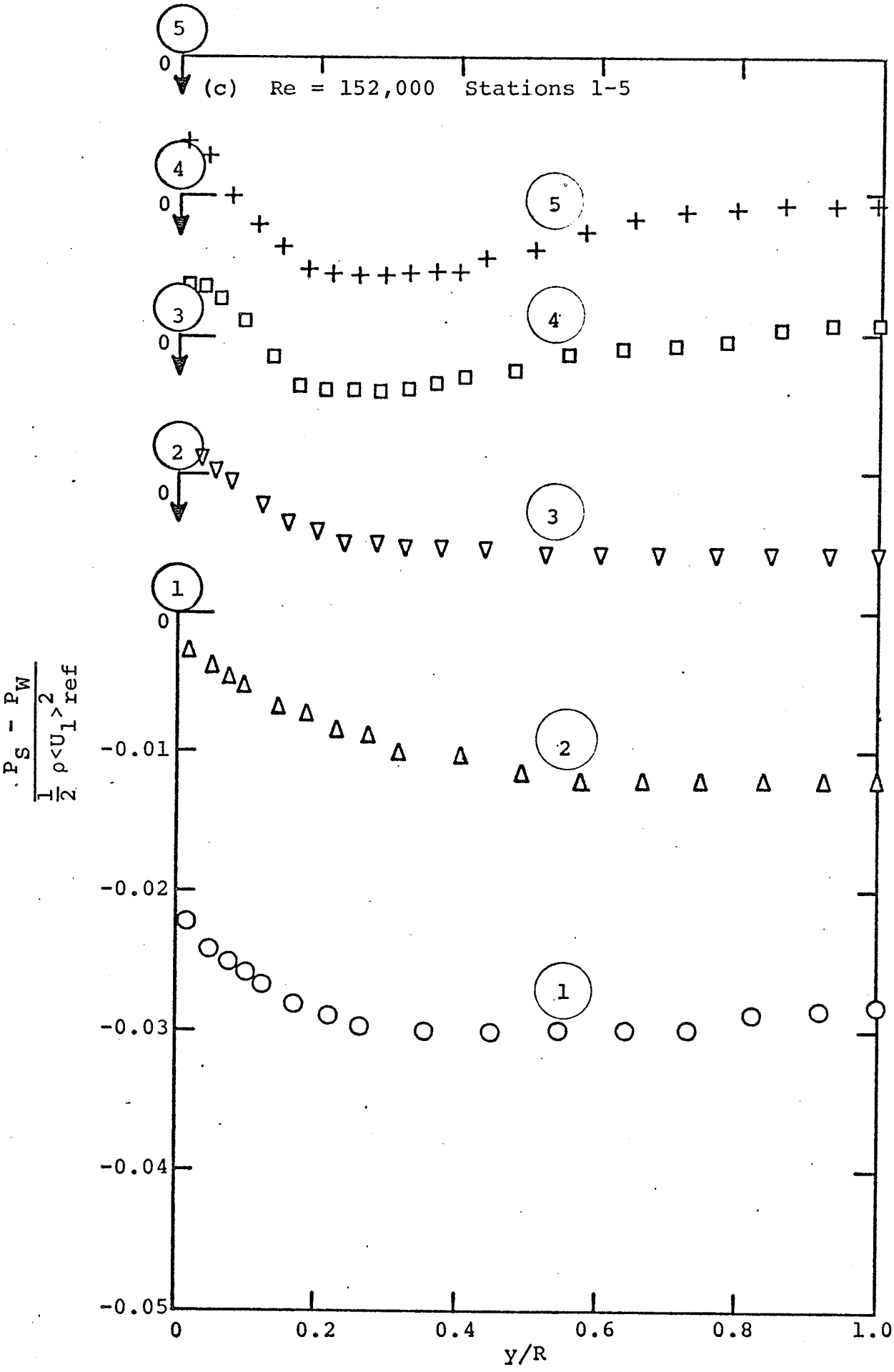

FIGURE 8. Variation of mean static pressure.

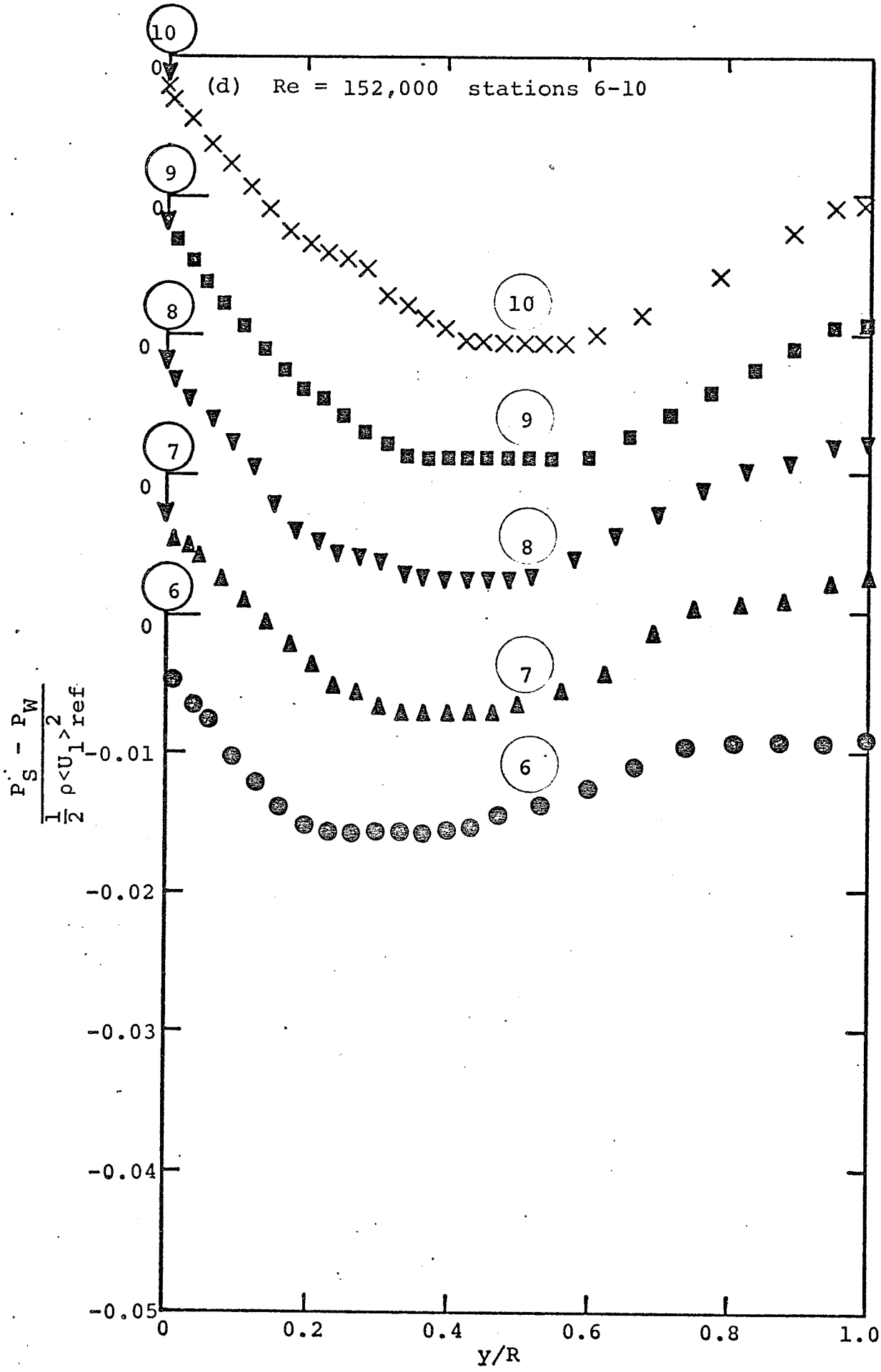

FIGURE 8. Variation of mean static pressure.

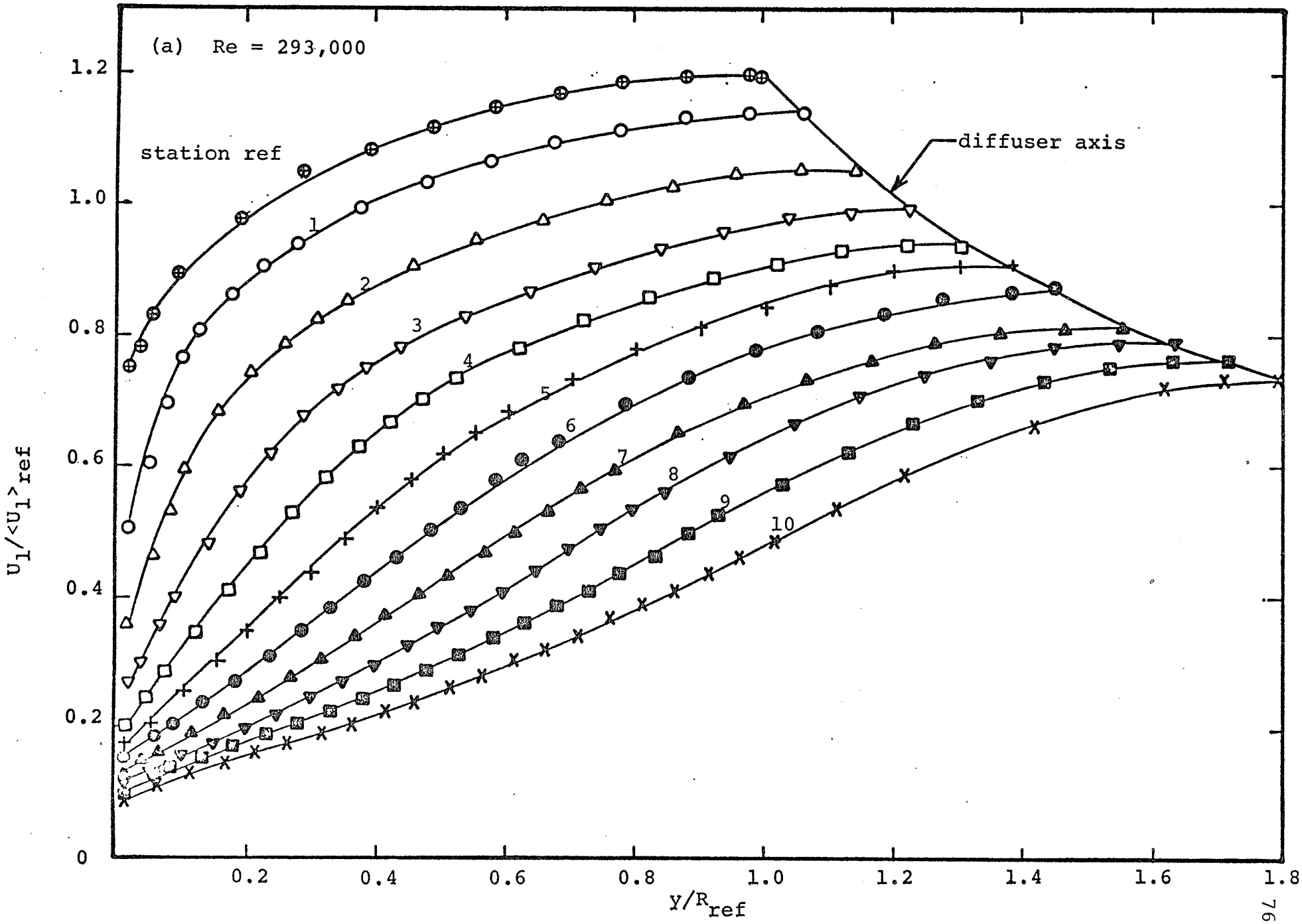

FIGURE 9. Mean velocity profiles $U_1/\langle U_1\rangle_{ref}$.

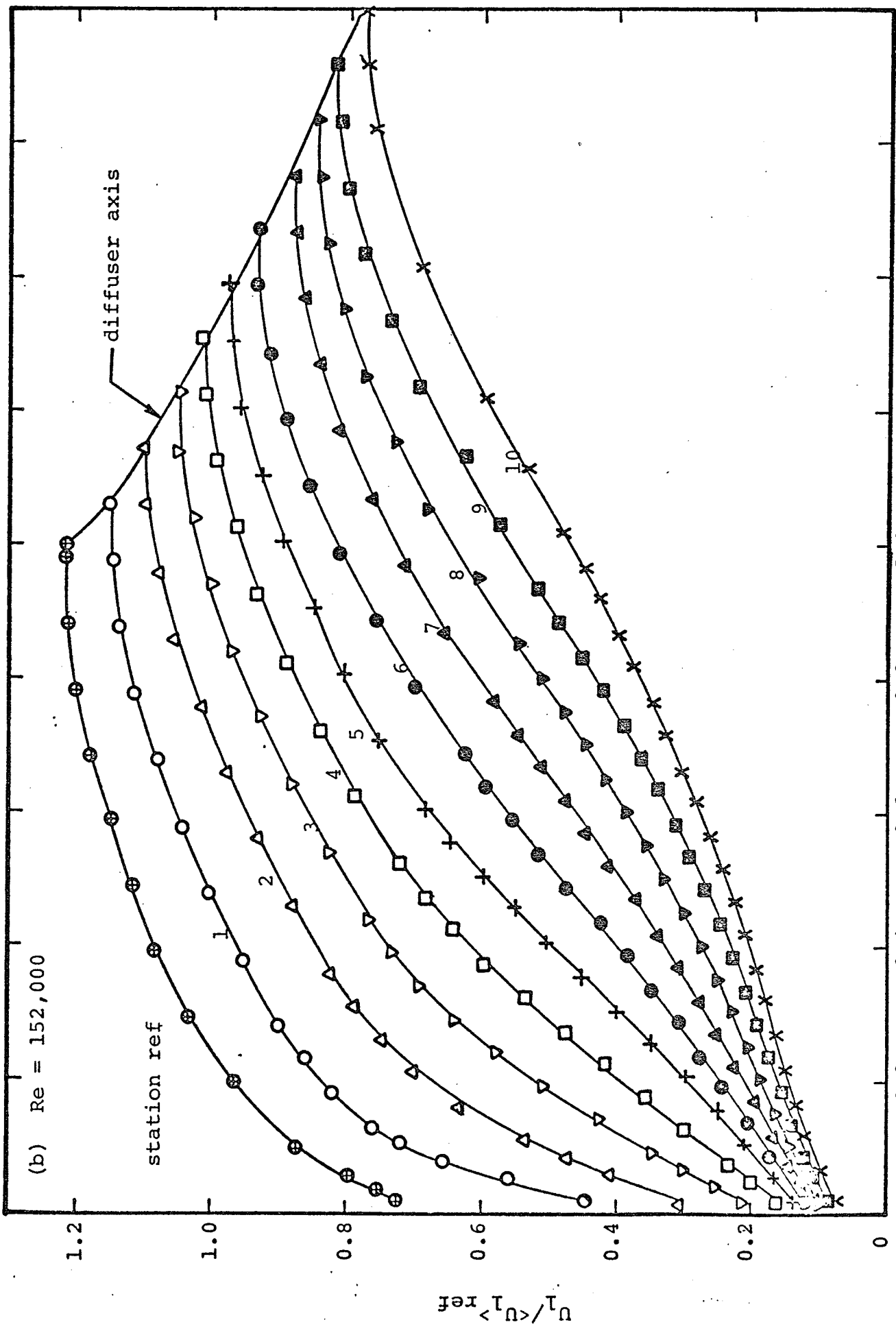

FIGURE 9. Mean velocity profiles $U_1/\langle U_1\rangle_{ref}$

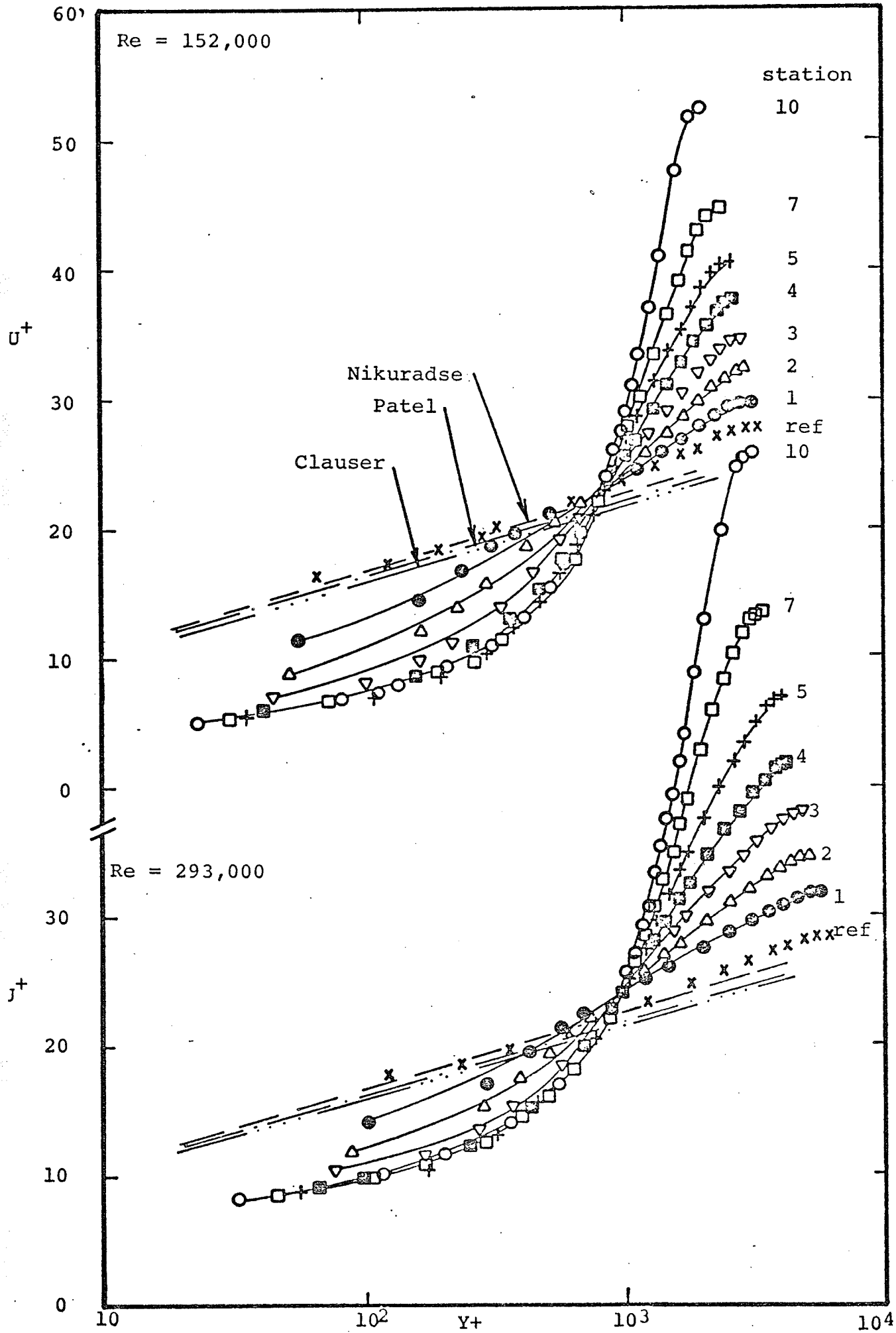

FIGURE 10(a). Diffuser velocity profiles in universal coordinates.

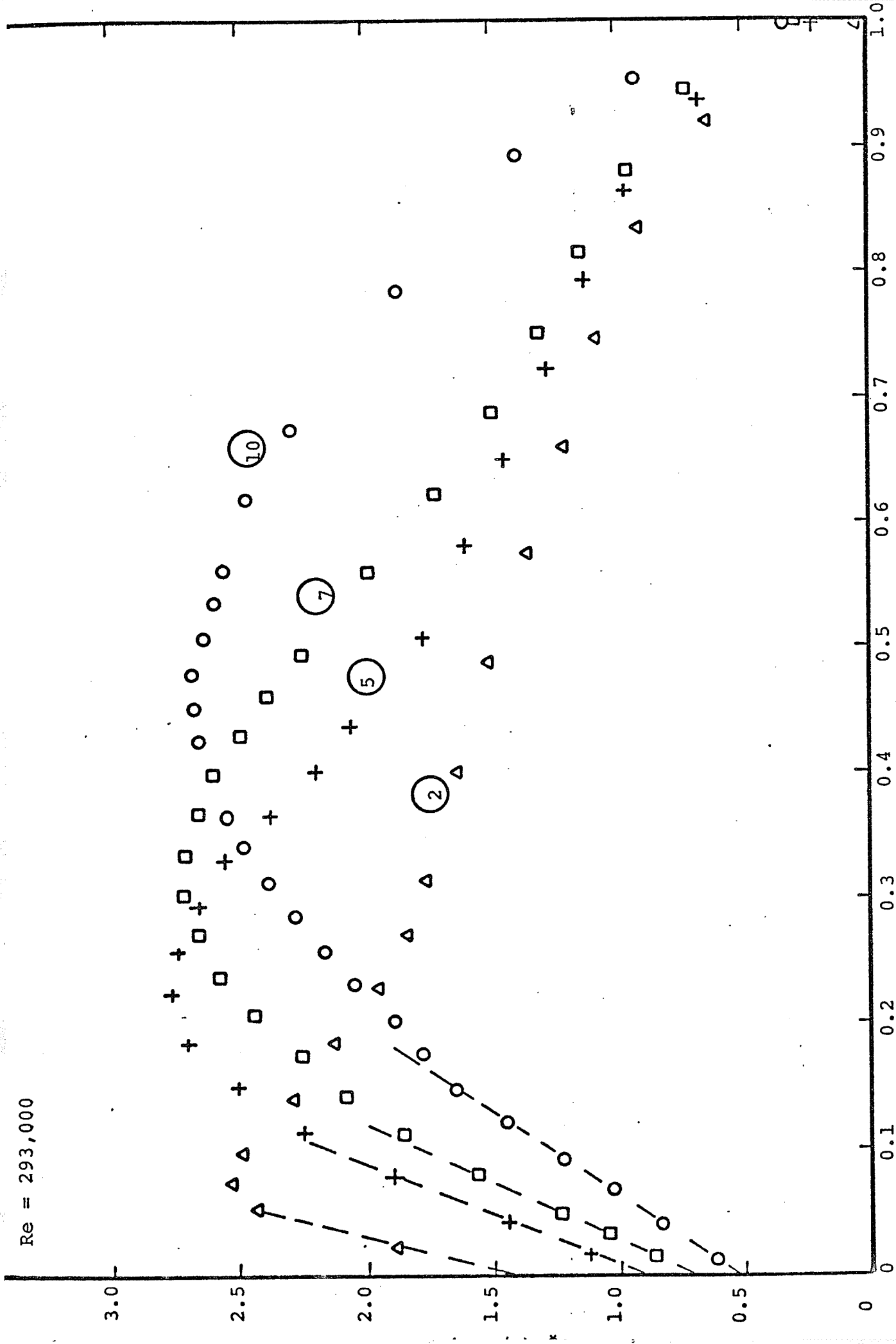

FIGURE 10(b). Variation of the total shear stress.

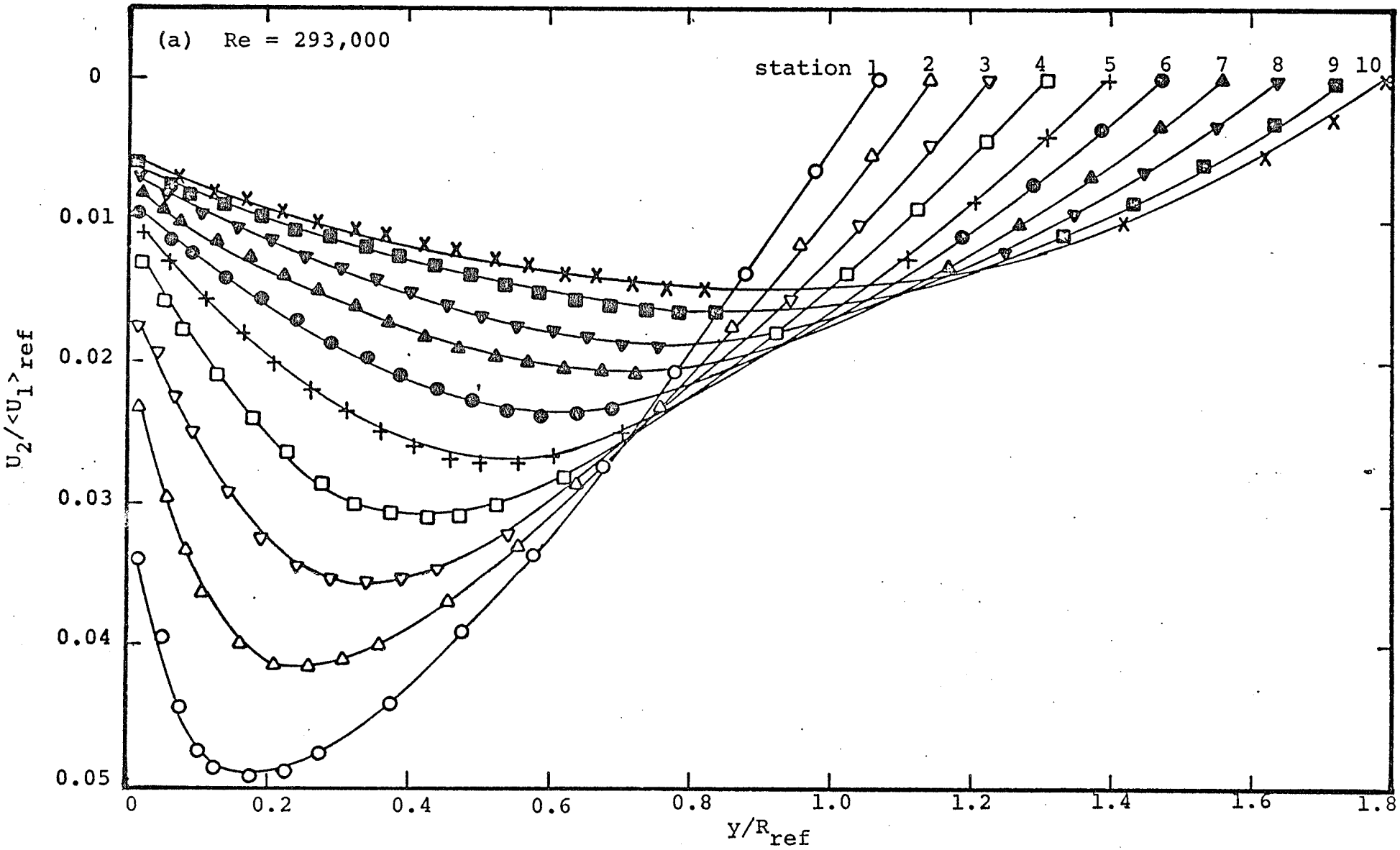

FIGURE 11. Mean velocity profiles $U_2/\langle U_1 \rangle_{ref}$.

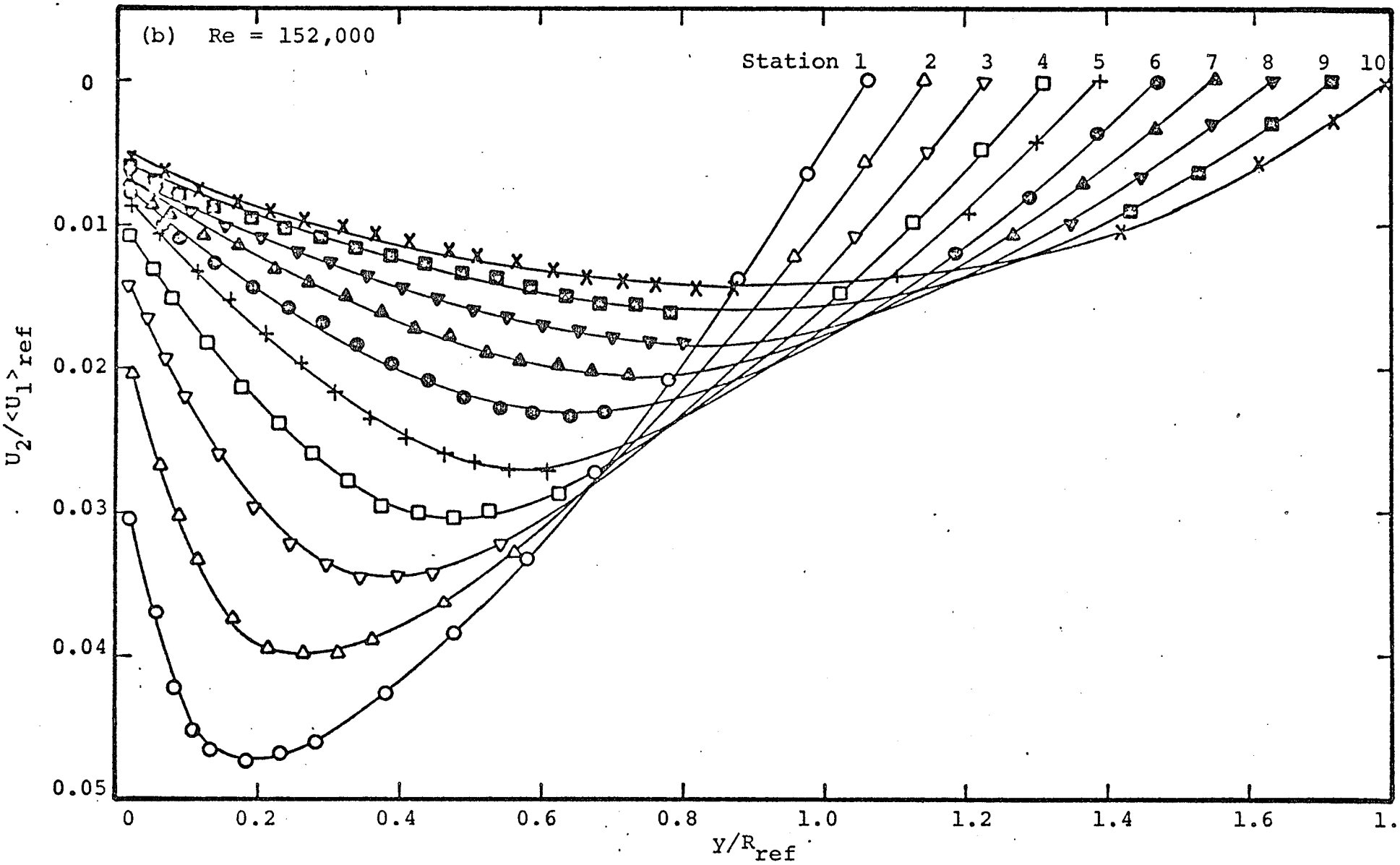

FIGURE 11. Mean velocity profiles $U_2/\langle U_1 \rangle_{ref}$.

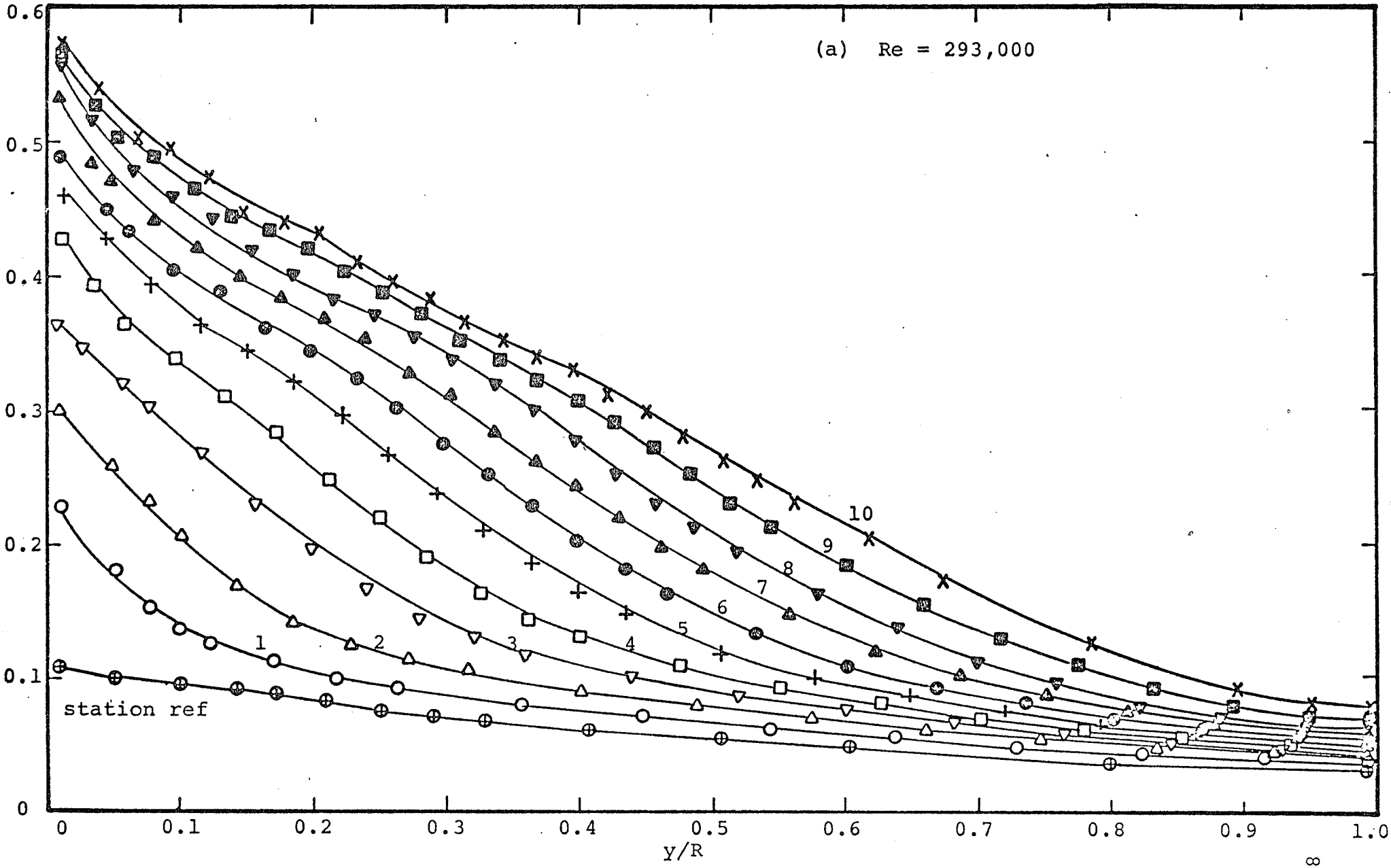

FIGURE 12 . Distribution of the turbulence intensities $\tilde{u}_1/U_1$, $\tilde{u}_2/U_1$ and $\tilde{u}_3/U_1$.

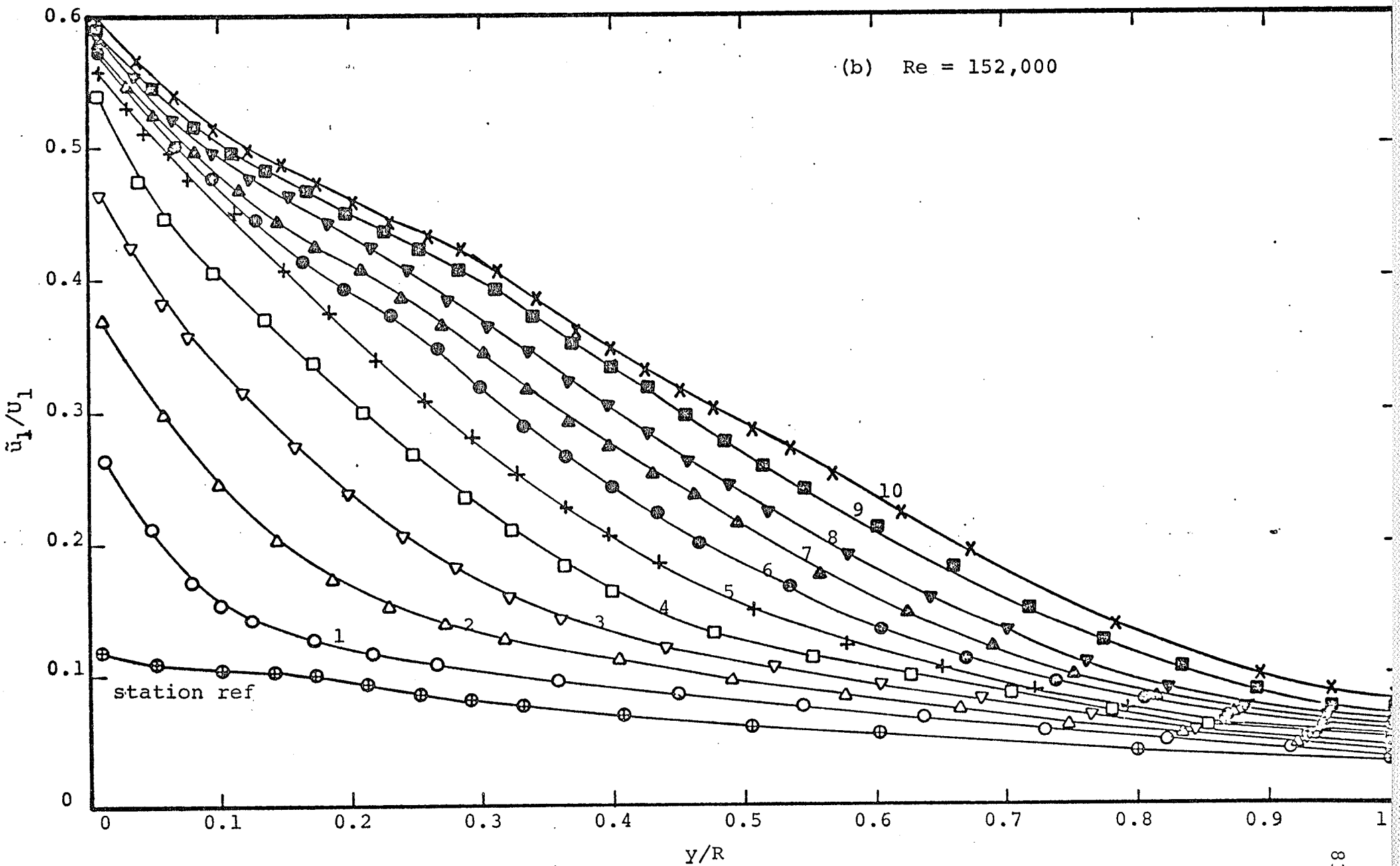

FIGURE 12 . Distribution of the turbulence intensities $\tilde{u}_1/U_1$, $\tilde{u}_2/U_1$ and $\tilde{u}_3/U_1$.

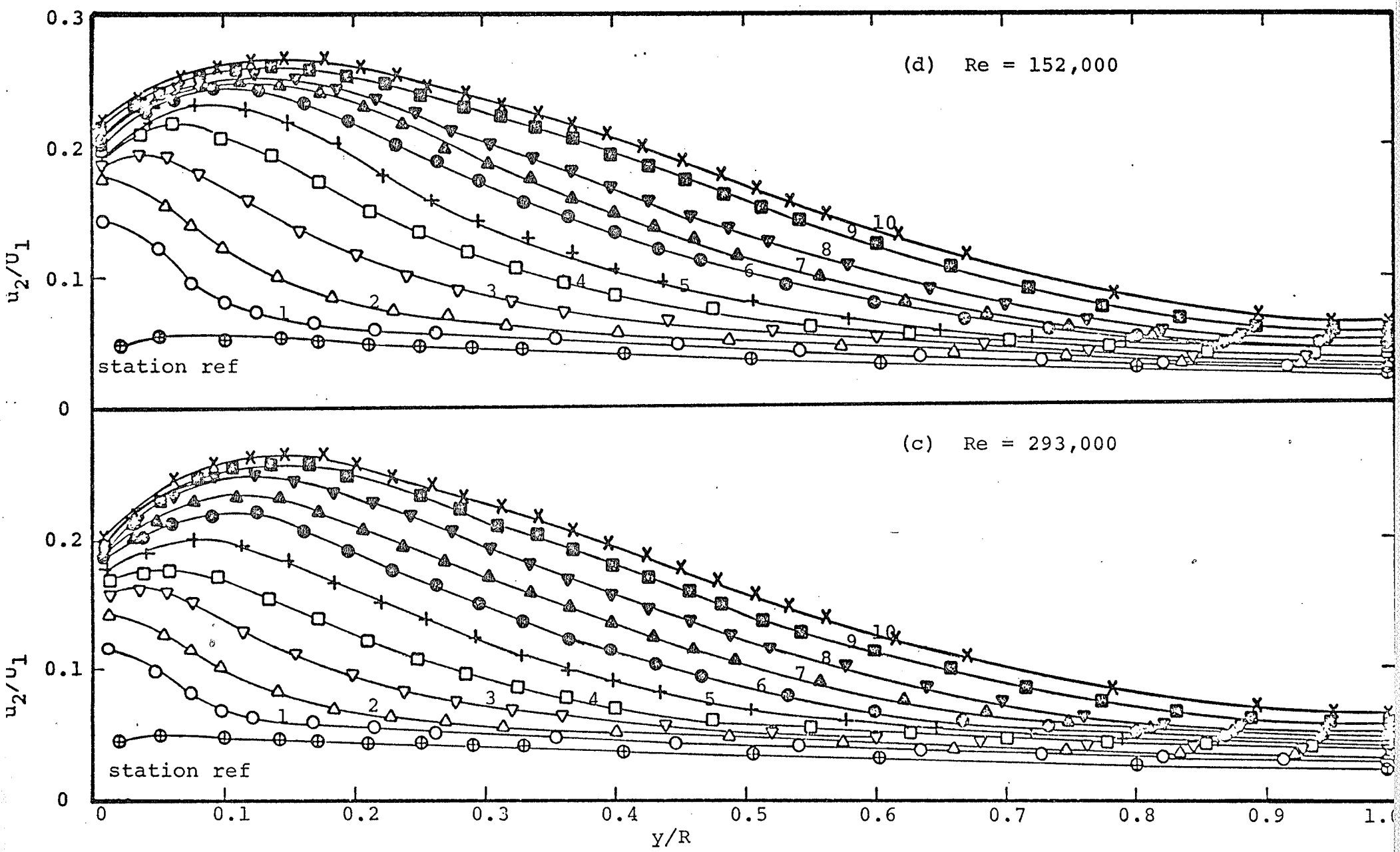

FIGURE 12. Distribution of the turbulence intensities $\tilde{u}_1/U_1$, $\tilde{u}_2/U_1$ and $\tilde{u}_3/U_1$.

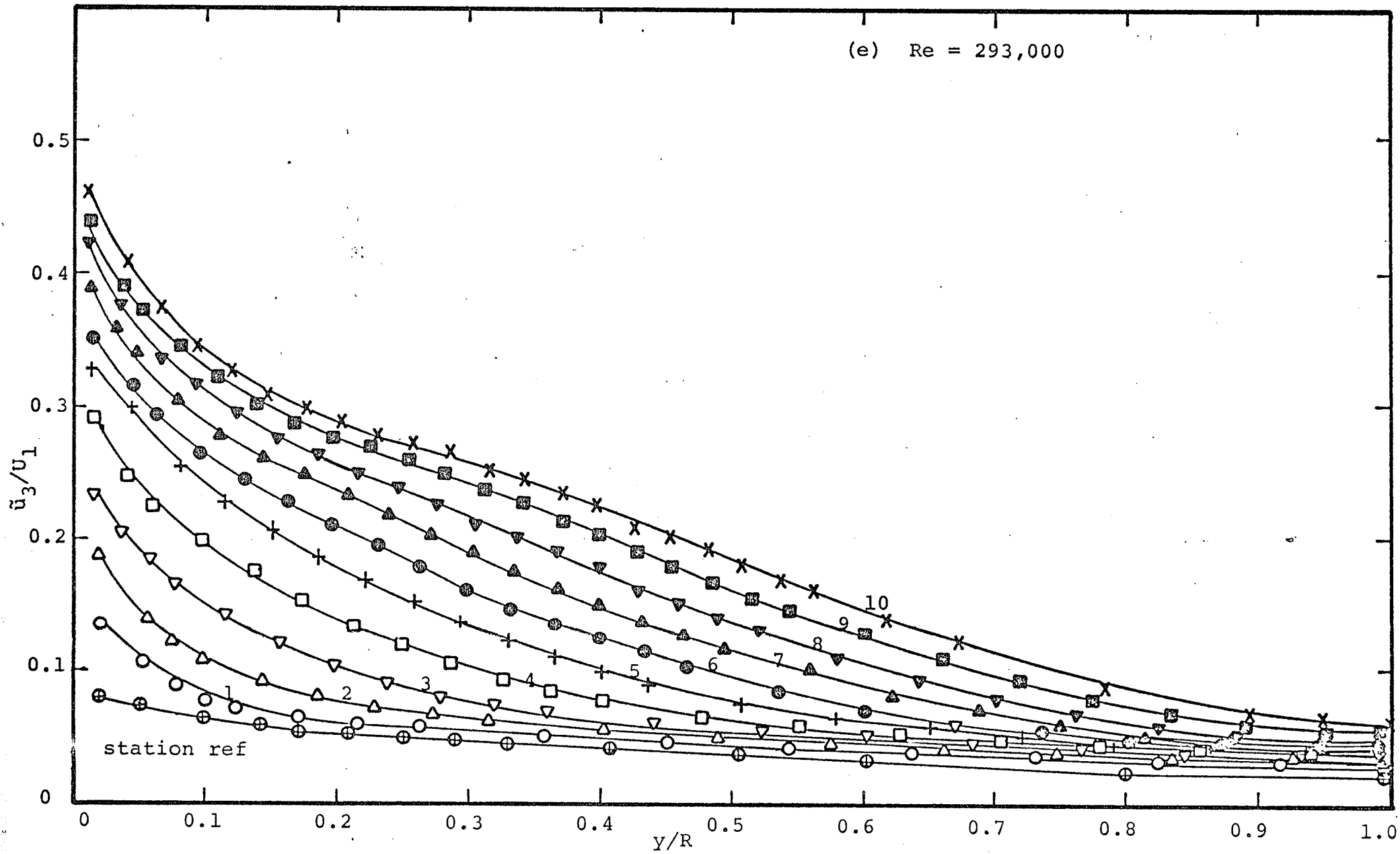

FIGURE 12 . Distribution of the turbulence intensities $\tilde{u}_1/U_1$, $\tilde{u}_2/U_1$ and $\tilde{u}_3/U_1$.

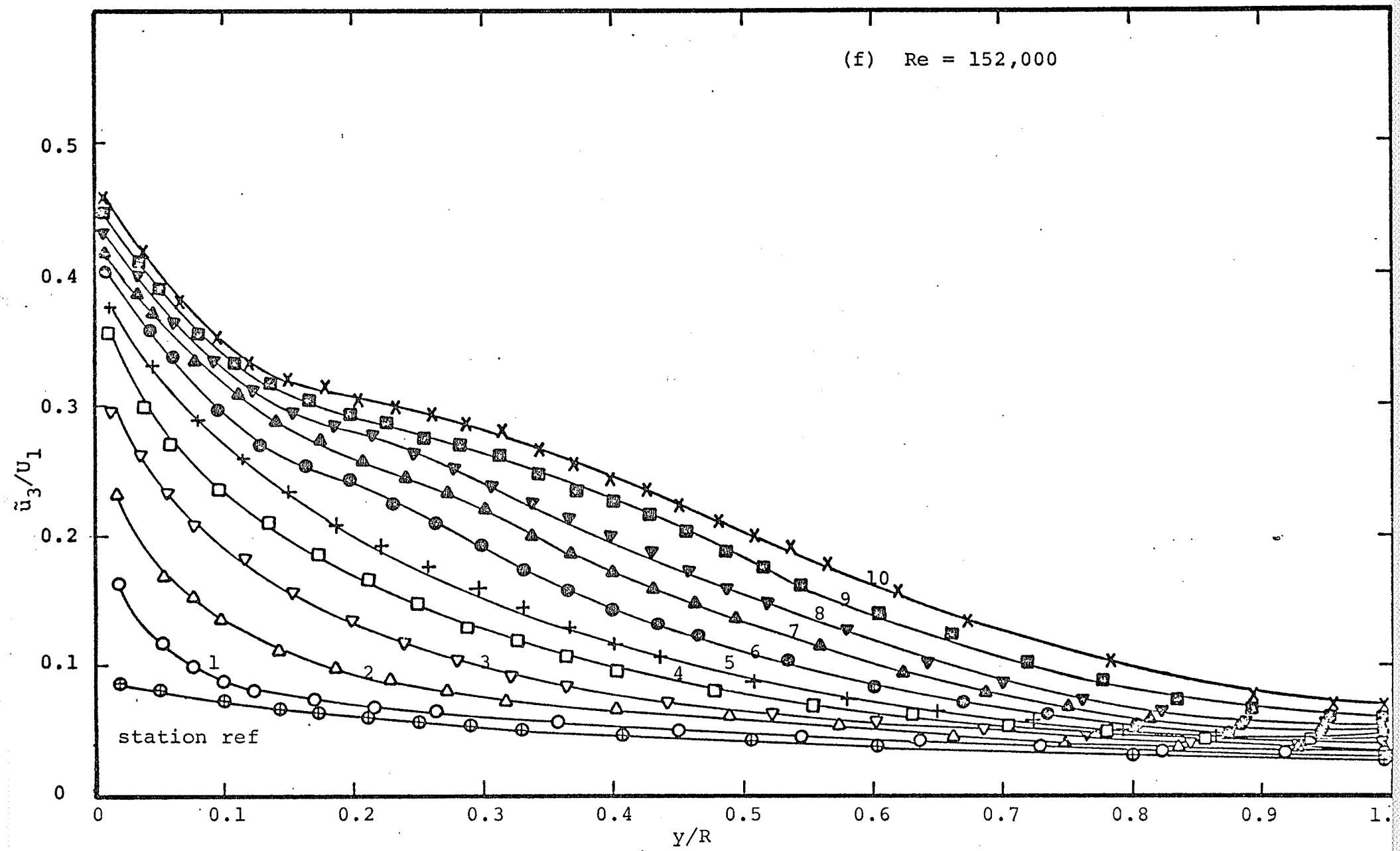

FIGURE 12 . Distribution of the turbulence intensities $\tilde{u}_1/U_1$, $\tilde{u}_2/U_1$ and $\tilde{u}_3/U_1$.

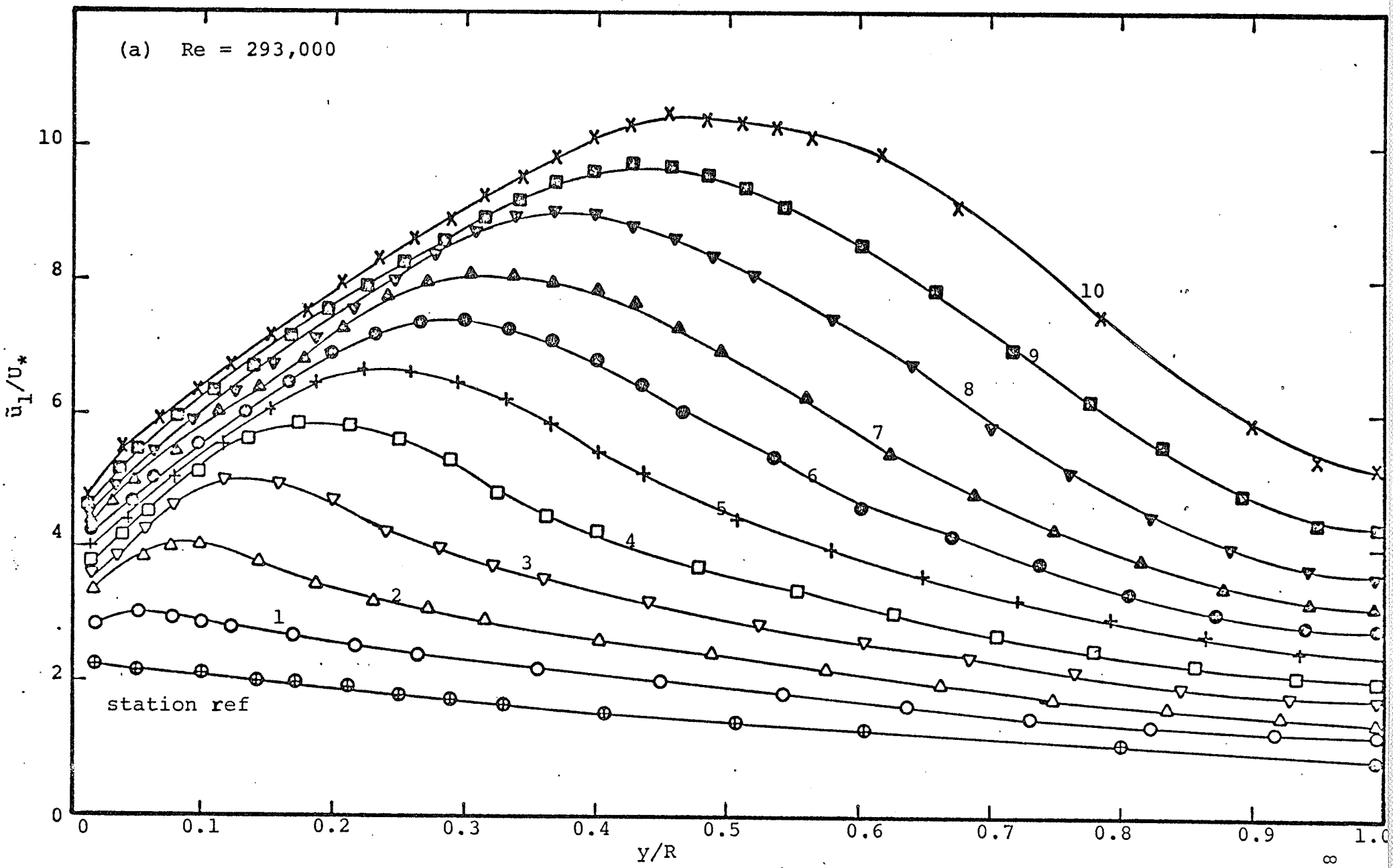

FIGURE 13. Distribution of the turbulence intensities $\tilde{u}_1/U_*$, $\tilde{u}_2/U_*$ and $\tilde{u}_3/U_*$.

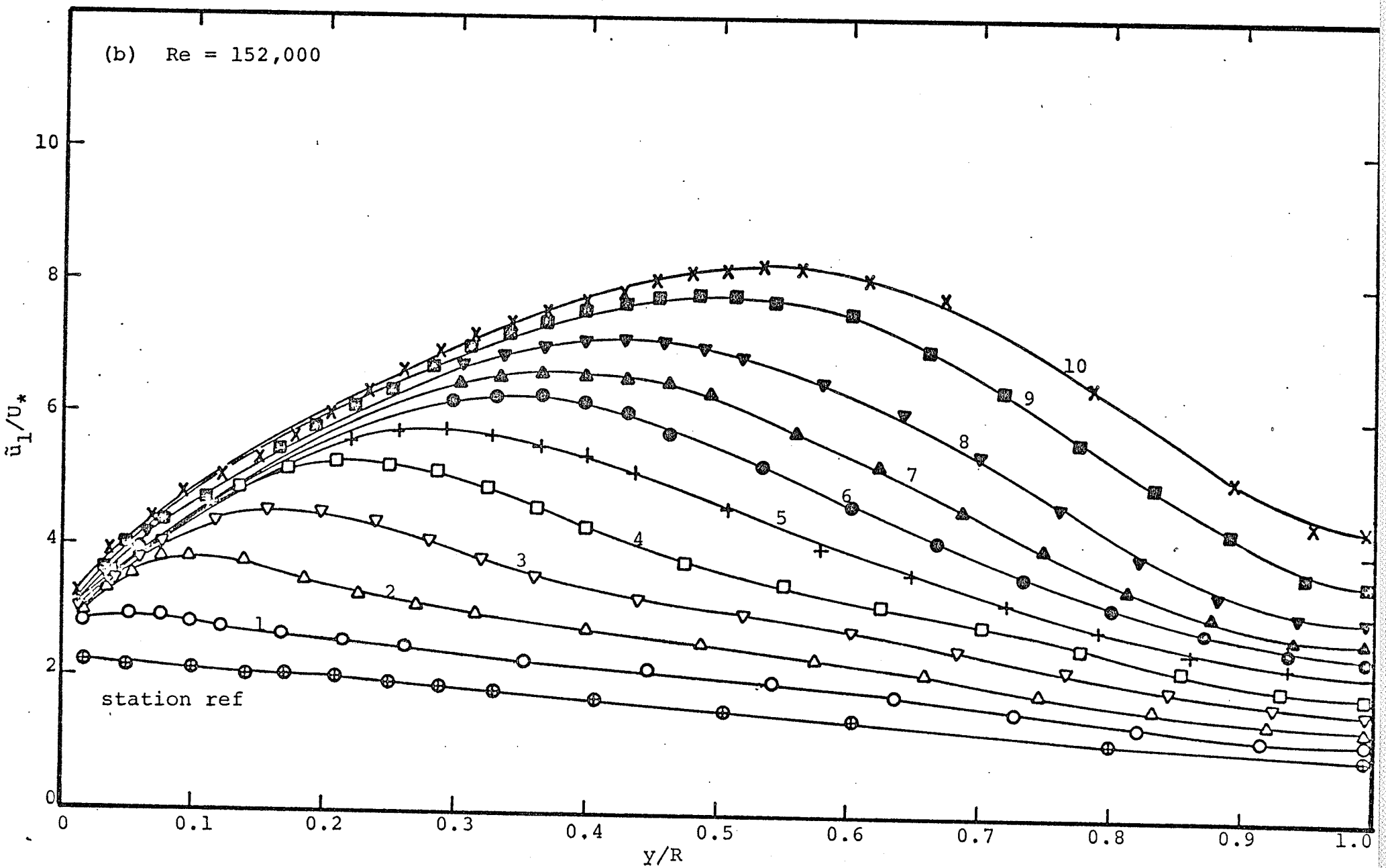

FIGURE 13. Distribution of the turbulence intensities $\tilde{u}_1/U_*$, $\tilde{u}_2/U_*$ and $\tilde{u}_3/U_1$.

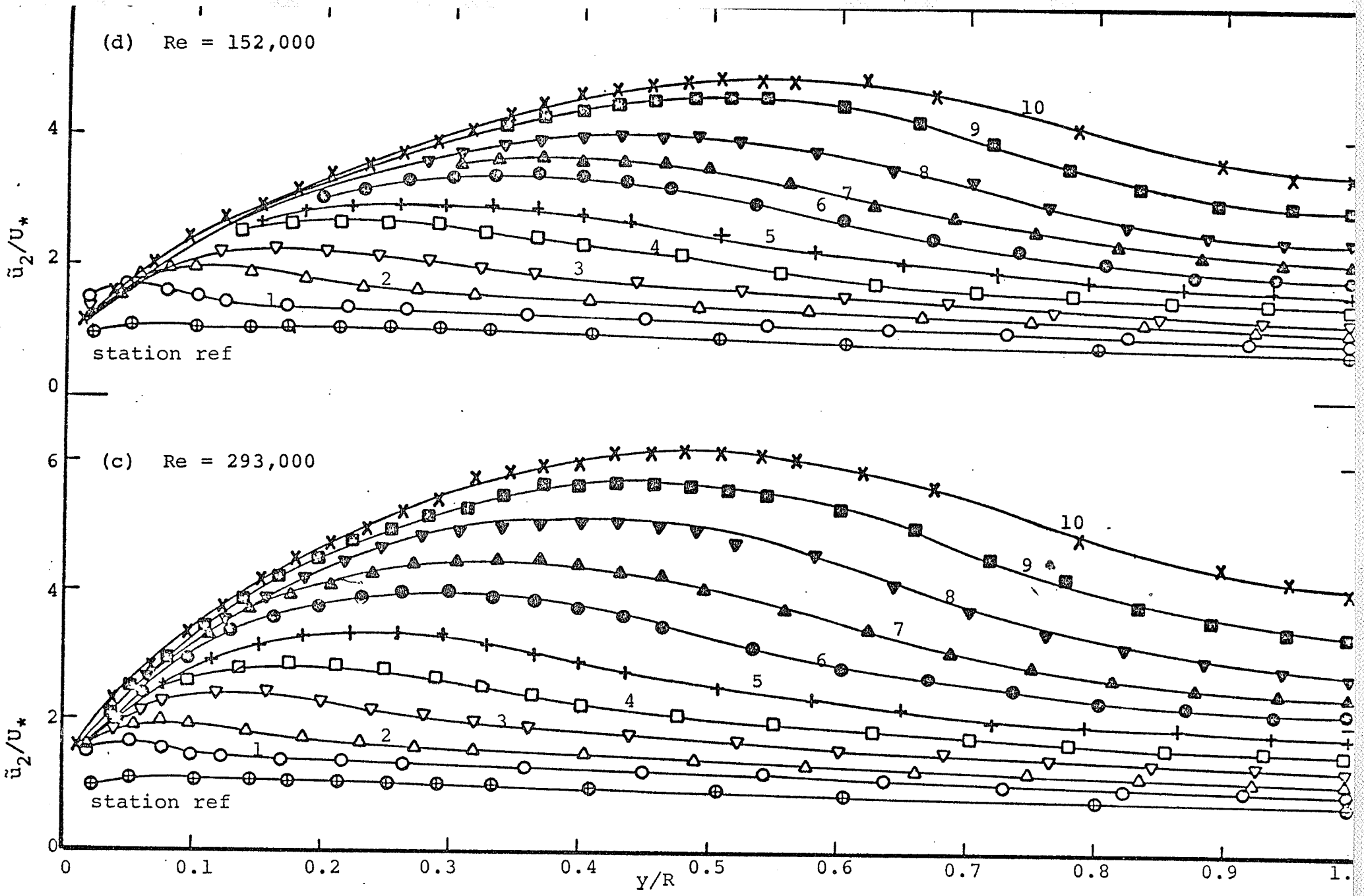

FIGURE 13. Distribution of the turbulence intensities $\tilde{u}_1/U_*$, $\tilde{u}_2/U_*$ and $\tilde{u}_3/U_*$.

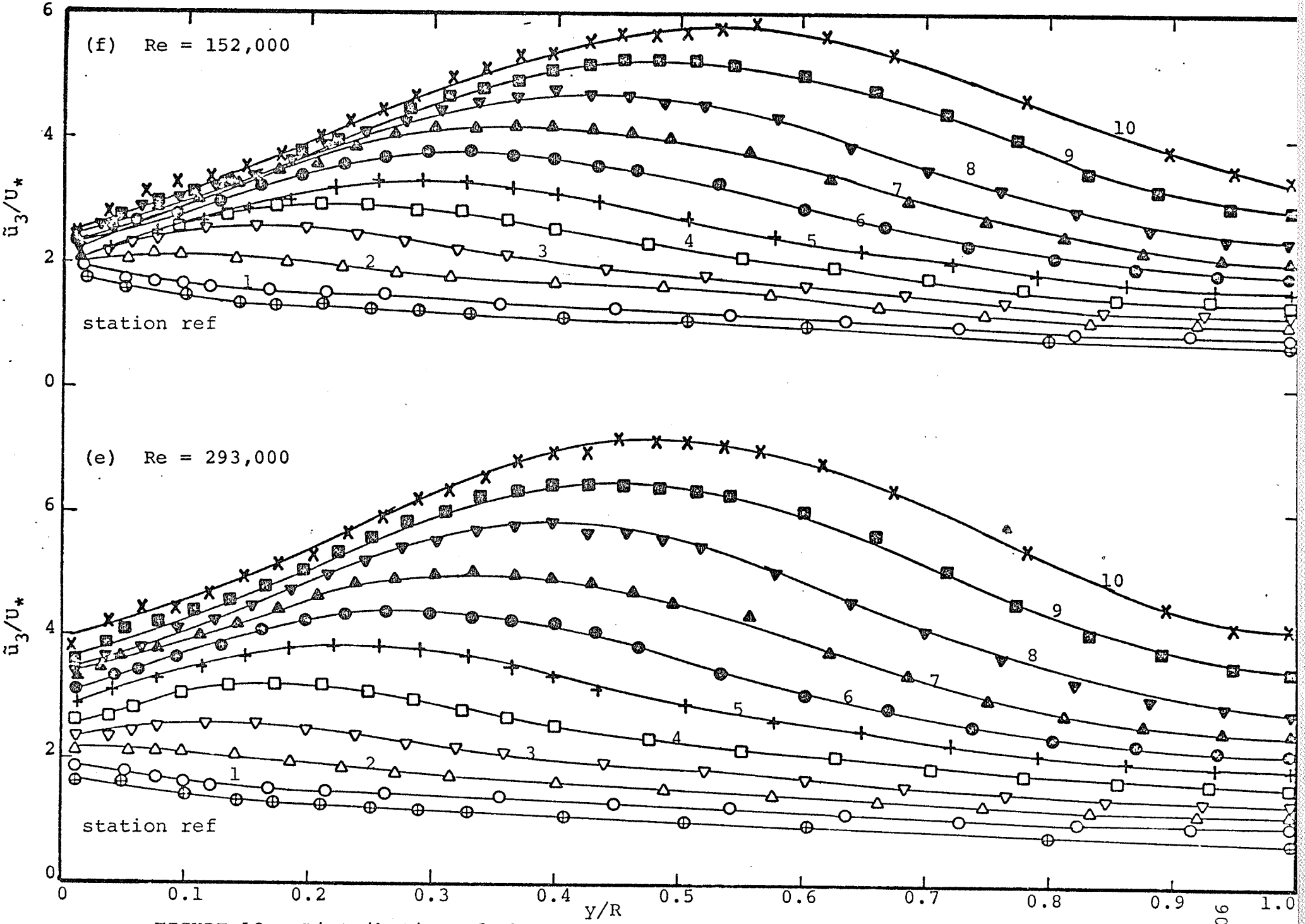

FIGURE 13. Distribution of the turbulence intensities $\tilde{u}_1/U_*$, $\tilde{u}_2/U_*$ and $\tilde{u}_3/U_*$.

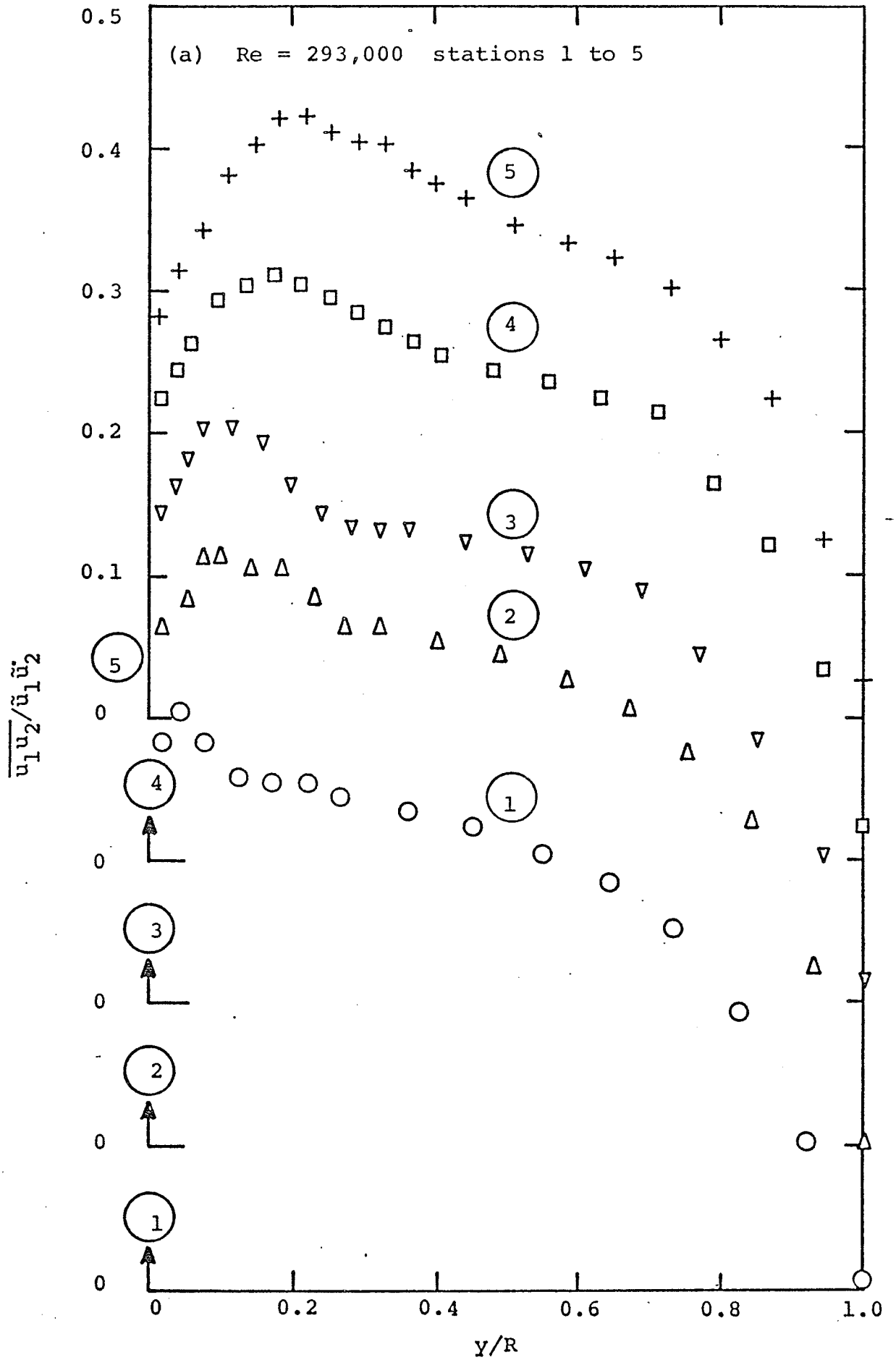

FIGURE 14. Variation of shear correlation coefficient, $\overline{u_1u_2}/\tilde{u}_1\tilde{u}_2$.

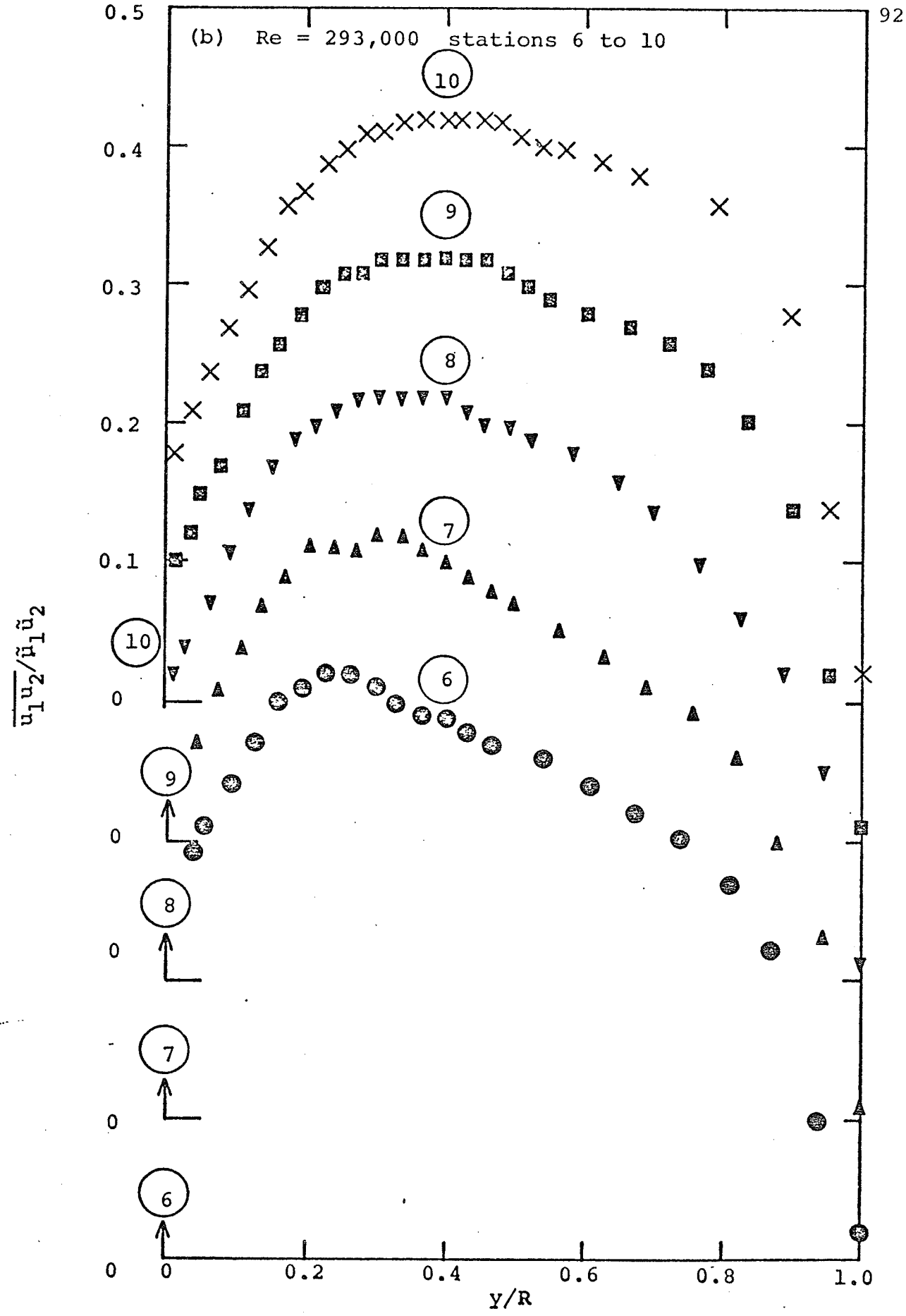

FIGURE 14. Variation of shear correlation coefficient, $\overline{u_1 u_2}/\tilde{u}_1\tilde{u}_2$.

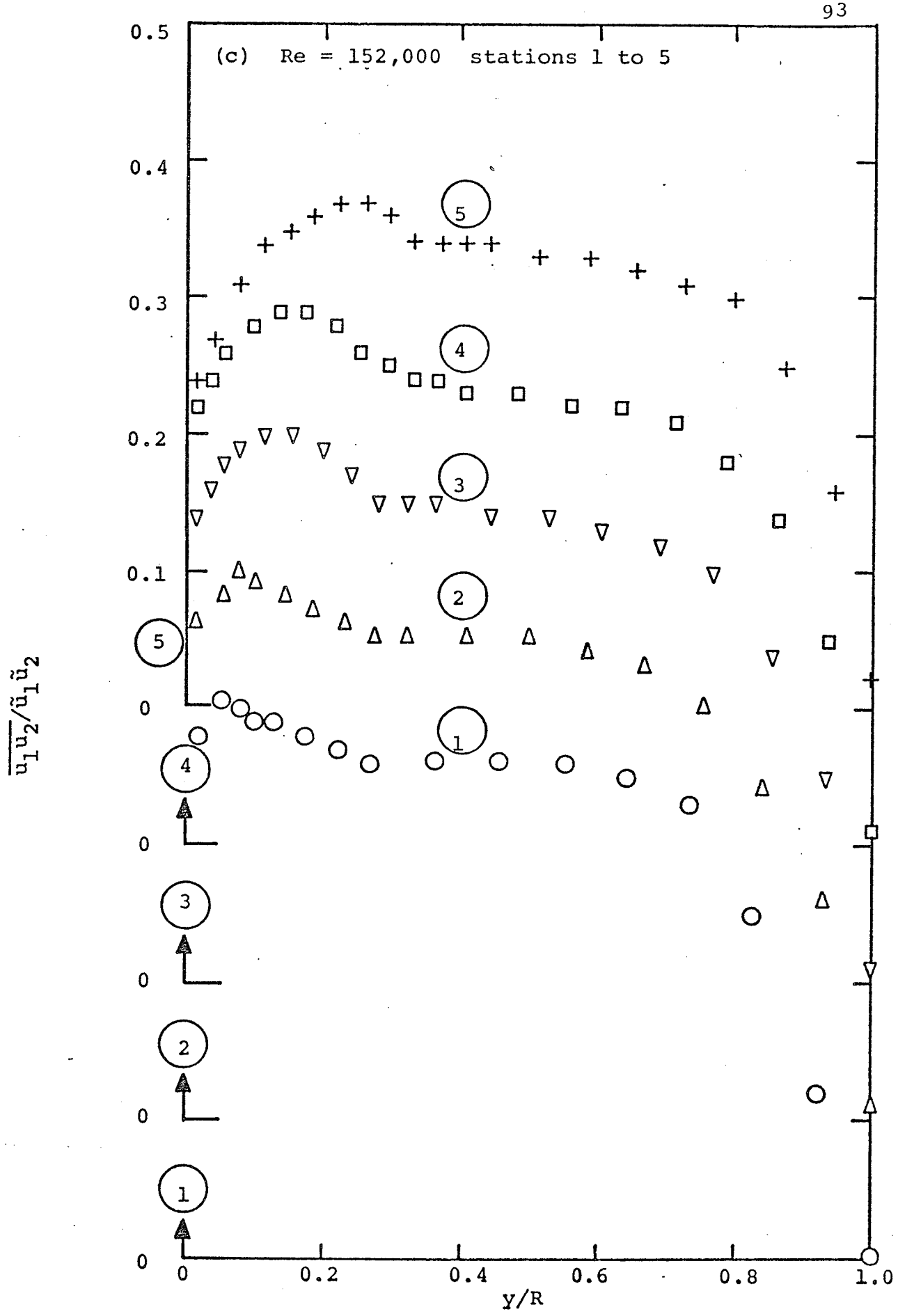

FIGURE 14. Variation of shear correlation coefficient, $\overline{u_1 u_2}/\tilde{u}_1\tilde{u}_2$.

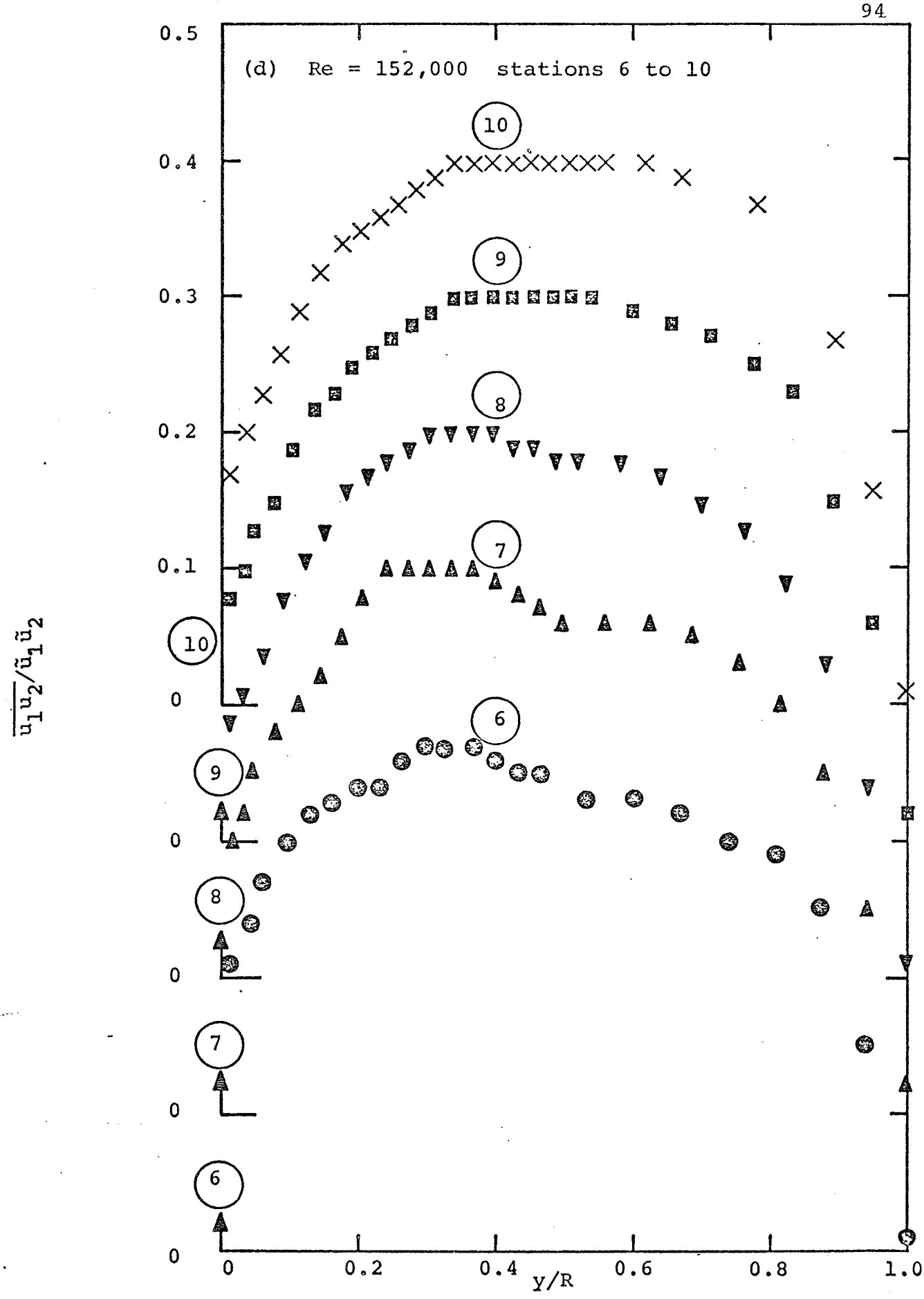

FIGURE 14. Variation of shear correlation coefficient, $\overline{u_1u_2}/\tilde{u}_1\tilde{u}_2$.

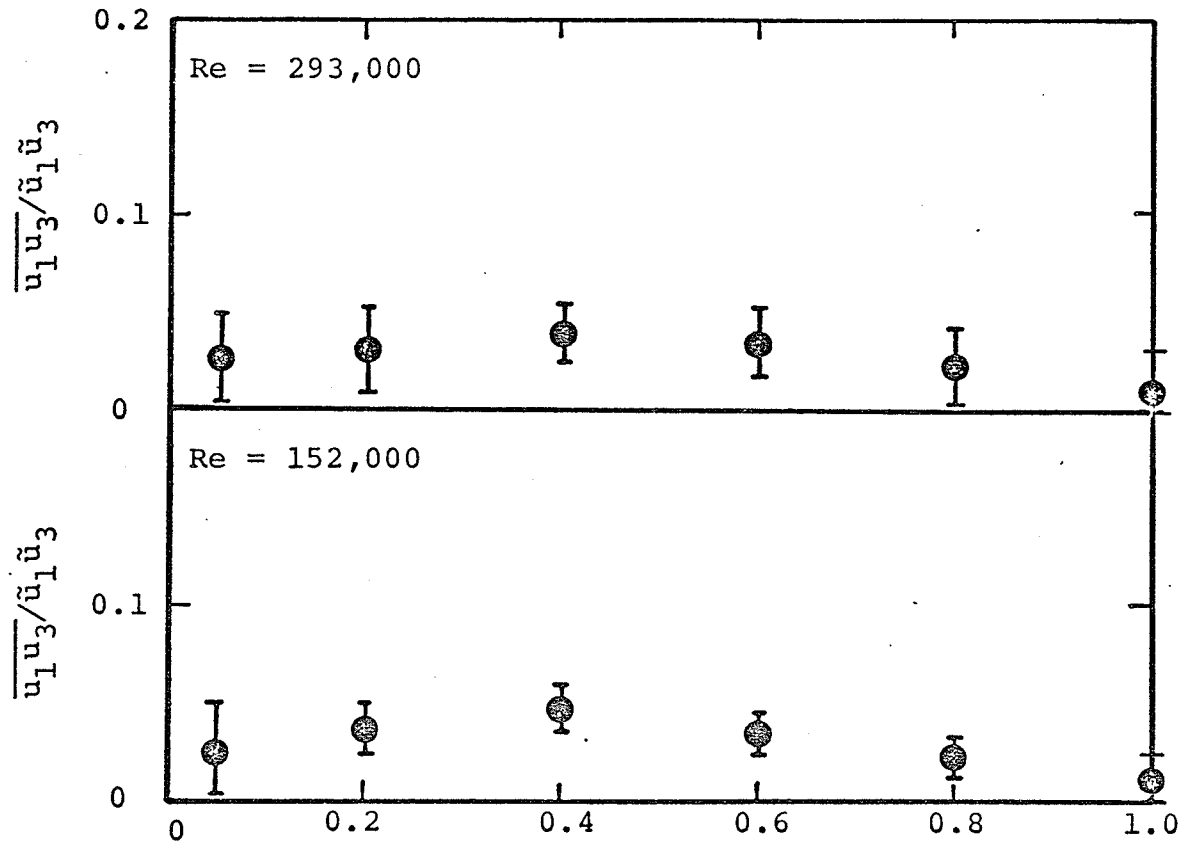

FIGURE 15. Variation of the shear correlation coefficient, $\overline{u_1u_3}/\tilde{u}_1\tilde{u}_3$.

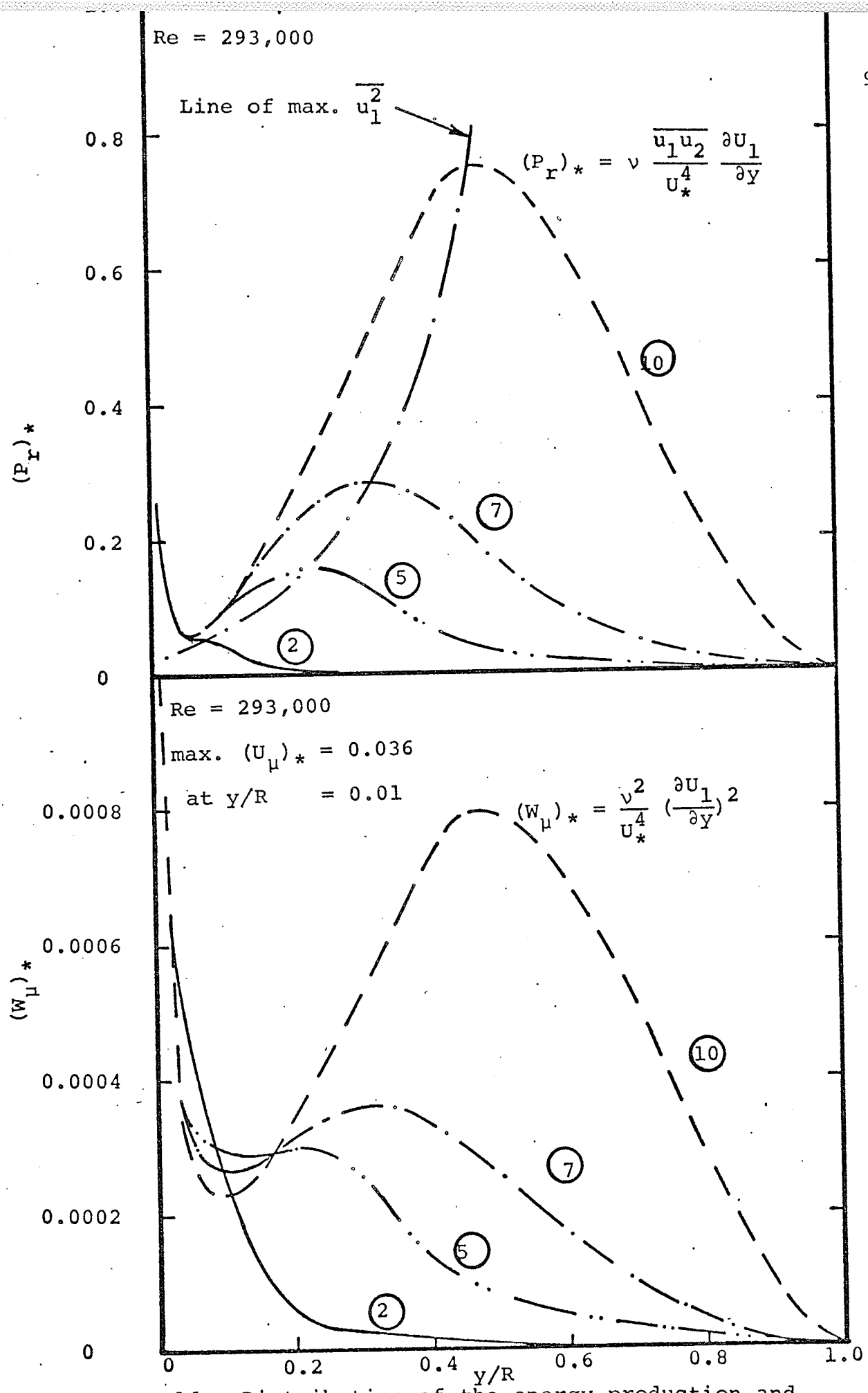

FIGURE 16. Distribution of the energy production and the direct viscous dissipation rates.

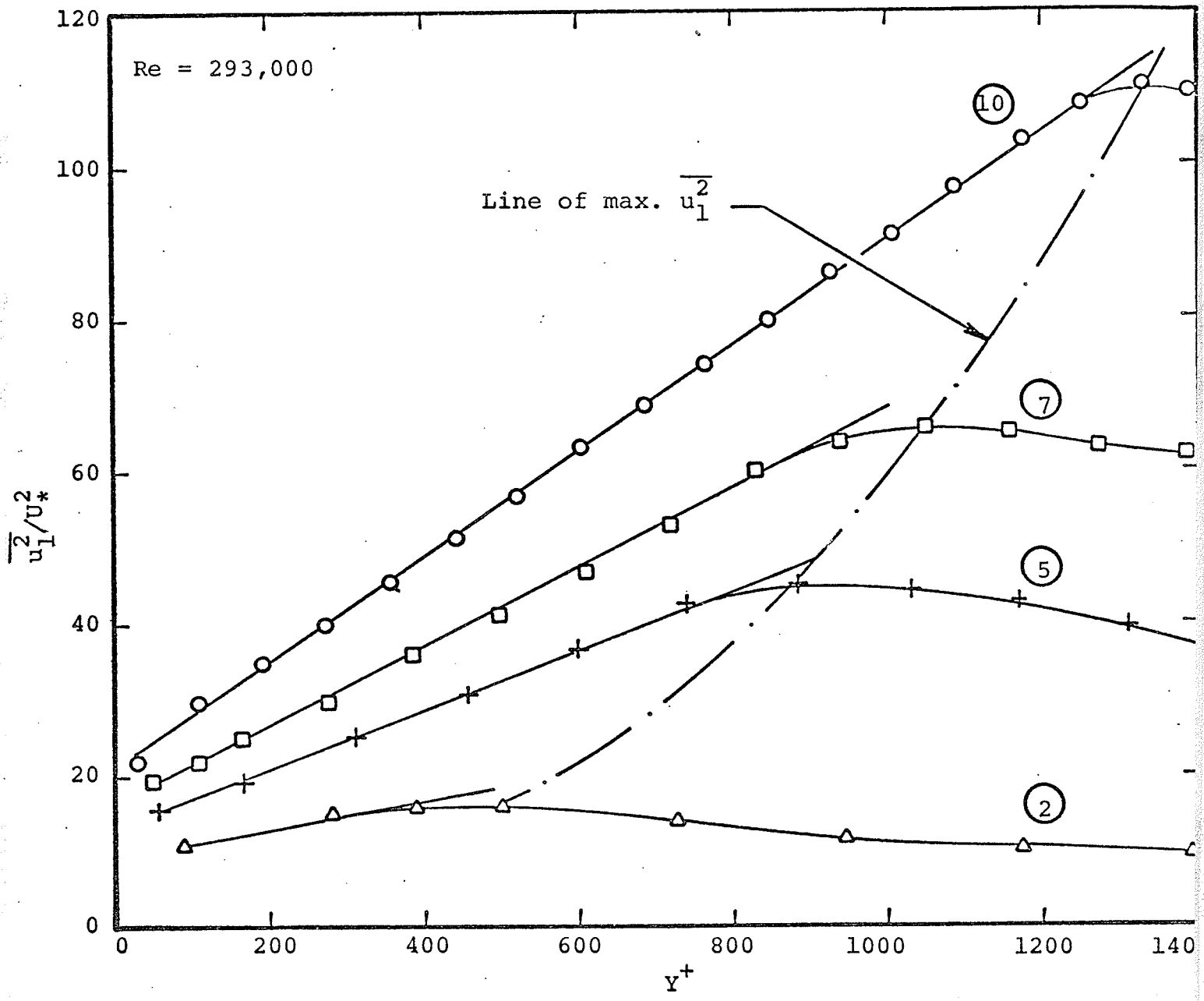

FIGURE 17. Distribution of $\overline{u_1^2}/U_*^2$ in the wall turbulent layer.

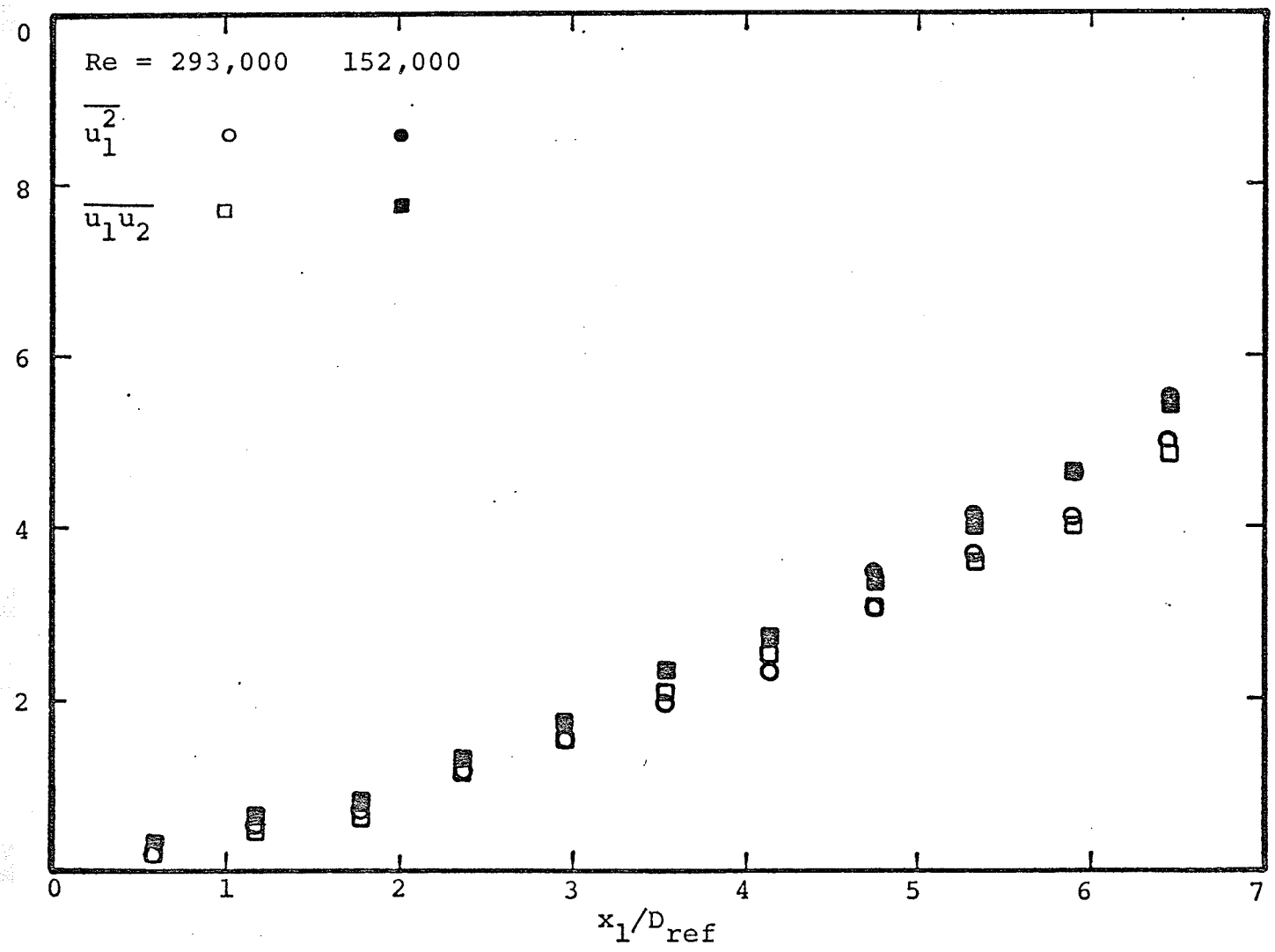

FIGURE 18. Position of maximum $\overline{u_1^2}$ and $\overline{u_1 u_2}$ as a function of the diffuser axial distance.

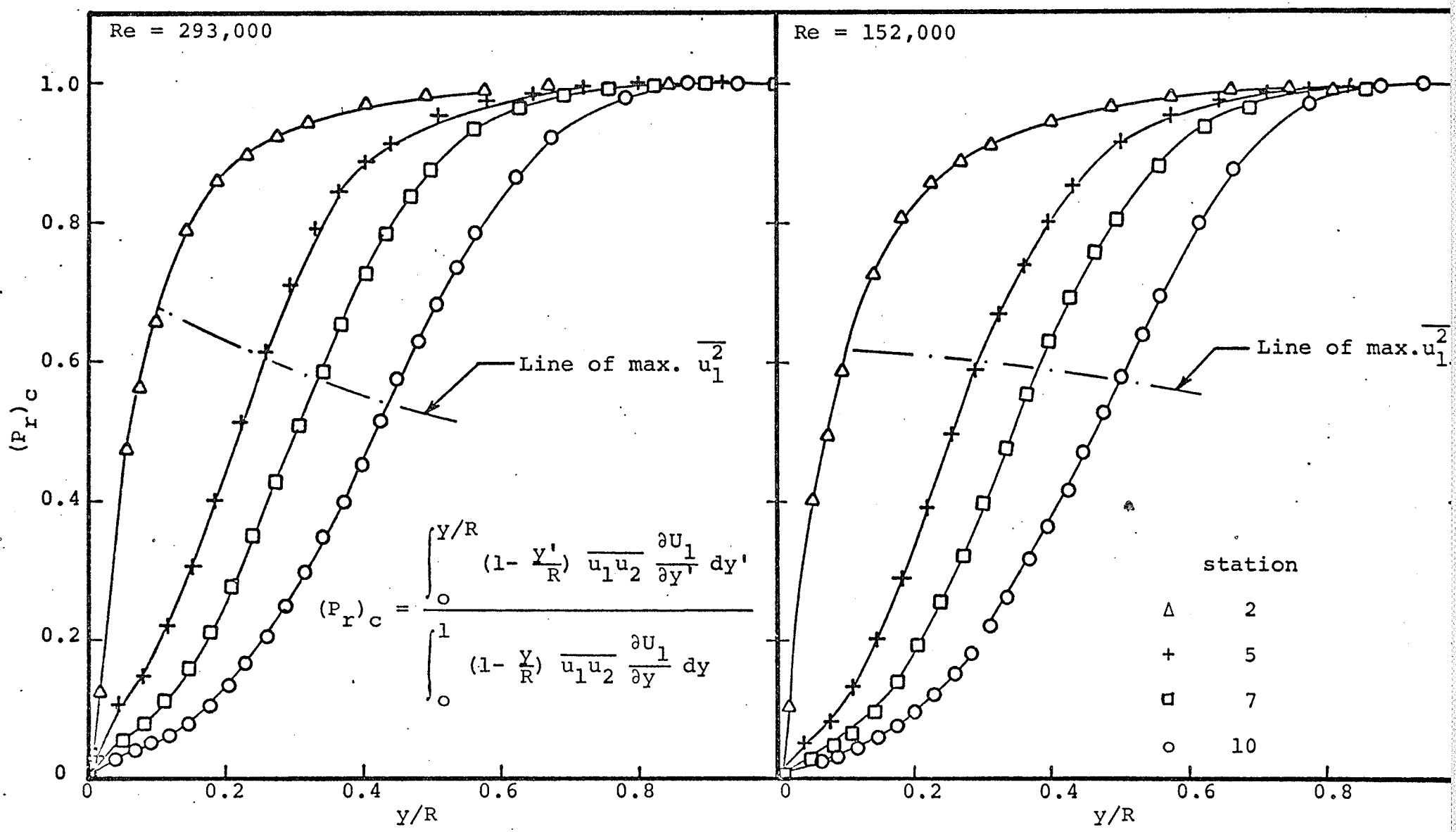

FIGURE 19. Cumulative turbulence energy production rate.

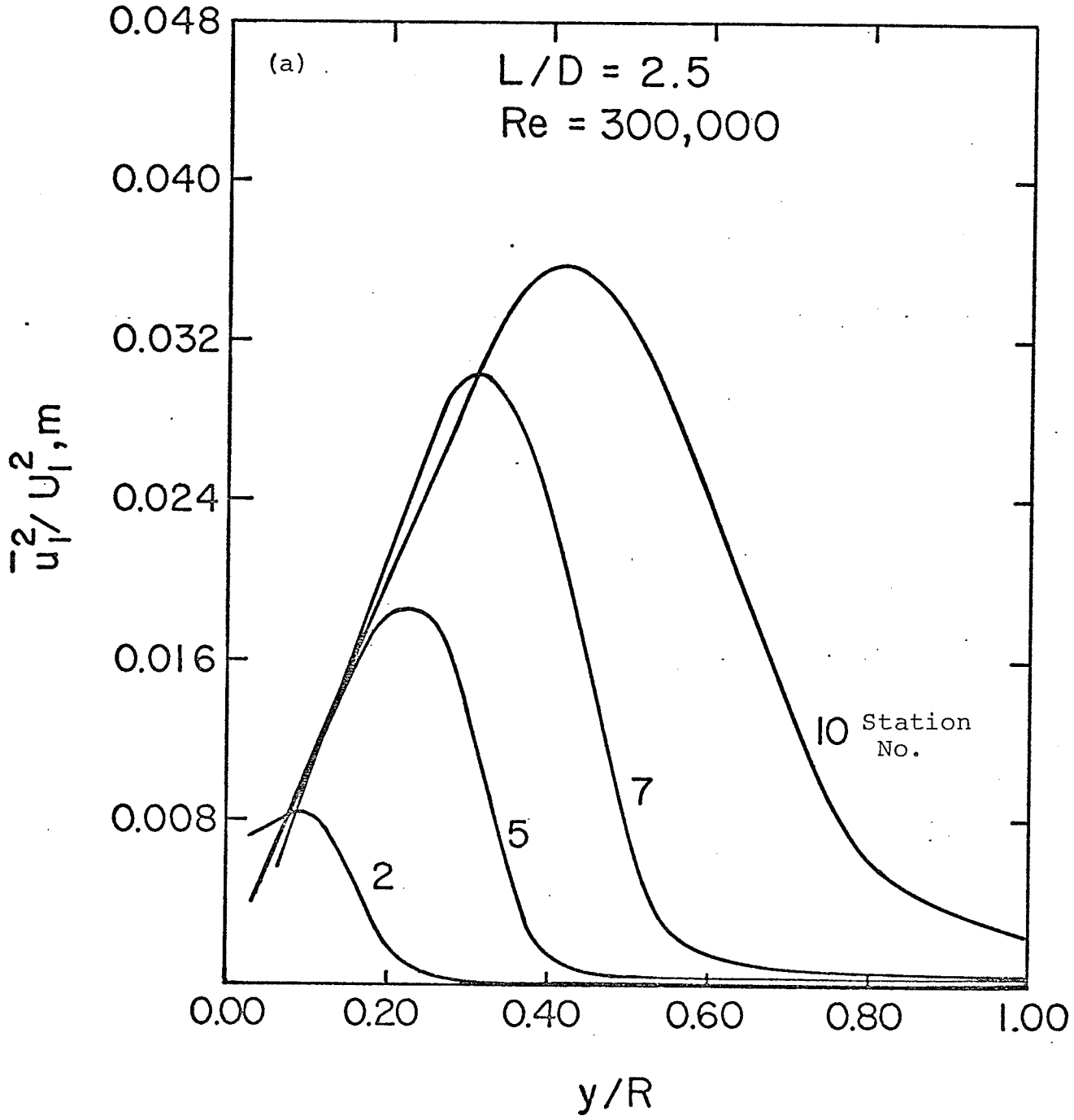

FIGURE 20. Distribution of $\overline{u_1^2}/U_{1,m}^2$.

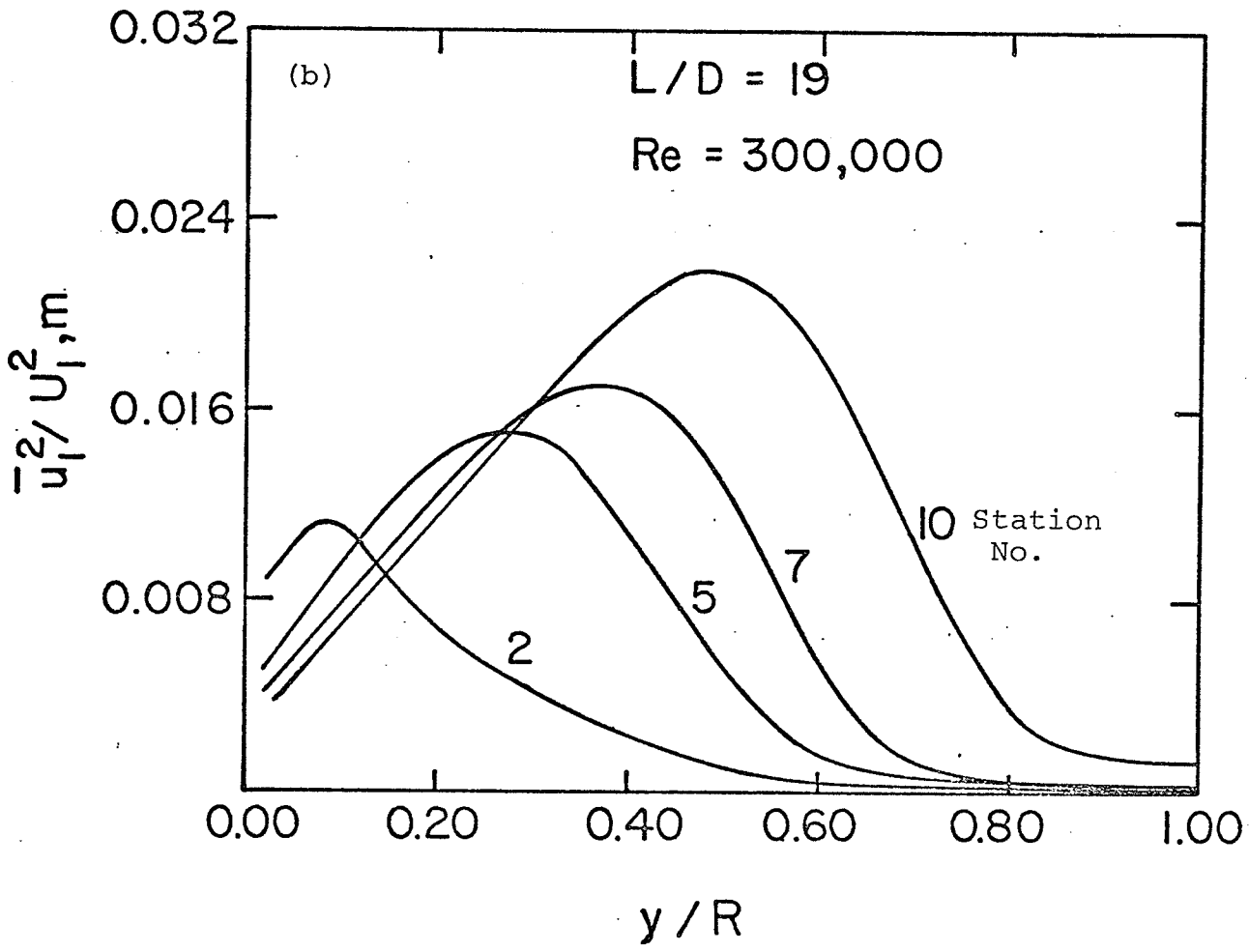

FIGURE 20. Distribution of $\overline{u_1^2}/U_{1,m}^2$.

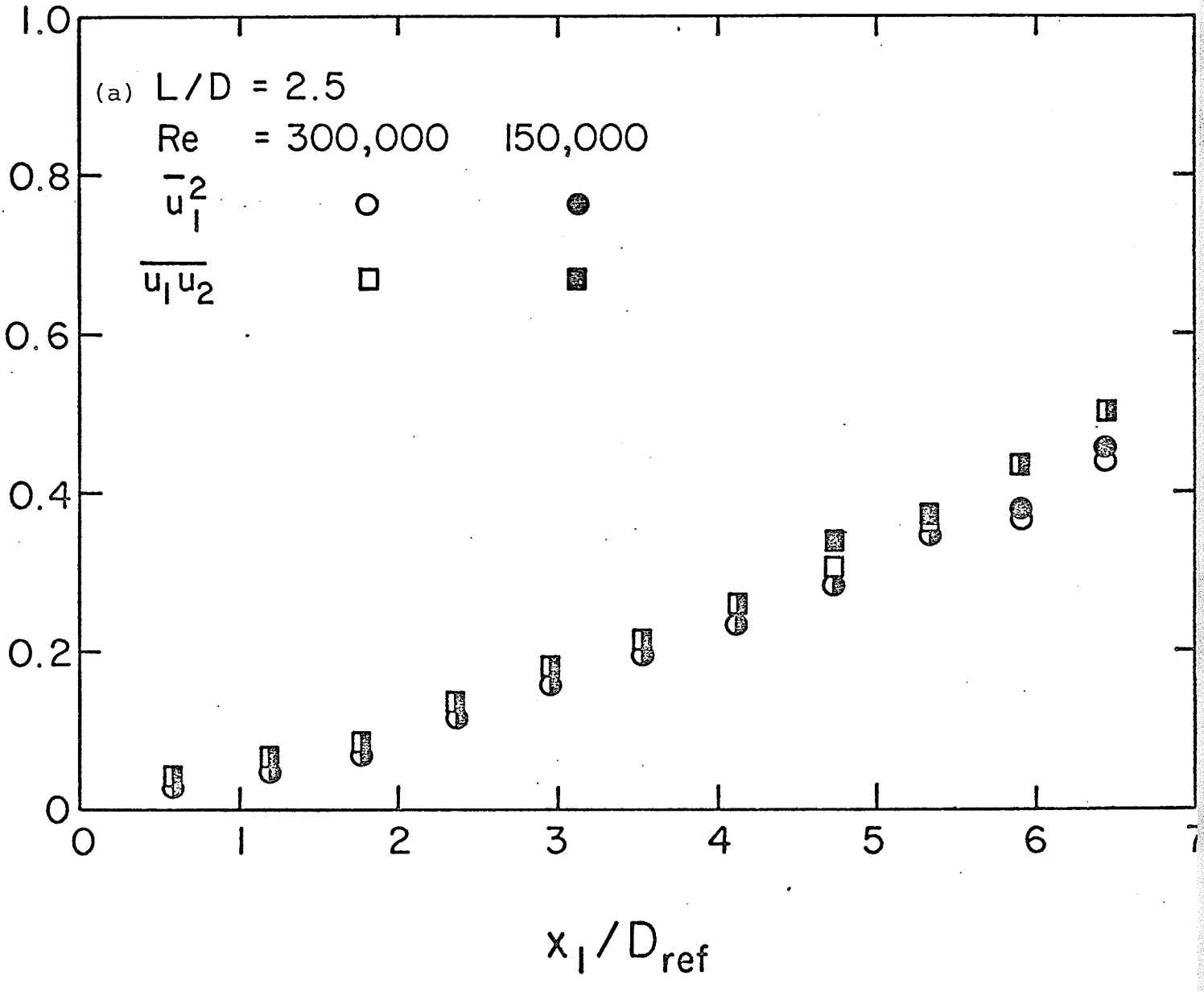

FIGURE 21. Position of maximum $\overline{u_1^2}$ and $\overline{u_1 u_2}$ as a function of the diffuser axial distance.

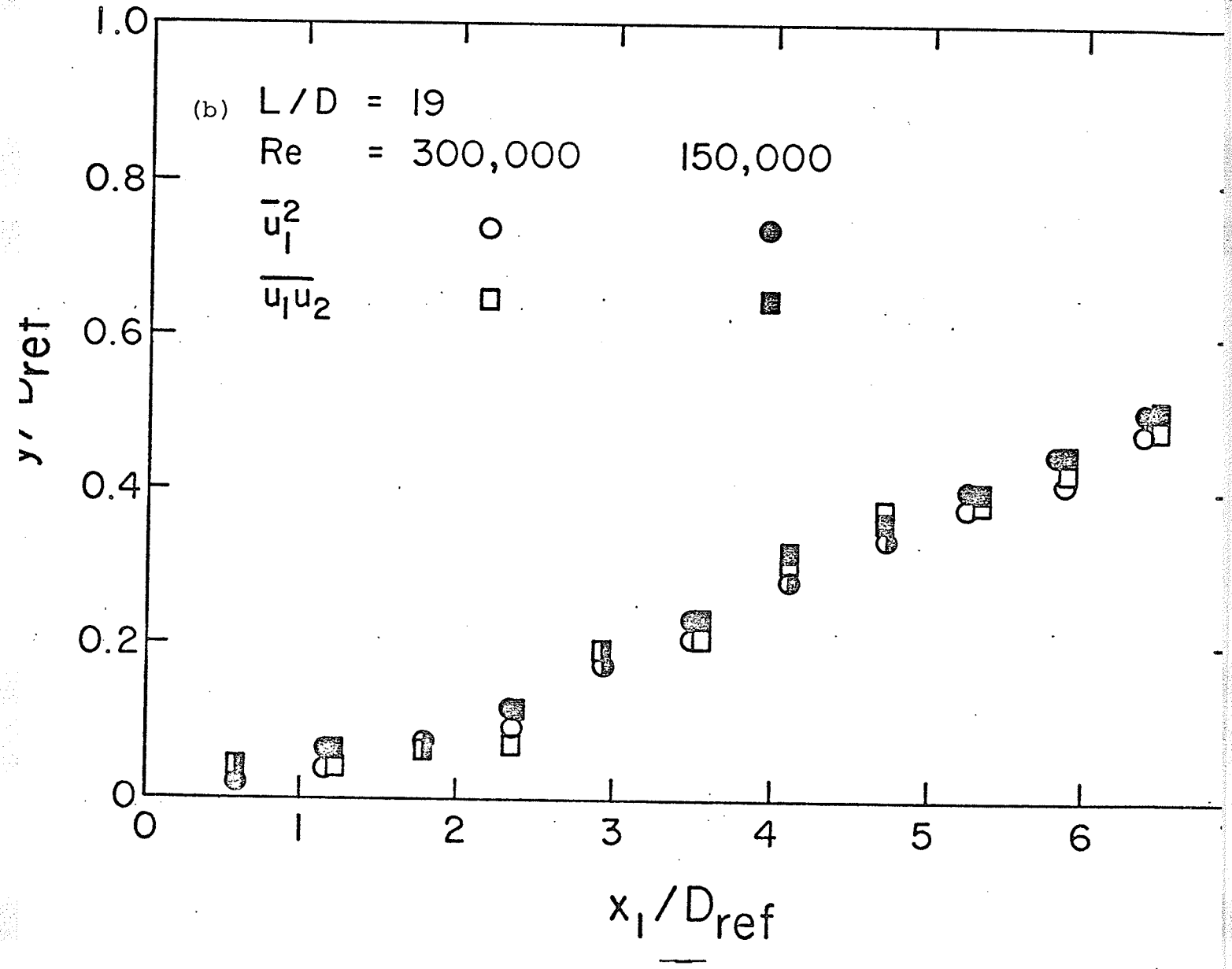

FIGURE 21. Position of maximum $\overline{u_1^2}$ and $\overline{u_1 u_2}$ as a function of the diffuser axial distance.

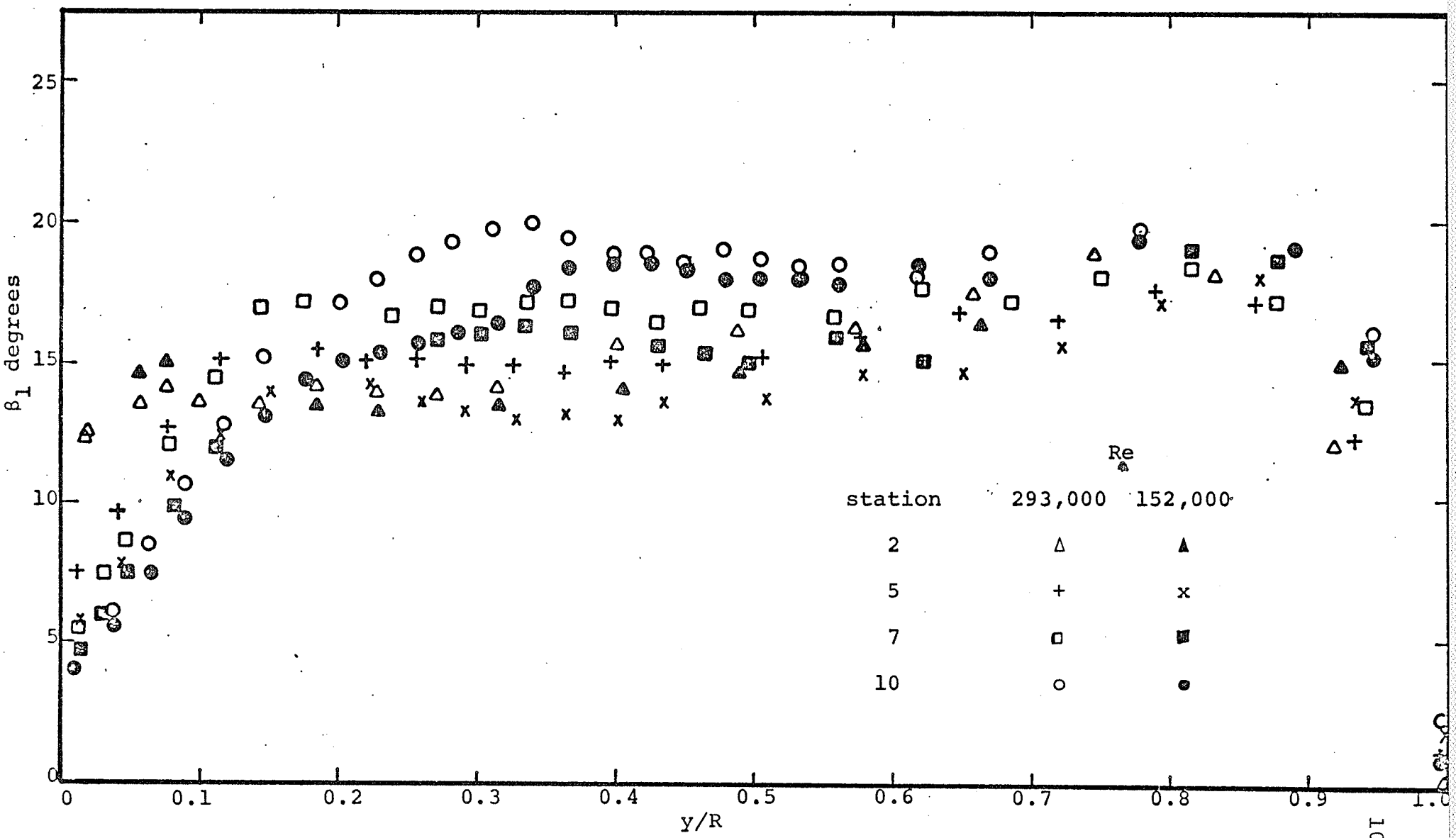

FIGURE 22. Variation of the angle β_1 between the principal axis of the turbulent stress tensor and the x_1-axis.

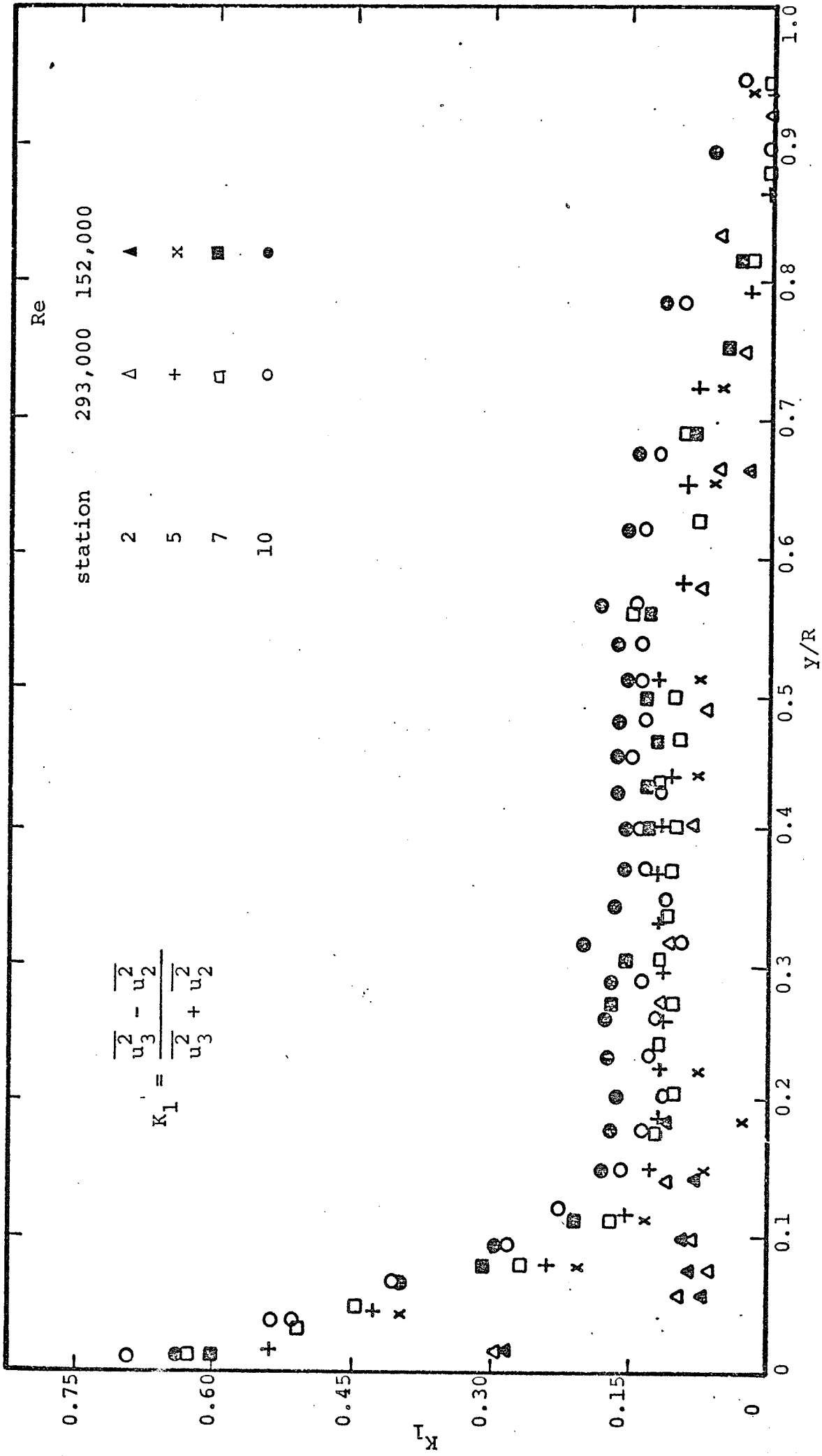

FIGURE 23. Distribution of the local structure parameter K_1.

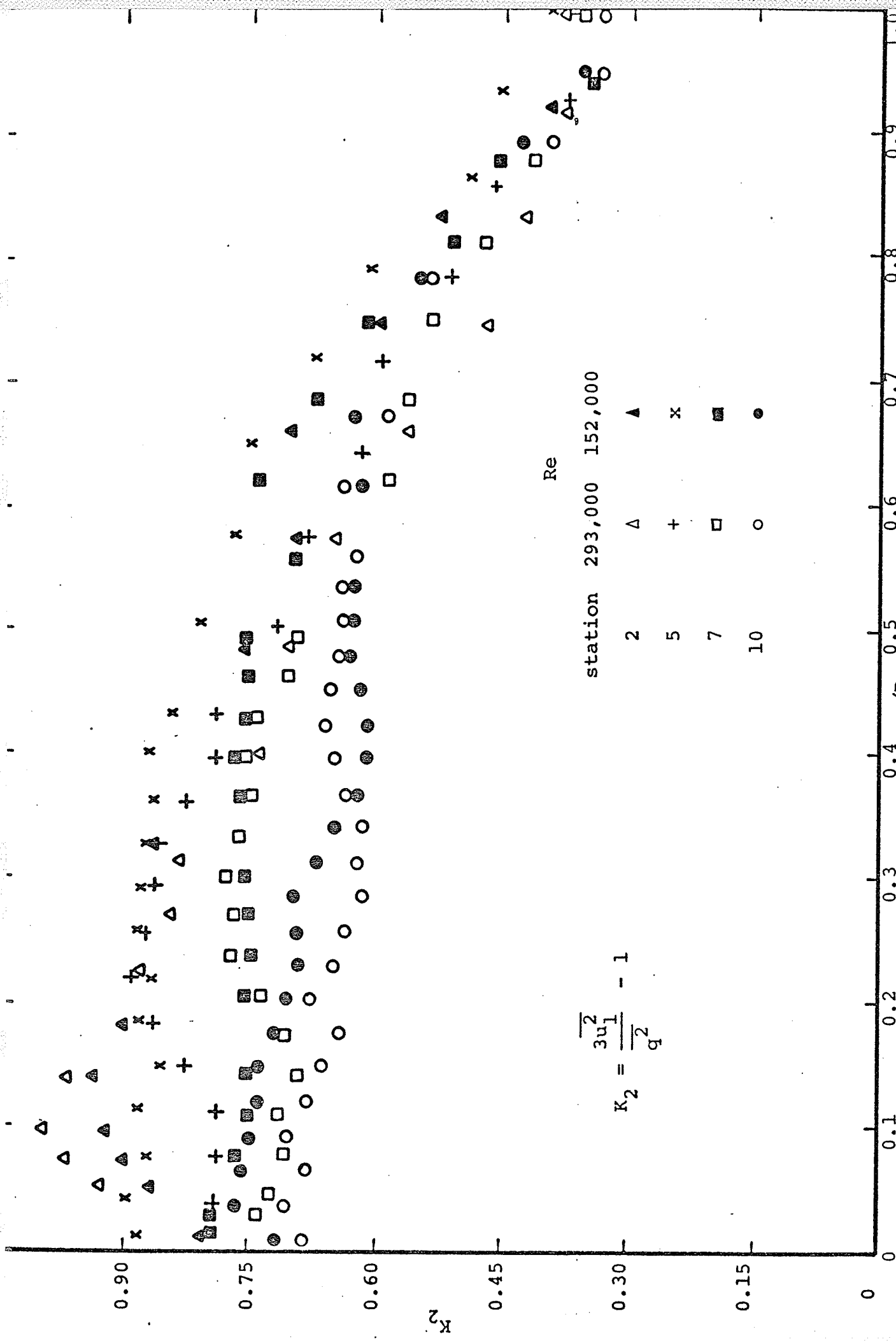

FIGURE 24. Distribution of the local structure parameter K_2.

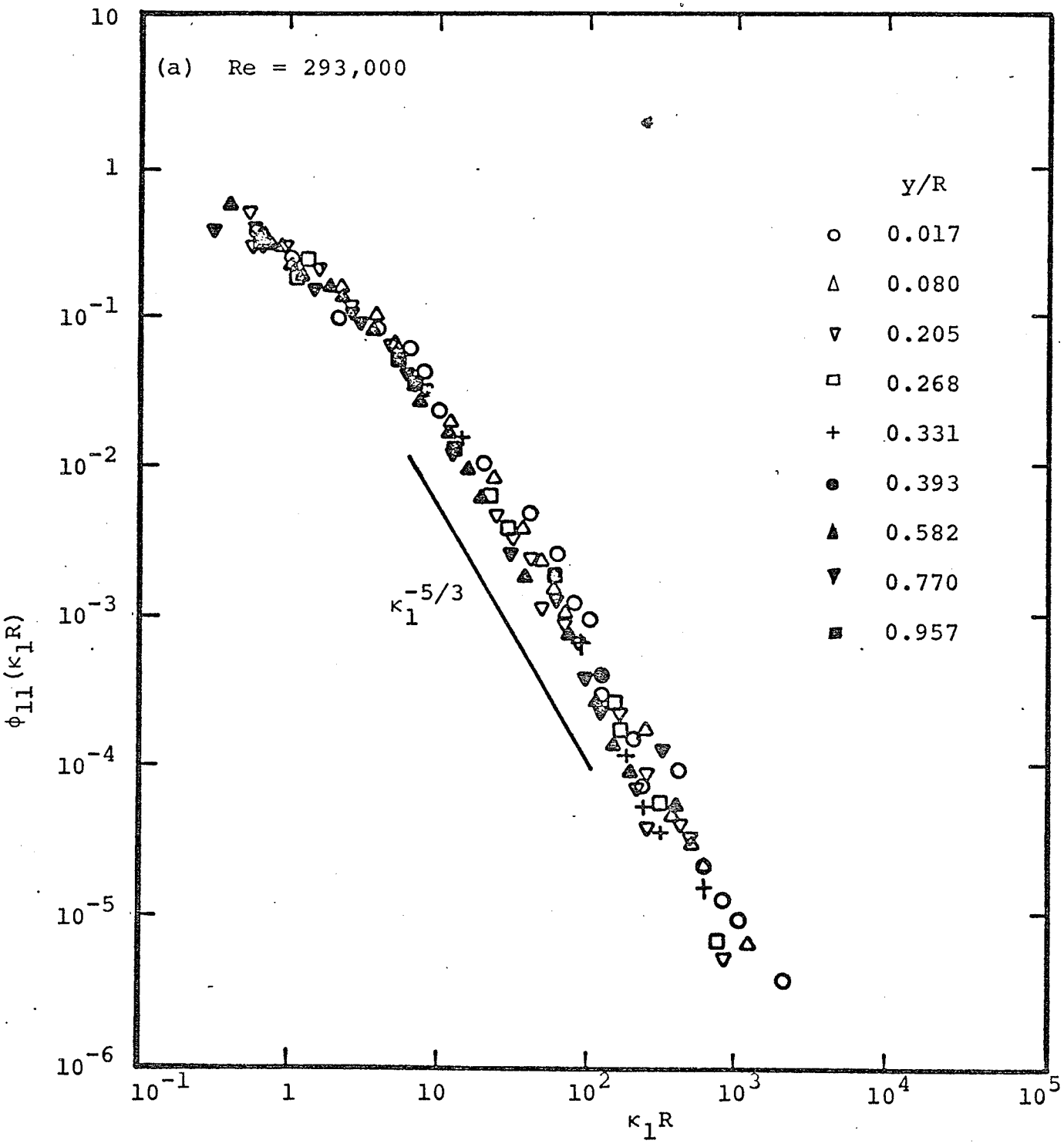

FIGURE 25. Normalised spectra of $\overline{u_1^2}$ (station 7).

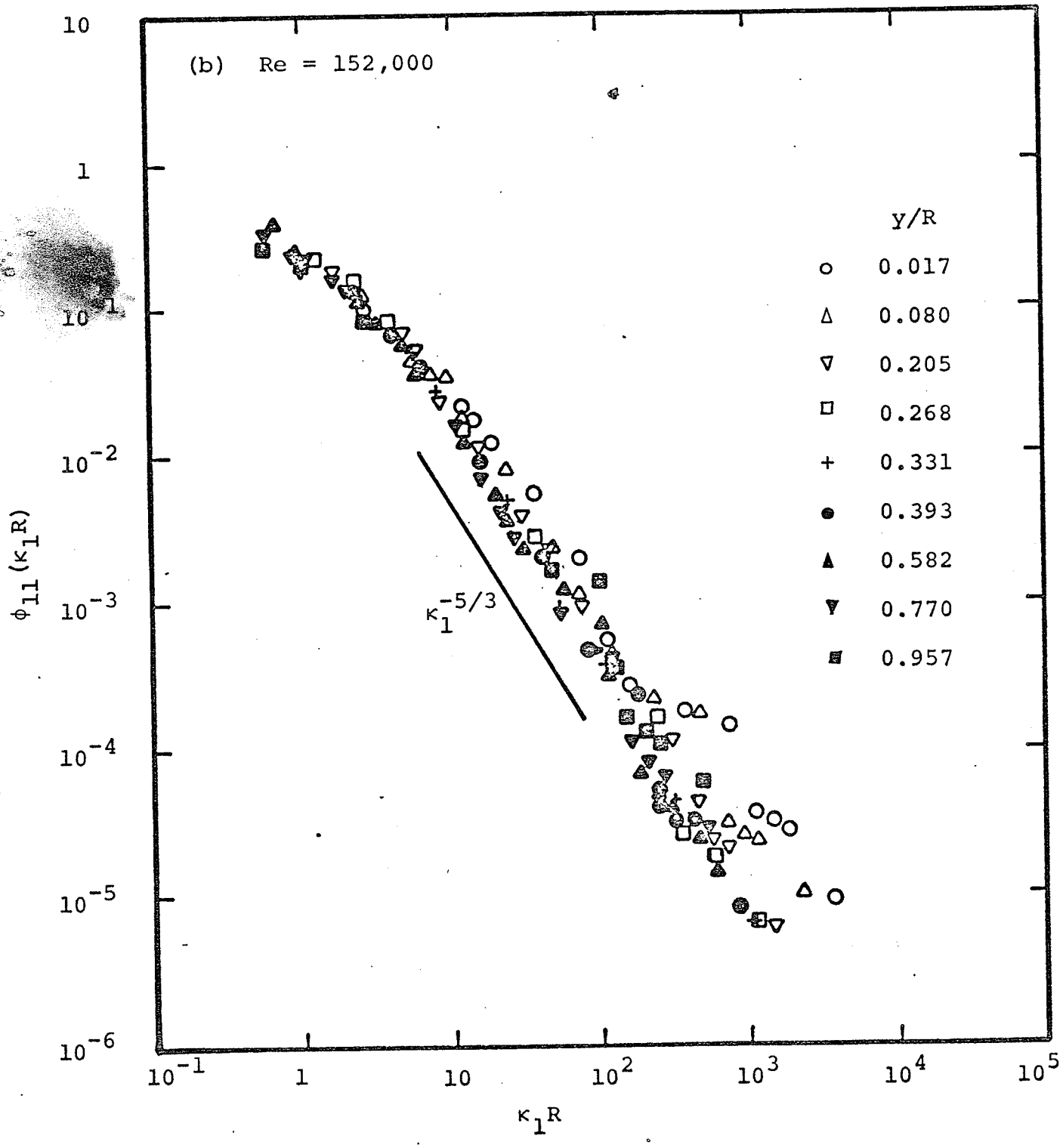

FIGURE 25. Normalised spectra of $\overline{u_1^2}$ (station 7).

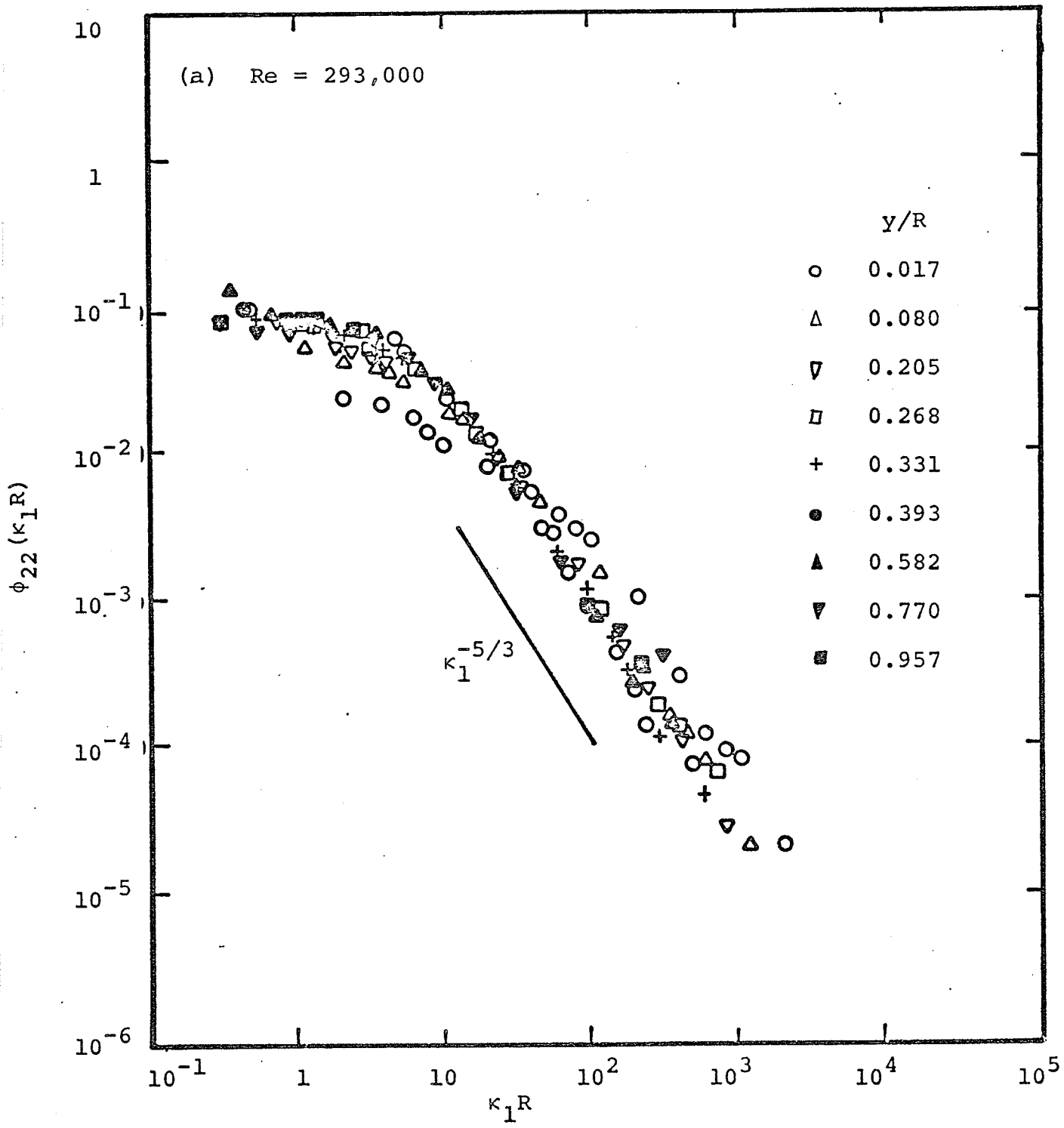

FIGURE 26. Normalised spectra of $\overline{u_2^2}$ (station 7).

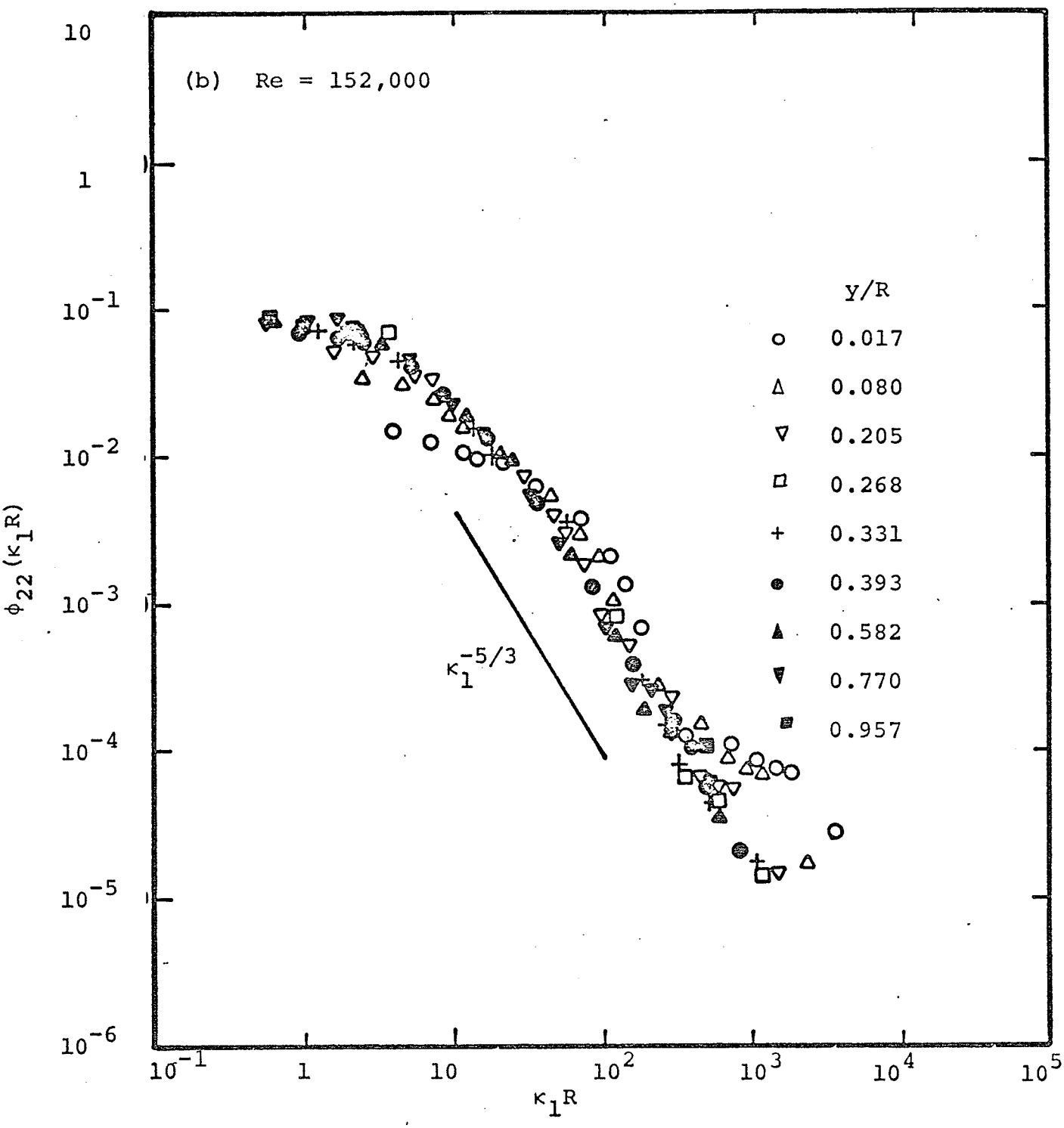

FIGURE 26. Normalised spectra of $\overline{u_2^2}$ (station 7).

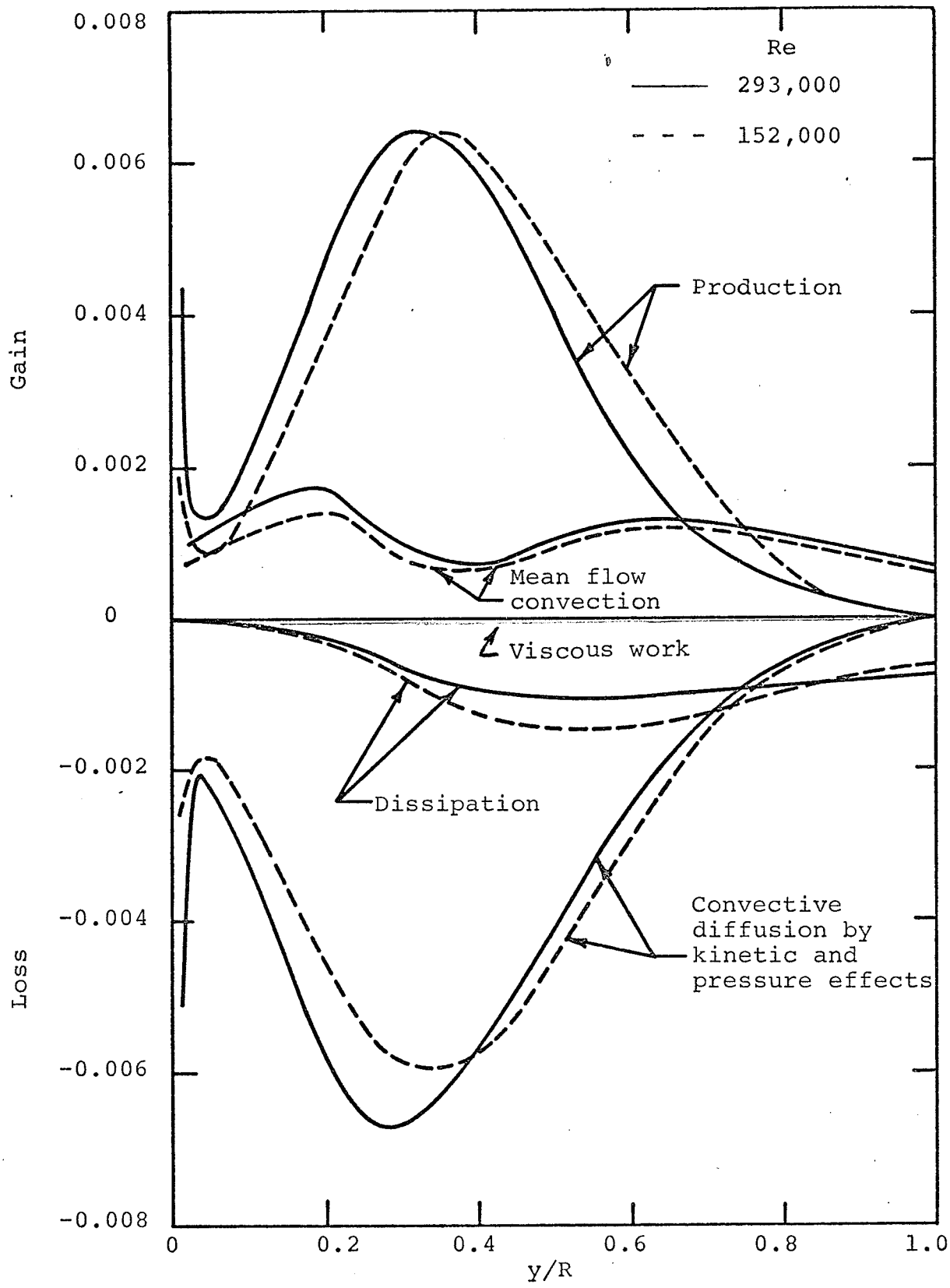

FIGURE 27. Turbulent kinetic energy balance (station 7).

VITA

PAUL AKAZUA CHRISTOPHER OKWUOBI

1935	Born, September 27, at Kaduna, Nigeria
1950	College Scholar at St. Patrick's College, Asaba, Nigeria
1958	State Scholar at the University College, Nigeria
1962	Graduated B.Sc.(Eng.) University of London, England
1962-68	Worked as Water Engineer and Ag. Senior Sanitary Engineer, Federal Ministry of Works, Lagos, Nigeria
1963	Studied Dam Engineering from Sept. to Dec. in Japan under the Technical Cooperation Plan
1965-66	Studied at Southampton University, England under The British Council Scholarship
1966	Appointed a Part-time lecturer in Hydraulics at the University of Lagos, Nigeria
1967	Graduated M.Sc.(Eng.) University of Southampton, England
1968-70	Studied at McGill University, Montreal; was a research assistant and instructor in fluid mechanics

1970-72 Studied at The University of Manitoba, Winnipeg; engaged in turbulence research and was an instructor in fluid mechanics.

Activities: Tennis, swimming and chess.

PUBLICATIONS

OKWUOBI, P. A. C. 1966 An investigation into the flow characteristics of a hollow weir offtake. M.Sc. dissertation, University of Southampton, Southampton, England.

OKWUOBI, P. A. C. AND SAVAGE, S. G. 1970 Calibration of the three component balance for use in the McGill cavitation tunnel. McGill University, Dept. of Civil Eng. and Applied Mechanics, Fluid Mechanics Note No. FML TN 70-1.

TRUPP, A. C., AZAD, R. S. WILSON, N. W. AND OKWUOBI, P. A. C. 1971 Turbulence in a straight conical diffuser. University of Salford Symposium on Internal Flows, paper 9.

OKWUOBI, P. A. C., AZAD, R. S. AND HAWALESHKA, O. 1972 Turbulence structure parameters in an inhomogeneous strain field. To be published in AIAA Journal.

OKWUOBI, P. A. C. AND AZAD, R. S. 1972 Turbulence investigation in a conical diffuser with fully developed flow at entry. The University of Manitoba, Dept. of Mech. Eng. Rep. ER 25.16.

OKWUOBI, P. A. C. AND AZAD, R. S. 1972 Turbulence investigation in a conical diffuser with partly developed flow at entry. The University of Manitoba, Dept. of Mech. Eng. Rep. ER 25.17.

OKWUOBI, P. A. C. AND AZAD, R. S. 1972 Turbulence in a conical diffuser with fully developed flow at entry. To be published in J. Fluid Mech.